Needle length control and secretion specificity switching in bacterial T3SS

Dissertation

der Mathematisch-Naturwissenschaftlichen Fakultät

der Eberhard Karls Universität Tübingen

zur Erlangung des Grades eines

Doktors der Naturwissenschaften

(Dr. rer. nat.)

vorgelegt von

Claudia Edith Torres-Vargas

aus Mexiko Stadt, Mexiko

Tübingen

2021

Gedruckt mit Genehmigung der Mathematisch-Naturwissenschaftlichen Fakultät der Eberhard Karls Universität Tübingen.

Tag der mündlichen Qualifikation:	29.06.2021
Dekan:	Prof. Dr. Thilo Stehle
1. Berichterstatter:	Prof. Dr. Samuel Wagner, PhD
2. Berichterstatter:	PD Dr. rer. nat. Monika Schütz

Table of contents

Abbreviations

BN	Blue Native polyacrylamide gel electrophoresis
CBD	Chaperone binding domain
CRP	cAMP receptor protein
Cryo-EM	Cryo-Electron Microscopy
DDM	N-Dodecyl-beta-D-Maltoside
EPEC	Enteropathogenic E. coli
GI	gastrointestinal
IM	inner membrane
LB	Luria Bertani
M	molar
MIS	maltose insertion site
µm	micrometre
ml	millilitre
ms	milliseconds
NC	Needle complex
NLuc	Nanoluc luciferase
nm	nanometre
OD_{600}	optical density at 600 nm
OM	outer membrane
*p*Bpa	*para*-benzoyl-phenylalanine
PBS	phosphate-buffered saline solution
PCR	polymerase chain reaction
pT10	plasmid Taco 10

PVDF	polyvinylidene fluoride
RBM	Ring-building motif
SCV	*Salmonella* containing vacuole
SDS PAGE	sodium dodecyl sulphate polyacrylamide gel electrophoresis
Sec-pathway	general secretory pathway
SPI-1	*Salmonella* pathogenicity island 1
SPI-2	*Salmonella* pathogenicity island 2
SPI-1IS	SPI-1 insertion site
TCA	trichloroacetic acid
TEM	Transmission electron microscopy
TPR	Tandem tetratricopeptide repeat
T3SS	Type three secretion system
T3S4	Type three secretion substrate specificity switching

Zusammenfassung

Das Typ III Sekretionssystem (T3SS) oder Injektisom ist eines der bestuntersuchten bakteriellen Sekretionssysteme, da es von entscheidender Wichtigkeit für die Virulenz einer Vielzahl von Pflanzen- und Tierpathogenen ist. Die Struktur des T3SS setzt sich zusammen aus der Basis, die in die bakterielle Zellhülle eingebettet ist und den Exportapparat beherbergt, zytoplasmatischen Bestandteilen, die an der Sekretion von Substraten beteiligt sind, dem Nadelfilament, und einer Translokationspore, die in die Membran der Wirtszelle eingebaut wird. Proteinsubstrate des T3SS werden nach ihrer Sekretionsreihenfolge in frühe, intermediäre und späte Substrate untergliedert. Der Aufbau des Nadelfilaments erfolgt durch Sekretion von drei frühen Substraten: der Nadeluntereinheit (SctF), dem Nadeladapter (SctI) sowie dem Nadellängenregulationsprotein (SctP). Sobald das Nadelfilament eine vorbestimmte Länge erreicht hat, ändert das T3SS seine Substratspezifität, um den Transport von intermediären und späten Substraten zu ermöglichen und den Aufbau des Injektisoms abzuschließen. Es wird vermutet, dass SctI und die Assemblierung des Nadeladapters beim Substratspezifitätswechsel sowie bei der Nadellängenkontrolle eine Rolle spielen. Obwohl die Aufrechterhaltung der Sekretionsreihenfolge und die Kontrolle der Nadellänge entscheidend für einen effizienten Aufbau und korrektes Funktionieren des T3SS sind, konnten die komplexen Mechanismen, die diese Prozesse steuern, bislang nicht abschließend aufgeklärt werden. Das Ziel der vorliegenden Arbeit ist es, ein besseres Verständnis des molekularen Mechanismus der Nadellängenkontrolle und deren Verbindung zum Substratspezifitätswechsel zu erlangen, indem I) ein genetisches System zur Synchronisierung des Aufbaus des T3SS konstruiert wird, und II) der Zusammenbau und das Interaktionsnetzwerk von SctI mittels in vivo photocrosslinking untersucht wird. Das im Rahmen dieser Arbeit erzeugte genetische System erlaubt es, den Zusammenbau des Injektisoms präzise zu steuern und zu synchronisieren. Wenngleich dieses System nicht direkt zur Strukturaufklärung geeignet ist, stellt es ein vielseitiges Werkzeug für zukünftige Studien des Aufbaus und der Regulation der Funktion des Injektisoms dar. Zusätzlich konnte in dieser Arbeit ein umfassendes Netzwerk von Protein-Protein-Interaktionen zwischen SctI und den Exportapparatkomponenten SctR und SctT beschrieben werden. Diese Daten unterstützen die Hypothese, dass

SctI als Adapter zwischen dem Exportapparat und dem Nadelfilament dient, weshalb wir vorschlagen, SctI fortan als Nadeladapter zu bezeichnen. Zuletzt konnte experimentell gezeigt werden, dass der Zusammenbau des Nadeladapters weder bei der Nadellängenkontrolle noch beim Wechsel der Substratspezifität eine Rolle spielt.

Summary

Type III secretion systems (T3SS) or injectisomes are one of the most investigated bacterial secretions systems, as they are pivotal for the virulence of several animal and plant pathogens. The T3SS consist of a membrane-embedded base that harbors the export apparatus, cytoplasmic components involved in secretion of proteins, a needle filament and a translocation pore inserted in the host cell membrane. Proteins secreted in type 3-dependent manner, also called substrates, are classified in three categories: early, middle and late, according to the order in which they are transported. Assembly of the needle structure requires the secretion of three early substrates: the needle (SctF), the rod (SctI) and the needle length regulator (SctP). As soon as the needle reaches its predetermined length, the T3SS switches its substrate specificity and allows the secretion of middle and late substrates to complete assembly of the injectisome. SctI and inner rod assembly are suggested to be involved in specificity switching and needle length control, respectively. Efficient assembly and functionality of the injectisome is assured by the ordered secretion of proteins and the needle length regulation, both processes governed by complex mechanisms that are not fully elucidated. The aim of this study was to improve the understanding of the molecular basis of needle length control and its relationship with substrate specificity switching by I) creating a genetic system to synchronize assembly of the T3SS, and II) characterizing the assembly and interaction network of SctI via *in vivo* photocrosslinking. This study provides an elaborate genetic system that permits to synchronize assembly of the injectisome. Although this system is not suitable for structural analyses, it is amenable to integration of further approaches, which makes it a resourceful tool to investigate relevant processes involved in the assembly and function regulation of the injectisome. In addition, this work encompasses a comprehensive network of protein-protein interactions between SctI and the export apparatus components SctR and SctT. These data point toward the adapter function of the inner rod between these two structures and therefore we propose to rename the inner rod “needle adapter”. Finally, this study provides experimental evidence that assembly of the inner rod is not involved in neither specificity switch nor in needle length control.

1 Introduction

1.1 *Salmonella* Typhimurium pathogenicity

Salmonella enterica serovar Typhimurium (generally referred to as *Salmonella* Typhimurium) is an important causal agent of human gastrointestinal (GI) tract infections (Kurtz et al., 2017) Numerous studies of *Salmonella* pathogenesis have provided remarkable insight into the essential role of type three secretion systems (T3SS) in successful colonization of eukaryotic tissues and bacterial dissemination (Haraga et al., 2008). *S.* Typhimurium expresses two different T3SS (described in sections bellow), one flagellar and two virulence-associated (injectisomes), the latter encoded within the *Salmonella* pathogenicity island 1 and 2, SPI-1 and SPI-2, respectively (Hansen-Wester and Hensel, 2001).

Salmonella infection starts with ingestion of bacteria in contaminated food or water, which allows the bacteria to enter and transit through the GI tract and transit through it until the small bowel. In this early phase of infection, *Salmonella* cells utilize the flagellar T3SS to get in close proximity to epithelial cells and initiate bacterial adhesion and invasion (Fig. 1A) (Stecher et al., 2005). Succeeding attachment, SPI-1 injectisome serves the injection of virulence proteins (effectors) responsible for triggering rearrangements in the cytoskeleton that result in the formation of membrane ruffles and engulfment of *Salmonella* cells (Fig 1B) (Fàbrega and Vila, 2013). The SPI-2 T3SS is activated inside the *Salmonella* containing vacuole (SCV) and mediates the translocation of effectors into the eukaryotic cytosol in order to promote intracellular survival and replication of *Salmonella* (Fig. 1C) (Fàbrega and Vila, 2013).

Besides its clinical relevance, *S.* Typhimurium serves as a model microorganism to study the molecular mechanisms of host-microorganism interactions and colonization of eukaryotic tissues. Moreover, both *Salmonella* T3SS, the flagellar and the virulence-associated, represent the archetype of this secretion system as they were the first to be visualized by electron microscopy and are so far, the best characterized ones (Galán and Iii, 1989; Kubori et al., 1988).

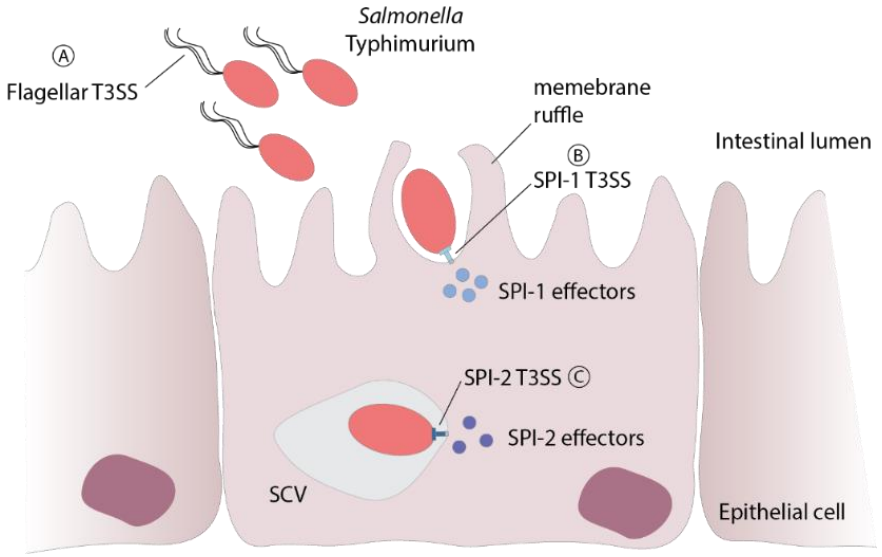

Fig. 1 Model of invasion of epithelial cells by *Salmonella* Typhimurium[1].
A. Once in the intestinal lumen *S.* Typhimurium uses the flagellar T3SS to approach epithelial cells and initiate adhesion. **B.** Subsequently, the SPI-1 injectisome enables injection of effector proteins into the host cell cytoplasm to induce formation of membrane ruffles and internalization of bacterial cells. **C.** The SPI-2 T3SS is activated inside the *Salmonella* containing vacuole (SCV) to translocate effectors into the eukaryotic cytoplasm and promote bacterial survival.

1.2 Structural organization of the bacterial T3SS

Secretion systems are complex machineries utilized by bacteria to transport a varied number of substrates such as proteins, nucleic acids and small molecules (Christie, 2019). So far, nine secretion systems have been discovered, being the T3SS one of the most investigated, owing to its medical and economical importance as T3SSs are found in many human, animal and plant pathogens (Buttner, 2012). As mentioned before, the T3SS is employed by two different molecular machineries: the flagellum and the virulence-associated injectisome. The first is a motility device used in chemotaxis, while the second is a specialised virulence determinant that facilitates translocation of virulence proteins from the bacterial cytoplasm to the eukaryotic cytosol (Diepold and Wagner, 2014).

Flagellar and virulence-associated T3SS have a common evolutionary origin and share general structural organization: both contain a core structure consisting of ring structures inserted in the inner (IM) and outer (OM) membranes connected by a periplasmic inner rod. The IM substructure is associated with the export apparatus, which is connected to the cytoplasmic components (Abby and Rocha, 2012; Gophna et al., 2003). This core structure is termed basal body in the

[1] Fig. 1 has been published in Microbiol. Mol. Biol. Rev. by Buttner 2012, and modified for its use in this thesis.

flagellum and needle complex (NC) in the injectisome, and it is connected to an extracellular hook/flagellin filament or the needle filament, respectively (Buttner, 2012). The structural organization of the virulence-associated T3SS will be thoroughly described in the following subsections as this study focuses on the *S.* Typhimurium injectisome encoded within the SPI-1. Note the name of individual components is given in agreement to the unified secretion and cellular translocation (Sct) nomenclature (Hueck, 1998; Wagner and Diepold, 2020). The injectisome consists of more than 20 proteins organized in four main substructures: i) the bacterial envelope-spanning base that harbors the export apparatus and encloses the secretion conduit, ii) the cytoplasmic sorting platform, iii) the hollow extracellular needle filament connected to the base through the periplasmic inner rod and iv) the needle tip and the translocation pore inserted in the host cell membrane (Fig. 2) (Wagner et al., 2018).

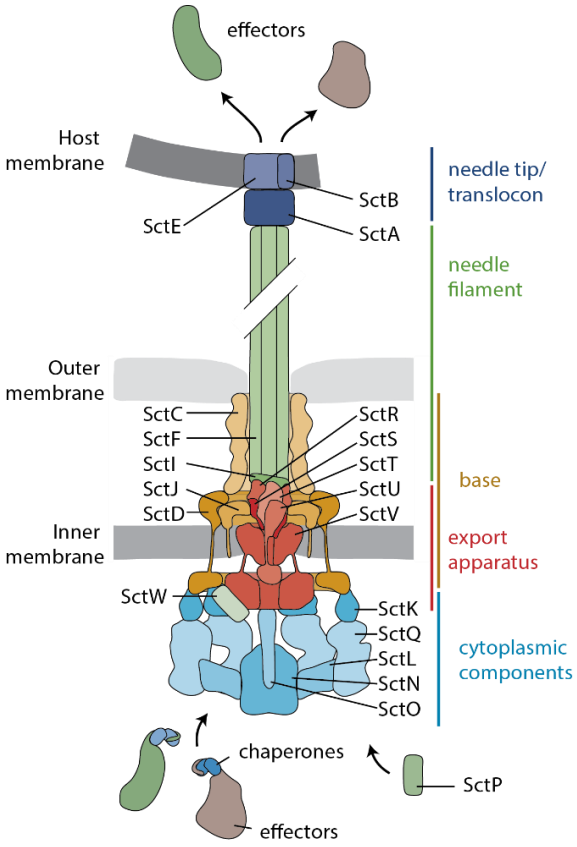

Fig. 2 Structure of the virulence-associated T3SS[2].
Simplified cartoon of the virulence associated-T3SS structure. The name of each component is given in accordance to the Sct unified nomenclature. The four main substructures are indicated: cytoplasmic components, base, needle filament and needle tip/translocation pore.

[2] Fig. 2 has been published in FEMS Microbiol. Lett. by Wagner et al., 2018, and adapted for its use in this thesis.

1.2.1 Base and export apparatus

The injectisome base is an array of membrane-embedded ring structures that anchors the T3SS to the bacterial envelope and consists of a single OM ring (SctC) and a set of two concentric rings inserted into the IM (SctD and SctJ), with a stoichiometry of 15-16:24:24, respectively (Schraidt et al., 2010). The OM ring structure is made up of 15-16 monomers of SctC, a member of the secretin protein family, also present in filamentous phage, type IV pili and T2SS (Deng et al., 2017). Cryo-EM analysis of the injectisome secretin provided remarkable insight into SctC structure organization, evincing three N- terminal domains (N0, N1, and N3) that extend deep into the periplasmic space and a C-terminal region that encompasses both the secretin domain and the S-domain (Worrall et al., 2016). A specialized lipoprotein named pilotin interacts with the S-domain in order to direct the secretin to the OM and facilitate its assembly (Silva et al., 2020). The central secretin domain is a highly conserved double layered β-barrel, with the outer β-sheet constituting the outer wall and the inner β-sheet supporting the outer wall and forming the periplasmic gate (Hu et al., 2018; Worrall et al., 2016). The N3 domain is contiguous to the inner β-barrel and is essential for oligomerization of SctC and undergoes discrete conformational changes during the assembly of the needle filament (Hu et al., 2018; Worrall et al., 2016). The N0 and N1 domains belong to the family of small α/β motifs coined ring-building motifs (RBMs) (Spreter et al., 2009).

Twenty four copies of SctD form the outer IM ring, which is connected to the OM secretin structure via the interaction of the C-terminal D4 domain of SctC monomers with the N0 domain of SctC monomers, an interaction that stabilizes the whole base structure (Schraidt et al., 2010). The crystal structure of SctD revealed a cytoplasmic D1 domain within the N-terminal region, a transmembrane segment and a periplasmic region with three RBMs (D2, D3 and D4) in the protein C-terminal portion (Spreter et al., 2009). The inner IM SctJ ring displays a 24-fold symmetry and surrounds the export apparatus (Worrall et al., 2016). SctJ is a periplasmic lipoprotein which is structurally organized into a transmembrane segment in the C-terminus, followed by two N-terminal domains D1 and D2 that traverse the periplasm (Lunelli et al., 2020; Schraidt et al., 2010).

Discrete mutations in the periplasmic domains of SctJ have a selective negative effect on secretion functionality but do not affect SctJ assembly (Butan et al., 2019). Apart from scaffolding assembly of the export apparatus, SctJ presumably plays an active role in secretion by inducing conformational changes in the export apparatus to prime its secretion function (Butan et al., 2019).

A structural analysis of the injectisomes from *S.* Typhimurium and *S. flexneri* revealed a varying 15-16-fold symmetry in the OM secretin ring (Hu et al., 2019; Lunelli et al., 2020). These studies elucidated the elaborate solution for the mismatch in the 15:24:24 stoichiometry of the IM and OM rings. The secreting ring formed by 15 SctC subunits recruits an extra SctC monomer containing only the N1 and N0 domains, to form a hexadecameric ring and to complete a symmetric interface with the outer IM ring SctD, consisting of a repeating eightfold interface of one SctC and two SctD subunits (Hu et al., 2019; Lunelli et al., 2020).

The export apparatus is a funnel-shaped multimeric complex composed of five proteins: SctR, SctS, SscT, SctU and SctV, which are the most conserved components in flagellar and virulence-associated T3SSs, and essential for secretion as the export apparatus forms the entrance of the export channel for secreted proteins (Wagner et al., 2010). In initial stages, the NC base is suggested to be impermeable to substrates due to the closed conformation of the export apparatus (Kuhlen et al., 2018, 2020). Although the five export apparatus components were predicted to be membrane-embedded proteins, recent cryo-EM studies demonstrated its actual extramembrane location within the periplasmic space at the core of the NC base (Butan et al., 2019; Kuhlen et al., 2018; Worrall et al., 2016). Interestingly, membrane remodeling and thinning was observed in the area surrounding the assembled export apparatus, leading to the proposition that the significantly decreased thickness permits the export apparatus tip to entirely span the membrane and consequently facilitates the passage of secreted substrates in a type 3-dependent manner across the IM (Butan et al., 2019).

The C-terminal domain of SctV ($SctV_C$), the major export apparatus component, forms a nonameric ring located directly under the export apparatus and above

the sorting platform, and it has recently been proposed to direct secreted proteins to the entrance of the export apparatus conduit (Abrusci et al., 2013; Butan et al., 2019). SctU possesses two main domains connected by a flexible linker: the N-terminus ($SctU_N$) contains four transmembrane domains that form two hairpins connected by a loop ($SctU_L$), and the large cytoplasmic C-terminal domain ($SctU_C$), which undergoes autocleavage in the conserved NPTH motif, producing two subdomains: $SctU_{CN}$ and $SctU_{CC}$. This cleavage event is thought to be related to secretion specificity switching and, therefore, SctU was coined “switch protein” (Lavander et al., 2002; Monjarás Feria et al., 2015; Sorg et al., 2007; Zarivach et al., 2008). The three minor export apparatus proteins SctR, SctS and SctT in conjunction with SctU form a helical complex in the IM termed the export gate. Prior to activation of type 3 secretion, this complex adopts a closed conformation gating the entrance of the secretion conduit (Kuhlen et al., 2018, 2020). Three identified restricting points in the export gate contribute to the complex closure: a methionine loop in SctR, a large hydrophobic insertion in SctT and a molecular latch in SctS. $SctU_N$, $SctU_L$ and $SctU_{CN}$ are instead thought to facilitate opening of the export gate (Kuhlen et al., 2018, 2020). The signal that initiates secretion triggers conformational rearrangements in the SctRSTU complex that open the export gate and allow passage of substrates and assembly of the inner rod on top of the export apparatus, giving in this way continuity to the secretion channel and providing the foundation for needle assembly (Dietsche et al., 2016; Kuhlen et al., 2018, 2020).

1.2.2 Cytoplasmic components and chaperones

Five cytoplasmic components of the T3SS, namely SctK, SctQ, SctL, SctN and SctO, form a protein complex located just beneath the IM rings and the export apparatus (Fig. 2) (Hu et al., 2015, 2017). The T3SS-associated ATPase SctN is positively regulated by SctO and is involved in recognition and dissociation of chaperone-effector complexes, and the partial unfolding of effectors prior their secretion (Akeda and Galán, 2005; Romo-Castillo et al., 2014). Structural characterization of the cytoplasmic complex revealed a cage-like organization

with a SctN hexamer placed in the center and aligned with the central channel of SctV, thus highlighting the essential function of both SctN and SctV in facilitating substrates secretion (Hu et al., 2015, 2017). SctK, SctQ and SctL constitute the so-called sorting platform, a cytosolic complex that contributes to secretion hierarchy by recruiting and sorting out substrates (either free or in complex with their cognate chaperone) in a precise order (Lara-Tejero et al., 2011; Hu et al., 2015). The cytosolic components do not form a static structure in the cytoplasmic side of the injectisome, rather a dynamic and adaptive complex that fluctuates between a free state in the bacterial cytoplasm and an IM-bound state in response to environmental conditions that activate secretion of substrates (Fig. 3) (Diepold et al., 2017).

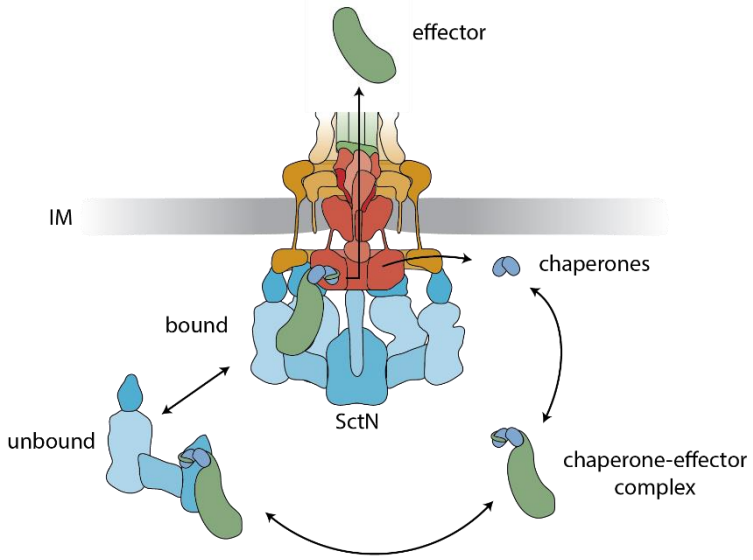

Fig. 3 Schematic representation of cytoplasmic components in their unbound and inner membrane-bound state[3].
Unbound cytoplasmic components form subcomplexes and associate with type 3 secretion substrates free or in complex with their cognate chaperone, as exemplified here. These complexes are recruited to the cytoplasmic face of the injectisome where chaperone-effector complexes are recognized by the major export apparatus SctV. Subsequently the ATPase SctN dissociates the effector protein from its chaperone, the first gets secreted into the culture supernatant in a partially unfolded conformation, while the latter is recycled to engage in the next cycle of secretion.

Secretion of substrates in type 3-dependent fashion is facilitated by multifunctional small cytoplasmic chaperones, which, apart from facilitating recruitment of substrates to the secretion machinery, also prevent degradation

[3] Fig. 3 has been published in FEMS Microbiol. Lett. by Wagner et al., 2018, and adapted for its use in this thesis.

and premature polymerization of their cognate substrate in the bacterial cytoplasm (Buttner, 2012; Creasey et al., 2003; Darwin and Miller, 2000). T3SS chaperones interact with specific regions within their substrates called chaperone binding domains (CBDs), and are classified according to their substrate specificity. Class I chaperones are dedicated to effector proteins and, in turn, divided into subcategories IA and IB, class II chaperones aid secretion of translocators and class III chaperones bind subunits of extracellular appendages like the needle and the flagellin filament (Cornelis, 2006; Izoré et al., 2011; Parsot et al., 2003). Class IA chaperones have a unique substrate (monocargo), while class IB bind to different effectors (multicargo), but both classes exhibit a conserved α/β fold and form homo- or heterodimers, around which the CBDs of cognate effectors are thought to wrap around (Fig. 1) (Birtalan et al., 2002; Birtalan and Ghosh, 2001). Chaperones of hydrophobic translocators are proposed to counteract the toxicity attributed to their cargo, and typically contain tandem tetratricopeptide repeats (TPRs) involved in protein-protein interactions (Job et al., 2010; Pallen et al., 2003).

1.2.3 Inner rod and needle

The extracellular portion of the injectisome is a hollow needle composed of hundreds of SctF copies polymerized in a right-handed helical structure with approximately eleven subunits per two turn (Demers et al., 2013; Loquet et al., 2012). Analysis of SctF atomic structure revealed a helical hairpin motif with the extended N-terminus located in the external surface of the needle and the conserved C-terminal domain facing the lumen (Loquet et al., 2012). The length of the needle varies among bacterial species and is strictly regulated to assure the injectisome functionality (Journet et al., 2003; Monjarás Feria et al., 2015; Tamano et al., 2002). Following their secretion, SctF monomers assemble the needle within the lumen of the OM secretin to build, in conjunction with the inner rod, a continuous secretion conduit that mediates the passage of effectors from the bacterial cytoplasm to the extracellular environment (Marlovits et al., 2004, 2006). The periplasmic inner rod SctI anchors the needle to the NC base by

connecting the helical assembly of the export apparatus to the helical needle filament (Dietsche et al., 2016; Kuhlen et al., 2018). Little is known about the exact stoichiometry and structure of the inner rod; however, each injectisome is proposed to solely comprise 6 subunits of SctI. Based on sequence conservation with the needle protein, it is likely that SctI assembles a helical structure in order to prime the helical assembly of the needle (Zilkenat et al., 2016). In addition to its structural function, the needle is presumably implicated in the mechanism of cell contact signal transmission and the consequent reprogramming of the secretion machinery (Explained in detail in the following sections) (Guo et al., 2019). Likewise, apart from laying the foundation for assembly of the needle structure, the function of the inner rod protein SctI has been expanded to the regulatory processes such as needle length control and secretion specificity switch (Cherradi et al., 2013; El Hajjami et al., 2018; Lefebre and Gálan, 2014; Marlovits et al., 2006).

1.2.4 Needle tip and translocation pore

Most injectisomes of animal pathogens have a needle tip complex assembled by 5 subunits of the hydrophilic translocator SctA at the distal end of the needle filament (Gaytán et al., 2016). Interestingly, the exception to this rule is the T3SS from enteropathogenic *E. coli* (EPEC), which has a flexible EspA filament that extends the needle and can reach up to 900 nm in length (Gaytán et al., 2016). Although the EspA filament serves to bridge the distance between EPEC and its target cells by traversing the thick mucus layer that covers the enterocytes, it still conserves the scaffolding function for assembly of the translocation pore attributed to the regular tip proteins (Marenne et al., 2003; Warawa et al., 1999).

Injection of effector proteins into the host cell cytosol is mediated by the two hydrophobic translocators, SctB and SctE, that hetero-oligomerize and assemble a protein complex in the eukaryotic membrane termed translocation pore (Ide et al., 2001; Lunelli et al., 2009). SctB and SctE are predicted to have two and one transmembrane segments, respectively, which are important for their localization in the membrane (Dasanayake et al., 2012; Marenne et al., 2003).

1.3 Assembly of the needle filament, role of cap proteins

In the flagellar T3SS assembly of the helical flagellin filament FliC is facilitated by an essential structure made up of five subunits of the cap protein FliD. Strains lacking *fliD* are reported to be deficient in filament formation and therefore non-motile (Yonekura et al., 2000; Yonekura et al., 2003). The cap complex attaches to the growing end of the flagellin filament where it promotes polymerization of FliC subunits using a rotational mechanism (Erhardt et al., 2010; Yonekura et al., 2000). In T3SS injectisomes, the pentameric needle tip complex was thought to cap the needle filament and promote its assembly. However, this notion is only supported by localization and structural commonalities between the cap and the tip complex (Deane et al., 2006; Mueller et al., 2016; Yonekura et al., 2003). In 2018, Kato and colleagues characterized the T3SS component OrgC (for oxygen regulated gene C) encoded within the *S.* Typhimurium SPI-1, and reported that it represents an early substrate and functions as cap-like protein responsible for promoting assembly of the needle filament and its condition of early substrate (Kato et al., 2018). The structural organization of OrgC shows that, despite of the low sequence conservation, its central core resembles the D1 domain of FliD, suggesting similarities in the molecular mechanism by which OrgC and FliD aid polymerization of needle and flagellin subunits, respectively (Al-Otaibi et al., 2020; Kato et al., 2018).

In sharp contrast to the flagellar cap complex, OrgC is not indispensable for needle elongation but solely required to nucleate its initial assembly within the secretin lumen, after which OrgC is no longer associated to the needle and most likely secreted to the extracellular environment (Kato et al., 2018). Nevertheless, the relevance of OrgC function is highlighted by the decreased number of fully assembled needle filaments and reduced secretion of middle and late substrates observed in bacterial strains devoid of this component.

1.4 Assembly pathways of the injectisome

Due to the modular design of the T3SS injectisome, its assembly proceeds in a coordinated stepwise fashion that consist of two main steps: one dependent on the general secretory pathway (Sec-dependent), which is used to insert components of the base and the export apparatus into the bacterial cell envelope, and one T3SS-dependent (Tsirigotaki et al., 2017). In an attempt to explain injectisome assembly pathway, two models were proposed: the inside-out model and the outside-in model (Diepold and Wagner, 2014).

Assembly of the injectisome is nucleated by the export apparatus, formation of this protein complex starts with insertion of a SctR pentamer into the IM and further recruitment of SctT, SctS and SctU to form the helical assembly of the export gate. This in turn recruits SctV and presumably contributes to lift up the export apparatus from the membrane towards the periplasmic space, reaching in this way its ultimate extramembrane location within the injectisome base (Fig. 4A) (Dietsche et al., 2016; Kuhlen et al., 2018; Wagner et al., 2010).

According to the inside-out model, a completely assembled export apparatus recruits SctJ and SctD to form the IM rings, and subsequent recruitment of the cytoplasmic components to this subcomplex secretion of early substrates. Once assembled, the inner rod SctI locally activates peptidoglycan lytic enzymes residing in the periplasm to make a hole above the IM subcomplex, where 15 copies of SctC assemble around the SctR pentamer with the aid of the pilotin. Subsequently, an additional SctC subunit (encompassing only the N1 and N0 domains) is recruited to complete the symmetric interface with the outer IM ring SctD. Assembly of the injectisome terminates with formation of the needle filament (Fig. 4B) (Hu et al., 2018; Hu et al., 2020).

In contrast, the outside-in model argues for an earlier action of the peptidoglycan lytic enzymes to mediate, in conjunction with the pilotin, assembly of the secretin pore in the OM, which recruits SctD to form the outer IM ring. In an independent assembly step, the export apparatus recruits SctJ to form a subcomplex that is recruited to secretin pore, and SctD to complete the base. Association of the cytoplasmic components to the base activates type 3 secretion of early substrates

that assemble the inner rod and needle filament within the secretin, finalizing assembly of the injectisome (Fig. 4C) (Diepold et al., 2010; Sukhan et al., 2001).

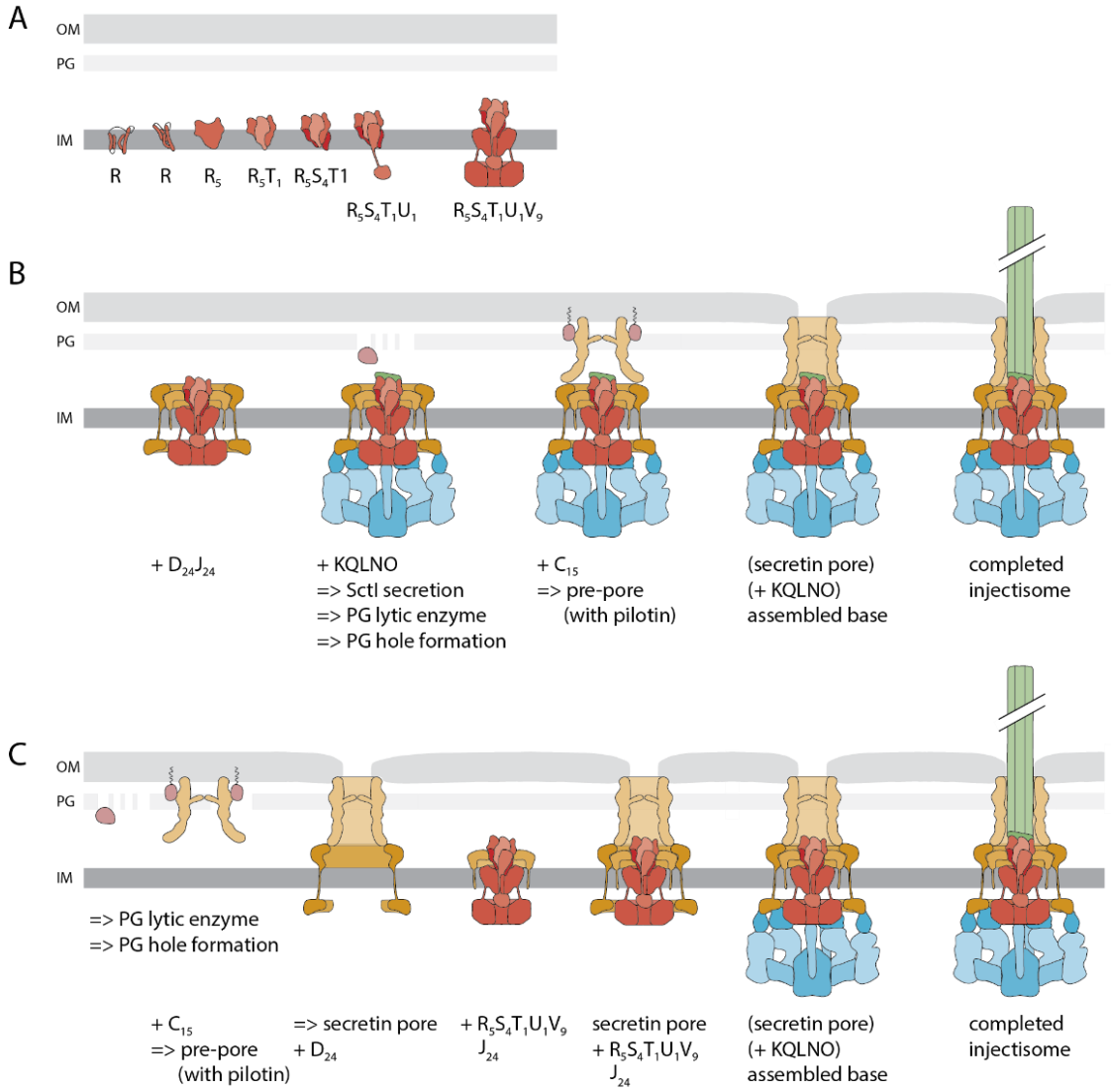

Fig. 4 Assembly pathways of the injectisome[4].
Note the name of individual injectisome components is given according to the unified nomenclature but omitting the Sct prefix. **A.** Simplified representation of the stepwise assembly of the export apparatus. Assembly initiates with insertion of five SctR into the IM, where they adopt the appropriate conformation for helical assembly. Then, one SctT is recruited to the SpaR pentamer to stabilize it. Four SctS associate with the StR_5SctT_1 complex to form a helical assembly. Recruitment of one SctU and nine SctV completes the export apparatus, which raises from the IM towards the periplasm to reach its ultimate extramembrane location. **B.** Inside-out assembly pathway. In this model the fully assembled export apparatus (final structure in A) recruits 24 SctD and 24 SctJ that form the IM rings around it. Then, the cytoplasmic components associate with the IM subcomplex to initiate type 3-dependent secretion of early substrates, which locally activate peptidoglycan (PG) lytic enzymes to enable assembly of 15 SctC in the OM, aided by the pilotin, to form a pre-pore above the IM subcomplex. Completion of the secretin pore along with assembly of the needle filament completes assembly of the injectisome **C.** Outside-in assembly pathway. PG lytic enzymes locally make a hole in the PG layer and along with the pilotin, facilitate assembly of 15 SctC into an OM pre-pore that recruits 24 SctD to assemble the outer IM ring. In an independent assembly step, the export apparatus recruits 24 SctJ to assemble the inner IM ring. This IM subcomplex is then incorporated in $SctC_{15}SctD_{24}$. Further assembly of the injectisome proceeds as descried in B.

[4] Fig. 4 has been published in FEMS Microbiol. Lett. by Wagner et al., 2018, and adapted for its use in this thesis.

1.5 Secretion hierarchy and specificity switching

With the purpose of assuring the full assembly and functionality of the injectisome, a strict hierarchy controls the ordered secretion of proteins through the T3SS. These proteins, also called substrates, are classified in three different categories, namely early, middle and late, in accordance to the order in which they are transported. Substrates transported through the T3SS contain a secretion signal (20-30 amino acids in length) commonly contained within their N-terminal domain (Michiels and Cornelis, 1991; Sory et al., 1995). Despite the low sequence conservation, T3SS secretion signals share amino acid composition and the lack of a defined secondary structure. This disordered character provides the structural flexibility that presumably facilitates recognition of type 3 secretion substrates by the secretion machinery (Arnold et al., 2009).

Recruitment of the cytoplasmic components to the NC base (Fig. 5A) enables the T3SS to secrete the three early substrates: the inner rod (SctI), the needle (SctF) and the needle length regulator (SctP) (Fig. 5B). In the case of *S.* Typhimurium, a fourth early substrate, the cap-like protein OrgC, is secreted along with SctF subunits to nucleate their initial polymerization (Storz et al., 2018). Once the needle filament is complete and reaches its predetermined length, the secretion machinery is reprogrammed for the first time and its secretion specificity switches from early to middle substrates, i.e. the translocators (Fig. 5C). When the needle tip (SctA) and the translocation pore (SctB and SctE) are assembled, a second reprogramming event in the secretion machinery takes place triggering a second switch in secretion specificity from middle to late substrates, the effectors, which now can be efficiently injected into the host cell cytoplasm (Fig. 5D).

The following two subsections will thoroughly describe the molecular basis of both reprogramming events, switch 1 and 2, that the secretion machinery undergoes during assembly of the injectisome.

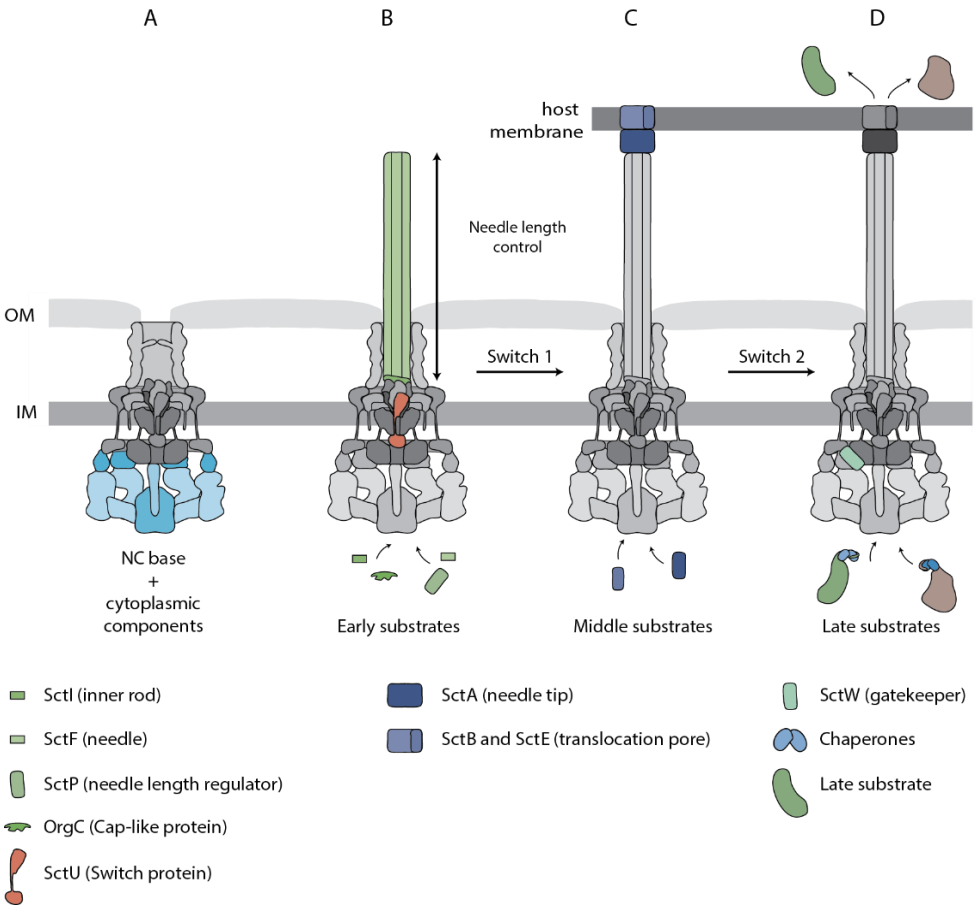

Fig. 5 Simplified illustration of the type 3 secretion hierarchy.
A. Recruitment of the cytoplasmic components to the NC base initiates the hierarchical secretion of early, middle and late substrates in type 3-dependent manner. **B.** Secreted early substrates SctI and SctF assemble the inner rod and needle, respectively. The cap-like protein OrgC is secreted along with SctF and facilitates initial assembly of the needle, the polymerization of which proceeds until it reaches its final length, a process controlled by SctP. Subsequently, the first switch in secretion specificity is triggered and middle substrates or translocators are now secreted. **C.** When the translocation pore is inserted in the host cell membrane, a second switch in secretion specificity is induced to secrete late substrates or effectors. **D.** Finally, late substrates are effectively injected directly into the host cell cytoplasm.

1.5.1 Secretion specificity switch 1

The first switch of secretion specificity happens only after the polymerization of a needle filament with appropriate length is completed, providing in this way, the foundation for needle tip and translocation pore assembly. Regulation of the secretion specificity switch 1 is attributed to the export apparatus component SctU. As afore-mentioned, this protein undergoes autocleavage in the highly conserved NPTH motif contained within its cytoplasmic C-terminal domain, $SctU_C$ (Deane et al., 2008; Monjarás Feria et al., 2015; Zarivach et al., 2008). Autocleavage in $SctU_C$ was long believed to be the trigger signal for specificity switching, however, study of the autocleavage kinetics debunked this

supposition, as it was discovered that the autoproteolytic processing of SctU occurs spontaneously and shortly after the protein is produced and the C-terminal domain is folded (Monjarás Feria et al., 2015). Hence, it was clarified that it is not the autocleavage *per se* that induces the switch in secretion specificity but rather the conformational flexibility conferred by it (Monjarás Feria et al., 2015). Genetic analysis of *sctP* deletion mutants revealed defects in secretion of middle and late substrates ranging from slight reduction to complete abrogation. Those observations led to the assumption that besides playing a central role in needle length control, SctP actively contributes to the efficient effectuation of secretion specificity switch (Journet et al., 2003; Kubori et al., 2000; Moriya et al., 2006). Indeed, the region of SctP responsible for this function is suggested to lie within the C-terminal domain and is commonly referred to as T3S4 domain (for type three secretion substrate specificity switching) (Agrain et al., 2005; Minamino et al., 2004). Consequently, needle length control and secretion specificity switch were spatially and temporally linked, notion supported by the direct interaction between $SctP_C$ and $SctU_C$, detected in flagellar and some virulence-associated T3SS (Botteaux et al., 2008; Lorenz and Büttner, 2011; Minamino et al., 1999). Although the biological relevance of the $SctP_C$-$SctU_C$ interaction is yet to be demonstrated *in vivo*, it is proposed to induce conformational changes in these domains that trigger the transition of the machinery into the mode of secretion of middle substrates (Lorenz and Büttner, 2011; Zarivach et al., 2008).

1.5.2 Secretion specificity switch 2

The secretion machinery is required to hold its specificity for middle substrates until the translocation pore is inserted into the host cell membrane and switch to late substrates as soon as the cell sensing signal is conveyed to the cytoplasmic side of the injectisome. This strict control of secretion specificity enables the efficient translocation of effector proteins directly into the eukaryotic cytosol. Reduced secretion of middle substrates and hyper-secretion of effectors are commonalities of *sctW* deletion mutants. Consequently, the bifunctional SctW protein was coined “gatekeeper”, which is a selective regulator of the second

specificity switch that prevents premature secretion of effectors and promotes secretion of translocators (Cheng et al., 2001; Deng et al., 2004; Yu et al., 2010, 2018). Although the detailed molecular mechanism of the secretion specificity switch 2 remains unclear, it is proposed that SctW binds to $SctV_C$, to facilitate recognition of translocator-chaperone complexes and physically block the binding of effectors (Gaytán et al., 2018; Portaliou et al., 2017; Yu et al., 2018). Once the signal of cell contact is transmitted to the secretion machinery, SctW disengages from $SctV_C$ allowing the late substrates to be secreted after being dissociated from their cognate chaperones by the ATPase SctN (Gaytán et al., 2018; Yu et al., 2018). After its release, SctW is secreted to the extracellular environment, degraded in the bacterial cytoplasm or recycled for another round of hierarchical secretion in newly assembled injectisomes (Cheng et al., 2001; Yu et al., 2010). Although numerous studies have shed light on the complex mechanism underlying the second specificity switch, and revealed the active role of further T3SS components, many aspects of this regulatory process remain elusive.

1.6 Needle length control

One of the most distinctive features of both flagellar and virulence-associated T3SSs is the rigorous control of the length of their extracellular appendages to guarantee the T3SS functionality, either motility or injection of virulence proteins (Hirano et al., 2005; Journet et al., 2003; Tamano et al., 2002). Different bacterial species have needles of varying length and, based on experimental evidence, it was suggested that needle length evolved in an attempt to match the size of specific structures at the bacterial and host cell surface (Mota et al., 2005). This prompted bacteria to develop sophisticated regulatory mechanisms to strictly regulate needle length. In this section, the models proposed for needle length control in virulence-associated T3SS will be described in detail.

1.6.1 Ruler model

The ruler model was postulated to clarify how needle length is controlled in the injectisome of *Yersinia enterocolitica* and originated from the observed linear correlation between the size of the SctP protein and the length of the needle filament. Varying the size of SctP with insertions or deletions, indeed, results in long and short needles, respectively, leading to the suggestion that SctP functions as a molecular ruler (Journet et al., 2003). In this model, SctI and SctF subunits are secreted along with SctP, which measures the length of the needle while traveling through the secretion channel: SctP interacts with the tip of the needle via its N terminus and is pulled through as the needle grows, bringing the C-terminal domain close to the export apparatus (Fig. 6A). Once SctP is completely extended and the needle reaches its predetermined length, further polymerization of SctF subunits is interrupted and switch of secretion specificity is triggered by the productive interaction of $SctP_C$ with the switch protein, $SctU_C$ (Fig. 6B). Specificity switching reprograms the secretion machinery and triggers secretion of intermediate and late substrates (Fig. 6C).

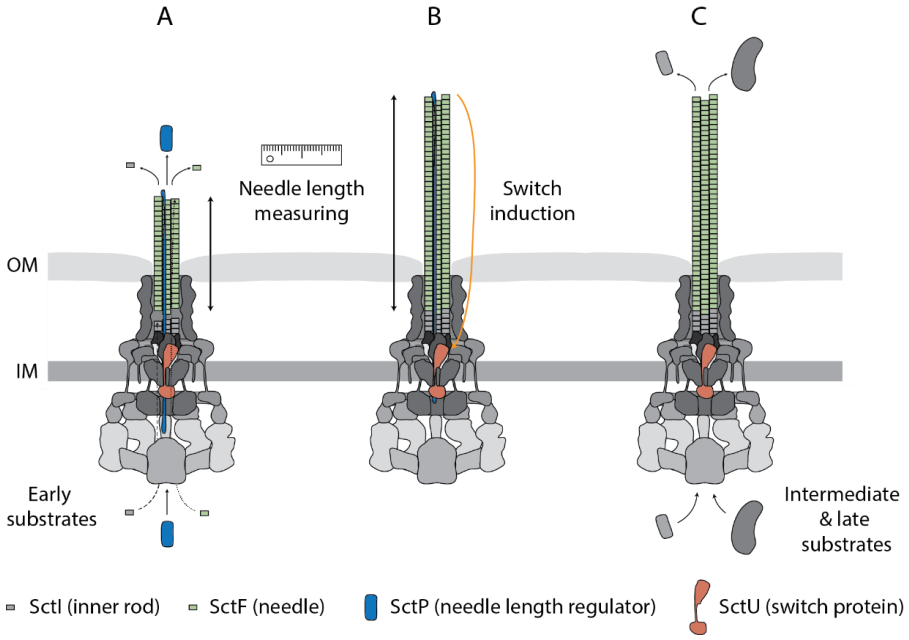

Fig. 6 Model of needle length control by the molecular ruler mechanism.
A. After being secreted, subunits of SctI and SctF polymerize into the inner rod and the needle, respectively. SctP travels through the secretion channel and measures the needle length. As the filament grows, SctP is pulled through, bringing $SctP_C$ close to the export apparatus. **B.** When SctP is fully extended and the needle reaches its predetermined length, further polymerization of SctF subunits is stopped and secretion specificity switching is triggered by the interaction of $SctP_C$ and $SctU_C$. **C.** Subsequently, secretion of intermediate and late substrates takes place.

1.6.2 Timer model

The timer model was postulated in an attempt to explain the structural differences observed in cryo-EM-analysed NCs isolated from wild type and Δ*sctP S.* Typhimurium strains (Marlovits et al., 2006). Deletion of *sctP* resulted in loss of two structures within the base: the socket and the inner rod. This led to the assumption that SctP plays a critical role in stabilizing the proper conformation of the socket, which in turn allows the inner rod to assemble (Marlovits et al., 2006). Additionally, it was showed that the concentration of the SctI and SctF subunits influenced needle length, as overexpression of SctI resulted in short needles and vice versa, overproduction of SctF monomers gave rise to long needles. Altogether, these results provided the foundation for the proposal of the timer model, which years later was consolidated by Lefebre and colleagues. These authors conducted an exhaustive alanine-scanning mutagenesis of the entire SctI length, and identified several residues that contributed to needle length control and regulation of secretion hierarchy (Lefebre and Gálan, 2014).

According to this model, both structures the inner rod (SctI) and the needle filament (SctF) assemble simultaneously, and the role of the protein SctP is restricted to facilitating SctI assembly (Fig. 7A). The duration of inner rod assembly determines the time span in which the SctF subunits are allowed to polymerize into the filament, thereby dictating needle length. Termination of the assembly of the inner rod halts further elongation of the needle and leads to conformational changes in the cytoplasmic side of the NC base that switch the secretion specificity, triggering type 3-dependent secretion of middle and late substrates (Fig. 7B).

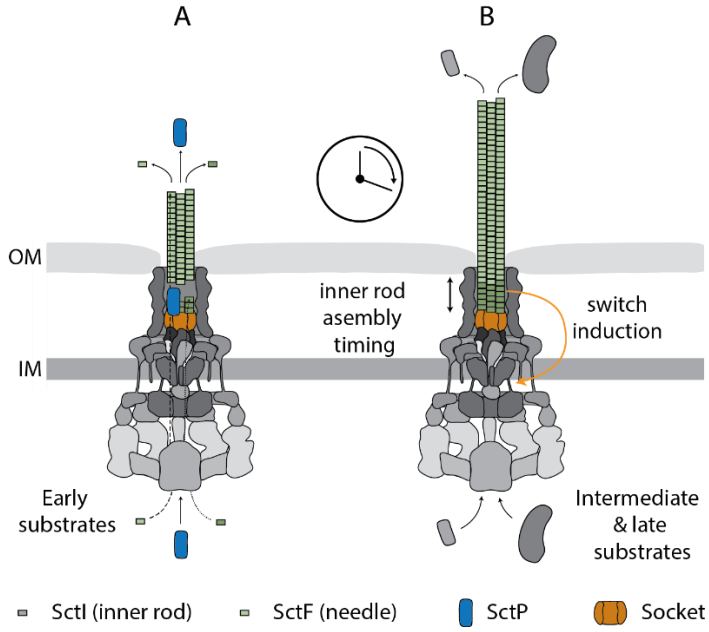

Fig. 7 Model of needle length control by the timer mechanism.
A. The socket-like structure is stabilized by SctP. Assembly of the inner rod but not the needle filament is assisted by SctP, both structures form simultaneously. **B.** Completion of the inner rod stops needle elongation, determining in this was its length. At the same time, secretion specify switching is effectuated as a result of conformational changes in the cytoplasmic side of the NC. Then intermediate and late substrates are secreted.

1.7 Host cell sensing

Secretion of effector proteins activates upon direct contact with the host cell, event interpreted as the activating signal conveyed through the injectisome to the cytoplasmic side of the NC base in order to reprogram the secretion machinery and initiate type 3 secretion of late substrates. Up until now, numerous chemical signals that activate type 3 secretion have been reported, such as calcium, pH, amino acids and cholesterol. However, the precise structural components of the T3SS involved in the detection of such signal and the molecular basis of its transmission have yet to be clarified (Diepold et al., 2017; Gaytán et al., 2018; Torruellas et al., 2005; Yu et al., 2010). Noteworthy progress in this regard has been achieved with the emerging structural and functional characterization of the translocation pore, the needle tip and the needle filament (Guo et al., 2019; Roehrich et al., 2013; Russo et al., 2019). The translocation pore undergoes conformational changes within minutes after the early contact with the eukaryotic cell. Such rearrangements are presumably the early trigger of the signalling cascade that ultimately activates secretion of effectors (Russo et al., 2019). The

needle tip is implicated in host cell sensing as SctA variants harbouring point mutations in the C- terminal domain are no longer responsive to the secretion activating signal (Roehrich et al., 2013). Likewise, the needle filament is suggested to play a key role in cell sensing and signalling as a number of SctF mutants are observed to restrict the secretion machinery specificity impeding its transition from early to middle substrates (Guo et al., 2019; Torruellas et al., 2005).

2. Aim of the study

In an attempt to improve the understanding of the molecular basis of needle length control and its relationship with substrate specificity switching, this study aims to create a genetic system that allows the synchronization of NC base assembly and type 3-dependent secretion. Such a system would be exploited to address the following questions:

1. What is the role of the inner rod assembly in needle length control and substrate specificity?

2. How is assembly of the inner rod promoted by SctP?

3. Material and methods

3.1 Chemicals and materials

All chemicals and materials used in this study were purchased from Sigma-Aldrich, AppliChem, ROTH, Merck, Merck Millipore, Beckman Coulter, Novagen, Thermo Pierce, Eppendorf, Anatrace, Promega, Bachem and Qiagen unless otherwise specified.

3.2 Bacterial strains and growth conditions

Salmonella Typhimurium strains used in this study are listed in Table 1. *S.* Typhimuriun strains were cultured with low aeration at 37°C in Luria Bertani (LB) broth supplemented with 0.3 M NaCl to induce expression of genes of SPI-1 (Monjarás Feria et al., 2015; Torres-Vargas et al., 2019; Kuhlen et al., 2020). While *E. coli* strains were cultured at 37°C in LB broth and used for plasmid DNA replication. As required, bacterial cultures were supplemented with tetracycline (12.5 µg/ml), streptomycin (50 µg/ml), chloramphenicol (10 µg/ml), ampicillin (100 µg/ml) or kanamycin (25 µg/ml).

Table 1. Bacterial strains

***Salmonella* strain**	**Genotype**	**Reference**
SB300	wild type (SL1344)	Kaniga et al., 1995
SB762	wild type (SL1344, flhD::tet)	Kaniga et al., 1995
SB1907	SpaP^{FLAG}, *flhD::tet*	Wagner et al., 2010
SB1909	SpaR^{FLAG}, *flhD::tet*	Wagner et al., 2010
SB2326	Δ*invJ*, *flhD::tet*	Monjarás Feria et al., 2015
MIB3340	SpaP$_{G2X}$^{FLAG}, *flhD::tet*	Dietsche et al., 2016
MIB3348	PrgJ$_{S2X}$, *flhD::tet*	Torres-Vargas et al., 2019
MIB3350	PrgJ$_{T5X}$, *flhD::tet*	Torres-Vargas et al., 2019
MIB3392	PrgJ$_{P8X}$, *flhD::tet*	Torres-Vargas et al., 2019
MIB3394	PrgJ$_{E9X}$, *flhD::tet*	Torres-Vargas et al., 2019
MIB3396	PrgJ$_{N10X}$, *flhD::tet*	Torres-Vargas et al., 2019

MIB4042	PrgJ$_{V12X}$, *flhD::tet*	Torres-Vargas et al., 2019
MIB4246	PrgJ$_{Q15X}$, *flhD::tet*	Torres-Vargas et al., 2019
MIB4044	PrgJ$_{N18X}$, *flhD::tet*	Torres-Vargas et al., 2019
MIB4046	PrgJ$_{S21X}$, *flhD::tet*	Torres-Vargas et al., 2019
MIB4048	PrgJ$_{T24X}$, *flhD::tet*	Torres-Vargas et al., 2019
MIB4050	PrgJ$_{S28X}$, *flhD::tet*	Torres-Vargas et al., 2019
MIB3855	PrgJ$_{L29X}$, *flhD::tet*	Torres-Vargas et al., 2019
MIB4052	PrgJ$_{L33X}$, *flhD::tet*	Torres-Vargas et al., 2019
MIB4054	PrgJ$_{Q35X}$, *flhD::tet*	Torres-Vargas et al., 2019
MIB4056	PrgJ$_{F37X}$, *flhD::tet*	Torres-Vargas et al., 2019
MIB4058	PrgJ$_{S40X}$, *flhD::tet*	Torres-Vargas et al., 2019
MIB4060	PrgJ$_{A43X}$, *flhD::tet*	Torres-Vargas et al., 2019
MIB4062	PrgJ$_{V46X}$, *flhD::tet*	Torres-Vargas et al., 2019
MIB4064	PrgJ$_{Q49X}$, *flhD::tet*	Torres-Vargas et al., 2019
MIB4066	PrgJ$_{T52X}$, *flhD::tet*	Torres-Vargas et al., 2019
MIB4068	PrgJ$_{I55X}$, *flhD::tet*	Torres-Vargas et al., 2019
MIB4070	PrgJ$_{D57X}$, *flhD::tet*	Torres-Vargas et al., 2019
MIB4072	PrgJ$_{L60X}$, *flhD::tet*	Torres-Vargas et al., 2019
MIB4074	PrgJ$_{D63X}$, *flhD::tet*	Torres-Vargas et al., 2019
MIB3731	PrgJ$_{L67X}$, *flhD::tet*	Torres-Vargas et al., 2019
MIB3732	PrgJ$_{S70X}$, *flhD::tet*	Torres-Vargas et al., 2019
MIB4076	PrgJ$_{Q71X}$, *flhD::tet*	Torres-Vargas et al., 2019
MIB3733	PrgJ$_{I74X}$, *flhD::tet*	Torres-Vargas et al., 2019
MIB3734	PrgJ$_{Y77X}$, *flhD::tet*	Torres-Vargas et al., 2019
MIB3735	PrgJ$_{L79X}$, *flhD::tet*	Torres-Vargas et al., 2019
MIB4078	PrgJ$_{Y80X}$, *flhD::tet*	Torres-Vargas et al., 2019
MIB4080	PrgJ$_{V81X}$, *flhD::tet*	Torres-Vargas et al., 2019
MIB3406	PrgJ$_{M83X}$, *flhD::tet*	Torres-Vargas et al., 2019
MIB4082	PrgJ$_{L87X}$, *flhD::tet*	Torres-Vargas et al., 2019
MIB4084	PrgJ$_{V92X}$, *flhD::tet*	Torres-Vargas et al., 2019
MIB3408	PrgJ$_{V95X}$, *flhD::tet*	Torres-Vargas et al., 2019
MIB3410	PrgJ$_{L98X}$, *flhD::tet*	Torres-Vargas et al., 2019

MIB3412	PrgJ$_{S101X}$, *flhD::tet*	Torres-Vargas et al., 2019
MIB3560	SpaP^{FLAG} PrgJ$_{S2X}$, *flhD::tet*	Torres-Vargas et al., 2019
MIB3562	SpaP^{FLAG} PrgJ$_{T5X}$, *flhD::tet*	Torres-Vargas et al., 2019
MIB3564	SpaP^{FLAG} PrgJ$_{P8X}$, *flhD::tet*	Torres-Vargas et al., 2019
MIB3566	SpaP^{FLAG} PrgJ$_{E9X}$, *flhD::tet*	Torres-Vargas et al., 2019
MIB3568	SpaP^{FLAG} PrgJ$_{N10X}$, *flhD::tet*	Torres-Vargas et al., 2019
MIB4086	SpaP^{FLAG} PrgJ$_{V12X}$, *flhD::tet*	Torres-Vargas et al., 2019
MIB3570	SpaP^{FLAG} PrgJ$_{Q15X}$, *flhD::tet*	Torres-Vargas et al., 2019
MIB4088	SpaP^{FLAG} PrgJ$_{N18X}$, *flhD::tet*	Torres-Vargas et al., 2019
MIB4090	SpaP^{FLAG} PrgJ$_{S21X}$, *flhD::tet*	Torres-Vargas et al., 2019
MIB4162	SpaP^{FLAG} PrgJ$_{T24X}$, *flhD::tet*	Torres-Vargas et al., 2019
MIB4164	SpaP^{FLAG} PrgJ$_{S28X}$, *flhD::tet*	Torres-Vargas et al., 2019
MIB3598	SpaP^{FLAG} PrgJ$_{L29X}$, *flhD::tet*	Torres-Vargas et al., 2019
MIB4166	SpaP^{FLAG} PrgJ$_{L33X}$, *flhD::tet*	Torres-Vargas et al., 2019
MIB4168	SpaP^{FLAG} PrgJ$_{Q35X}$, *flhD::tet*	Torres-Vargas et al., 2019
MIB4170	SpaP^{FLAG} PrgJ$_{F37X}$, *flhD::tet*	Torres-Vargas et al., 2019
MIB4172	SpaP^{FLAG} PrgJ$_{S40X}$, *flhD::tet*	Torres-Vargas et al., 2019
MIB4174	SpaP^{FLAG} PrgJ$_{A43X}$, *flhD::tet*	Torres-Vargas et al., 2019
MIB4176	SpaP^{FLAG} PrgJ$_{V46X}$, *flhD::tet*	Torres-Vargas et al., 2019
MIB4178	SpaP^{FLAG} PrgJ$_{Q49X}$, *flhD::tet*	Torres-Vargas et al., 2019
MIB4180	SpaP^{FLAG} PrgJ$_{T52X}$, *flhD::tet*	Torres-Vargas et al., 2019
MIB4182	SpaP^{FLAG} PrgJ$_{I55X}$, *flhD::tet*	Torres-Vargas et al., 2019
MIB4184	SpaP^{FLAG} PrgJ$_{D57X}$, *flhD::tet*	Torres-Vargas et al., 2019
MIB4186	SpaP^{FLAG} PrgJ$_{L60X}$, *flhD::tet*	Torres-Vargas et al., 2019
MIB4188	SpaP^{FLAG} PrgJ$_{D63X}$, *flhD::tet*	Torres-Vargas et al., 2019
MIB4248	SpaP^{FLAG} PrgJ$_{L67X}$, *flhD::tet*	Torres-Vargas et al., 2019
MIB4250	SpaP^{FLAG} PrgJ$_{S70X}$, *flhD::tet*	Torres-Vargas et al., 2019
MIB4190	SpaP^{FLAG} PrgJ$_{Q71X}$, *flhD::tet*	Torres-Vargas et al., 2019
MIB4272	SpaP^{FLAG} PrgJ$_{I74X}$, *flhD::tet*	Torres-Vargas et al., 2019
MIB4274	SpaP^{FLAG} PrgJ$_{Y77X}$, *flhD::tet*	Torres-Vargas et al., 2019
MIB4276	SpaP^{FLAG} PrgJ$_{L79X}$, *flhD::tet*	Torres-Vargas et al., 2019
MIB4192	SpaP^{FLAG} PrgJ$_{Y80X}$, *flhD::tet*	Torres-Vargas et al., 2019

MIB4194	SpaP^{FLAG} PrgJ$_{V81X}$, *flhD::tet*	Torres-Vargas et al., 2019
MIB3578	SpaP^{FLAG} PrgJ$_{M83X}$, *flhD::tet*	Torres-Vargas et al., 2019
MIB4196	SpaP^{FLAG} PrgJ$_{L87X}$, *flhD::tet*	Torres-Vargas et al., 2019
MIB4198	SpaP^{FLAG} PrgJ$_{V92X}$, *flhD::tet*	Torres-Vargas et al., 2019
MIB3580	SpaP^{FLAG} PrgJ$_{V95X}$, *flhD::tet*	Torres-Vargas et al., 2019
MIB3610	SpaP^{FLAG} PrgJ$_{L98X}$, *flhD::tet*	Torres-Vargas et al., 2019
MIB4244	SpaP^{FLAG} PrgJ$_{S101X}$, *flhD::tet*	Torres-Vargas et al., 2019
MIB4278	SpaR^{FLAG} PrgJ$_{S2X}$, *flhD::tet*	Torres-Vargas et al., 2019
MIB4280	SpaR^{FLAG} PrgJ$_{T5X}$, *flhD::tet*	Torres-Vargas et al.,2019
MIB4282	SpaR^{FLAG} PrgJ$_{P8X}$, *flhD::tet*	Torres-Vargas et al., 2019
MIB4284	SpaR^{FLAG} PrgJ$_{E9X}$, *flhD::tet*	Torres-Vargas et al., 2019
MIB4286	SpaR^{FLAG} PrgJ$_{N10X}$, *flhD::tet*	Torres-Vargas et al., 2019
MIB4200	SpaR^{FLAG} PrgJ$_{V12X}$, *flhD::tet*	Torres-Vargas et al., 2019
MIB4288	SpaR^{FLAG} PrgJ$_{Q15X}$, *flhD::tet*	Torres-Vargas et al., 2019
MIB4202	SpaR^{FLAG} PrgJ$_{N18X}$, *flhD::tet*	Torres-Vargas et al., 2019
MIB4204	SpaR^{FLAG} PrgJ$_{S21X}$, *flhD::tet*	Torres-Vargas et al., 2019
MIB4206	SpaR^{FLAG} PrgJ$_{T24X}$, *flhD::tet*	Torres-Vargas et al., 2019
MIB4208	SpaR^{FLAG} PrgJ$_{S28X}$, *flhD::tet*	Torres-Vargas et al., 2019
MIB4290	SpaR^{FLAG} PrgJ$_{L29X}$, *flhD::tet*	Torres-Vargas et al., 2019
MIB4210	SpaR^{FLAG} PrgJ$_{L33X}$, *flhD::tet*	Torres-Vargas et al., 2019
MIB4212	SpaR^{FLAG} PrgJ$_{Q35X}$, *flhD::tet*	Torres-Vargas et al., 2019
MIB4214	SpaR^{FLAG} PrgJ$_{F37X}$, *flhD::tet*	Torres-Vargas et al., 2019
MIB4216	SpaR^{FLAG} PrgJ$_{S40X}$, *flhD::tet*	Torres-Vargas et al., 2019
MIB4218	SpaR^{FLAG} PrgJ$_{A43X}$, *flhD::tet*	Torres-Vargas et al., 2019
MIB4220	SpaR^{FLAG} PrgJ$_{V46X}$, *flhD::tet*	Torres-Vargas et al., 2019
MIB4222	SpaR^{FLAG} PrgJ$_{Q49X}$, *flhD::tet*	Torres-Vargas et al., 2019
MIB4224	SpaR^{FLAG} PrgJ$_{T52X}$, *flhD::tet*	Torres-Vargas et al., 2019
MIB4226	SpaR^{FLAG} PrgJ$_{I55X}$, *flhD::tet*	Torres-Vargas et al., 2019
MIB4228	SpaR^{FLAG} PrgJ$_{D57X}$, *flhD::tet*	Torres-Vargas et al., 2019
MIB4230	SpaR^{FLAG} PrgJ$_{L60X}$, *flhD::tet*	Torres-Vargas et al., 2019
MIB4232	SpaR^{FLAG} PrgJ$_{D63X}$, *flhD::tet*	Torres-Vargas et al., 2019
MIB4292	SpaR^{FLAG} PrgJ$_{L67X}$, *flhD::tet*	Torres-Vargas et al., 2019

MIB4294	SpaR^{FLAG} PrgJ$_{S70X}$, *flhD::tet*	Torres-Vargas et al., 2019
MIB4234	SpaR^{FLAG} PrgJ$_{Q71X}$, *flhD::tet*	Torres-Vargas et al., 2019
MIB4296	SpaR^{FLAG} PrgJ$_{I74X}$, *flhD::tet*	Torres-Vargas et al., 2019
MIB4298	SpaR^{FLAG} PrgJ$_{Y77X}$, *flhD::tet*	Torres-Vargas et al., 2019
MIB4300	SpaR^{FLAG} PrgJ$_{L79X}$, *flhD::tet*	Torres-Vargas et al., 2019
MIB4236	SpaR^{FLAG} PrgJ$_{Y80X}$, *flhD::tet*	Torres-Vargas et al., 2019
MIB4238	SpaR^{FLAG} PrgJ$_{V81X}$, *flhD::tet*	Torres-Vargas et al., 2019
MIB4302	SpaR^{FLAG} PrgJ$_{M83X}$, *flhD::tet*	Torres-Vargas et al., 2019
MIB4240	SpaR^{FLAG} PrgJ$_{L87X}$, *flhD::tet*	Torres-Vargas et al., 2019
MIB4242	SpaR^{FLAG} PrgJ$_{V92X}$, *flhD::tet*	Torres-Vargas et al., 2019
MIB4304	SpaR^{FLAG} PrgJ$_{V95X}$, *flhD::tet*	Torres-Vargas et al., 2019
MIB4306	SpaR^{FLAG} PrgJ$_{L98X}$, *flhD::tet*	Torres-Vargas et al., 2019
MIB4308	SpaR^{FLAG} PrgJ$_{S101X}$, *flhD::tet*	Torres-Vargas et al., 2019
MIB4770	SpaP^{FLAG} PrgJ$_{S2X}$ Δ*invJ*, *flhD::tet*	Torres-Vargas et al., 2019
MIB4772	SpaP^{FLAG} PrgJ$_{T52X}$ Δ*invJ*, *flhD::tet*	Torres-Vargas et al., 2019
MIB4774	SpaP^{FLAG} PrgJ$_{I55X}$ Δ*invJ*, *flhD::tet*	Torres-Vargas et al., 2019
MIB4776	SpaP^{FLAG} PrgJ$_{Y77X}$ Δ*invJ*, *flhD::tet*	Torres-Vargas et al., 2019
MIB3674	SpaP^{FLAG} PrgJ$_{M83X}$ Δ*invJ*, *flhD::tet*	Torres-Vargas et al., 2019
MIB3676	SpaP^{FLAG} PrgJ$_{V95X}$ Δ*invJ*, *flhD::tet*	Torres-Vargas et al., 2019
MIB4778	SpaR^{FLAG} PrgJ$_{S21X}$ Δ*invJ*, *flhD::tet*	Torres-Vargas et al., 2019
MIB4780	SpaR^{FLAG} PrgJ$_{F37X}$ Δ*invJ*, *flhD::tet*	Torres-Vargas et al., 2019
MIB4862	SpaR^{FLAG} PrgJ$_{S40X}$ Δ*invJ*, *flhD::tet*	Torres-Vargas et al., 2019
MIB4864	SpaR^{FLAG} PrgJ$_{V81X}$ Δ*invJ*, *flhD::tet*	Torres-Vargas et al., 2019
MIB3612	SpaP$_{G2X}$^{FLAG} PrgJ$_{E9A}$, *flhD::tet*	Torres-Vargas et al., 2019
MIB3614	SpaP$_{G2X}$^{FLAG} PrgJ$_{N10A}$, *flhD::tet*	Torres-Vargas et al., 2019
MIB3616	SpaP$_{G2X}$^{FLAG} PrgJ$_{Q15A}$, *flhD::tet*	Torres-Vargas et al., 2019
MIB3618	SpaP$_{G2X}$^{FLAG} PrgJ$_{V17A}$, *flhD::tet*	Torres-Vargas et al., 2019
MIB3620	SpaP$_{G2X}$^{FLAG} PrgJ$_{N18A}$, *flhD::tet*	Torres-Vargas et al., 2019
MIB3622	SpaP$_{G2X}$^{FLAG} PrgJ$_{T24A}$, *flhD::tet*	Torres-Vargas et al., 2019
MIB3624	SpaP$_{G2X}$^{FLAG} PrgJ$_{L29A}$, *flhD::tet*	Torres-Vargas et al., 2019
MIB3626	SpaP$_{G2X}$^{FLAG} PrgJ$_{D63A}$, *flhD::tet*	Torres-Vargas et al., 2019
MIB3628	SpaP$_{G2X}$^{FLAG} PrgJ$_{Q71A}$, *flhD::tet*	Torres-Vargas et al., 2019

MIB3630	SpaP$_{G2X}^{FLAG}$ PrgJ$_{M83A}$, *flhD::tet*	Torres-Vargas et al., 2019
MIB3632	SpaP$_{G2X}^{FLAG}$ PrgJ$_{E96A}$, *flhD::tet*	Torres-Vargas et al., 2019
MIB3634	SpaP$_{G2X}^{FLAG}$ PrgJ$_{T97A}$, *flhD::tet*	Torres-Vargas et al., 2019
MIB3636	SpaP$_{G2X}^{FLAG}$ PrgJ$_{L98A}$, *flhD::tet*	Torres-Vargas et al., 2019
MIB4694	SpaP^{FLAG} PrgJ$_{M83X}$ PrgIM1K, *flhD::tet*	Torres-Vargas et al., 2019
MIB4764	SpaP^{FLAG} PrgJ$_{M83X}$ PrgIM1K Δ*invG*, *flhD::tet*	Torres-Vargas et al., 2019
MIB5002	SpaP^{FLAG} PrgJ$_{M83X}$ Δ*invG*, *flhD::tet*	Torres-Vargas et al., 2019
SB1905	Δ*spaS*, *flhD::tet*	Wagner et al*.*, 2010
SB1902	Δ*spaP*, *flhD::tet*	Wagner et al., 2010
MIB3212	ΔprgK, *flhD::tet*	Laboratory collection
MIB3338	Δ*invG*, *flhD::tet*	Laboratory collection
MIB3214	Δ*prgH*, *flhD::tet*	Laboratory collection
MIB3722	Δ*invC*, SipANLuc, *flhD::tet*	This study
MIB3325	Δ*orgB*, SipANLuc, *flhD::tet*	This study
MIB3724	Δ*orgA*, SipANLuc, *flhD::tet*	This study
MIB3723	Δ*invI*, SipANLuc, *flhD::tet*	This study
MIB3721	Δ*spaO*, SipANLuc, *flhD::tet*	This study
MIB5016	Δ*orgC*, SipDNLuc, *flhD::tet*	This study
MIB4572	MIS P_{araBAD} *spaS*, SipDNLuc, *flhD::tet*	This study
MIB4697	MIS P_{araBAD} *spaP*, SipDNLuc, *flhD::tet*	This study
MIB4698	MIS P_{araBAD} *prgK*, SipDNLuc, *flhD::tet*	This study
MIB4554	SPI1IS P_{araBAD} *spaS,* SipDNLuc*, flhD*::tet	This study
MIB4558	SPI1IS P_{araBAD} *spaS,* Δ*invC,* SipDNLuc*, flhD*::tet	This study
MIB4562	SPI1IS P_{araBAD} *spaP,* SipDNLuc*, flhD*::tet	This study
MIB4566	SPI1IS P_{araBAD} *spaP,* Δ*invC,* SipDNLuc*, flhD*::tet	This study

3.3 Molecular cloning

Expression and suicide plasmids described in Table 2 were constructed by one-step isothermal Gibson assembly (Gibson et al., 2009). PCR amplification of DNA molecules used for assembly was performed using the primers (Eurofins) listed

in Table 3 and Q5 Hot Start High-Fidelity polymerase (New England Biolabs) following the manufacturer´s protocol (https://international.neb.com/protocols/2012/08/30/pcr-using-q5-hot-start-high-fidelity-dna-polymerase-m0493). All constructs were verified by plasmid DNA sequencing (Eurofins).

Table 2. Plasmids

Plasmid	Description	Reference
pMIB5704	pSB890, $PrgJ_{S2X}$	Torres-Vargas et al., 2019
pMIB5705	pSB890, $PrgJ_{T5X}$	Torres-Vargas et al., 2019
pMIB5706	pSB890, $PrgJ_{P8X}$	Torres-Vargas et al., 2019
pMIB5707	pSB890, $PrgJ_{E9X}$	Torres-Vargas et al., 2019
pMIB5708	pSB890, $PrgJ_{N10X}$	Torres-Vargas et al., 2019
pMIB6221	pSB890, $PrgJ_{V12X}$	Torres-Vargas et al., 2019
pMIB5709	pSB890, $PrgJ_{Q15X}$	Torres-Vargas et al., 2019
pMIB6242	pSB890, $PrgJ_{N18X}$	Torres-Vargas et al., 2019
pMIB6222	pSB890, $PrgJ_{S21X}$	Torres-Vargas et al., 2019
pMIB6223	pSB890, $PrgJ_{T24X}$	Torres-Vargas et al., 2019
pMIB6224	pSB890, $PrgJ_{S28X}$	Torres-Vargas et al., 2019
pMIB3855	pSB890, $PrgJ_{L29X}$	Torres-Vargas et al., 2019
pMIB6225	pSB890, $PrgJ_{L33X}$	Torres-Vargas et al., 2019
pMIB6226	pSB890, $PrgJ_{Q35X}$	Torres-Vargas et al., 2019
pMIB6227	pSB890, $PrgJ_{F37X}$	Torres-Vargas et al., 2019
pMIB6228	pSB890, $PrgJ_{S40X}$	Torres-Vargas et al., 2019
pMIB6229	pSB890, $PrgJ_{A43X}$	Torres-Vargas et al., 2019
pMIB6230	pSB890, $PrgJ_{V46X}$	Torres-Vargas et al., 2019
pMIB6231	pSB890, $PrgJ_{Q49X}$	Torres-Vargas et al., 2019
pMIB6232	pSB890, $PrgJ_{T52X}$	Torres-Vargas et al., 2019
pMIB6233	pSB890, $PrgJ_{I55X}$	Torres-Vargas et al., 2019
pMIB6234	pSB890, $PrgJ_{D57X}$	Torres-Vargas et al., 2019
pMIB6235	pSB890, $PrgJ_{L60X}$	Torres-Vargas et al., 2019
pMIB6236	pSB890, $PrgJ_{D63X}$	Torres-Vargas et al., 2019

pMIB5947	pSB890, PrgJ$_{L67X}$	Torres-Vargas et al., 2019
pMIB5948	pSB890, PrgJ$_{S70X}$	Torres-Vargas et al., 2019
pMIB6237	pSB890, PrgJ$_{Q71X}$	Torres-Vargas et al., 2019
pMIB5949	pSB890, PrgJ$_{I74X}$	Torres-Vargas et al., 2019
pMIB5950	pSB890, PrgJ$_{Y77X}$	Torres-Vargas et al., 2019
pMIB5951	pSB890, PrgJ$_{L79X}$	Torres-Vargas et al., 2019
pMIB6238	pSB890, PrgJ$_{Y80X}$	Torres-Vargas et al., 2019
pMIB6239	pSB890, PrgJ$_{V81X}$	Torres-Vargas et al., 2019
pMIB5713	pSB890, PrgJ$_{M83X}$	Torres-Vargas et al., 2019
pMIB6240	pSB890, PrgJ$_{L87X}$	Torres-Vargas et al., 2019
pMIB6241	pSB890, PrgJ$_{V92X}$	Torres-Vargas et al., 2019
pMIB5714	pSB890, PrgJ$_{V95X}$	Torres-Vargas et al., 2019
pMIB5715	pSB890, PrgJ$_{L98X}$	Torres-Vargas et al., 2019
pMIB5716	pSB890, PrgJ$_{S101X}$	Torres-Vargas et al., 2019
pMIB5837	pSB890, PrgJ$_{E9A}$	Torres-Vargas et al., 2019
pMIB5838	pSB890, PrgJ$_{N10A}$	Torres-Vargas et al., 2019
pMIB5839	pSB890, PrgJ$_{Q15A}$	Torres-Vargas et al., 2019
pMIB5840	pSB890, PrgJ$_{V17A}$	Torres-Vargas et al., 2019
pMIB5841	pSB890, PrgJ$_{N18A}$	Torres-Vargas et al., 2019
pMIB5842	pSB890, PrgJ$_{T24A}$	Torres-Vargas et al., 2019
pMIB5846	SB890, PrgJ$_{L29A}$	Torres-Vargas et al., 2019
pMIB5847	pSB890, PrgJ$_{D63A}$	Torres-Vargas et al., 2019
pMIB5849	pSB890, PrgJ$_{Q71A}$	Torres-Vargas et al., 2019
pMIB5850	pSB890, PrgJ$_{M83A}$	Torres-Vargas et al., 2019
pMIB5843	pSB890, PrgJ$_{E96A}$	Torres-Vargas et al., 2019
pMIB5844	pSB890, PrgJ$_{T97A}$	Torres-Vargas et al., 2019
pMIB5845	pSB890, PrgJ$_{L98A}$	Torres-Vargas et al., 2019
pMIB5642	pSB890, *prgJ*	Torres-Vargas et al., 2019
pMIB5177	pSB890, Δ*invJ*	Torres-Vargas et al., 2019
pMIB6890	pSB890, PrgJ$_{M83X}$, PrgI$_{M1K}$	Torres-Vargas et al., 2019
pMIB5170	pSB890, Δ*invG*	Torres-Vargas et al., 2019
pSB3292	pBAD24, *hilA*	Lara-Tejero et al., 2011

pSup-pBpa		Ryu and Schultz, 2006
pMIB6217	P890, MIS P_{araBAD} *spaS*, SipDNLuc	This study
pMIB6218	P890, MIS P_{araBAD} *spaP*, SipDNLuc	This study
pMIB6219	P890, MIS P_{araBAD} *prgK*, SipDNLuc	This study
pMIB6727	P890, SPI1IS P_{araBAD} *spaS,*SipDNLuc	This study
pMIB6728	P890, SPI1IS P_{araBAD} *spaP,*SipDNLuc	This study
pMIB5942	pT10, *invC*	Laboratory collection
pMIB5941	pT10, *invI*	This study
pMIB5266	pT10, FLAG *spaO*	Laboratory collection
pMIB5790	pT10, *orgB*	This study
pMIB5789	pT10, *orgA*	This study
pMIB5726	pT10, *prgH* FLAG	Laboratory collection
pMIB5748	pT10, *invG* FLAG, *invH*	Laboratory collection
pMIB5727	pT10, *prgK* FLAG	Laboratory collection
pSB3598	pT10, *spaS*	Laboratory collection
pSB3416	pT10, *spaP*	Laboratory collection

Table 3. Primers

Primer name	Sequence 5'-3'
PrgJ_QC_890_S2X_f	gttaatcagttataaggtggattatgtagattgcaactattgtccctg
PrgJ_QC_890_S2X_r	cagggacaatagttgcaatctacataatccaccttataactgattaac
PrgJ_QC_890_T5X_f	gttataaggtggattatgtcgattgcatagattgtccctgagaatgccgttatag
PrgJ_QC_890_T5X_r	ctataacggcattctcagggacaatctatgcaatcgacataatccaccttataac
PrgJ_QC_890_P8X_f	gtcgattgcaactattgtctaggagaatgccgttatagggcaggcggtc
PrgJ_QC_890_P8X_r	gaccgcctgccctataacggcattctcctagacaatagttgcaatcgac
PrgJ_QC_890_E9X_f	gtcgattgcaactattgtcccttagaatgccgttatagggcag
PrgJ_QC_890_E9X_r	ctgccctataacggcattctaagggacaatagttgcaatcgac
PrgJ_QC_890_N10X_f	gattgcaactattgtccctgagtaggccgttatagggcag
PrgJ_QC_890_N10X_r	ctgccctataacggcctactcagggacaatagttgcaatc
PrgJ_V12X_QC_f	ctattgtccctgagaatgcctagatagggcaggcggtcaatatc

PrgJ_V12X_QC_r	gatattgaccgcctgccctatctaggcattctcagggacaatag
PrgJ_QC_890_Q15X_f	gagaatgccgttatagggtaggcggtcaatatcaggtc
PrgJ_QC_890_Q15X_r	gacctgatattgaccgcctaccctataacggcattctc
PrgJ_QC_890_N18X_f	gttatagggcaggcggtctagatcaggtctatggaaacggac
PrgJ_QC_890_N18X_r	gtccgtttccatagacctgatctagaccgcctgccctataac
PrgJ_S21X_QC_f	caggcggtcaatatcaggtagatggaaacggacattgtctc
PrgJ_S21X_QC_r	gagacaatgtccgtttccatctacctgatattgaccgcctg
PrgJ_T24X_QC_f	ggtcaatatcaggtctatggaataggacattgtctcgctg
PrgJ_T24X_QC_r	cagcgagacaatgtcctattccatagacctgatattgacc
PrgJ_S28X_QC_f	gtctatggaaacggacattgtctagctggatgaccggctac
PrgJ_S28X_QC_r	gtagccggtcatccagctagacaatgtccgtttccatagac
PrgJ_QC_890_L29X_f	gaaacggacattgtctcgtaggatgaccggctactc
PrgJ_QC_890_L29X_r	gagtagccggtcatcctacgagacaatgtccgtttc
PrgJ_L33X_QC_f	ctcgctggatgaccggtagctccaggctttttctgg
PrgJ_L33X_QC_r	ccagaaaaagcctggagctaccggtcatccagcgag
PrgJ_Q35X_QC_f	gatgaccggctactctaggctttttctggttcg
PrgJ_Q35X_QC_r	cgaaccagaaaaagcctagagtagccggtcatc
PrgJ_F37X_QC_f	ggctactccaggcttagtctggttcggcgattg
PrgJ_F37X_QC_r	caatcgccgaaccagactaagcctggagtagcc
PrgJ_S40X_QC_f	ctccaggctttttctggttaggcgattgccacggc
PrgJ_S40X_QC_r	gccgtggcaatcgcctaaccagaaaaagcctggag
PrgJ_A43X_QC_f	gctttttctggttcggcgatttagacggctgtggataaacagac
PrgJ_A43X_QC_r	gtctgtttatccacagccgtctaaatcgccgaaccagaaaaagc
PrgJ_S21X_QC_f	caggcggtcaatatcaggtagatggaaacggacattgtctc
PrgJ_S21X_QC_r	gagacaatgtccgtttccatctacctgatattgaccgcctg
PrgJ_T24X_QC_f	ggtcaatatcaggtctatggaataggacattgtctcgctg
PrgJ_T24X_QC_r	cagcgagacaatgtcctattccatagacctgatattgacc
PrgJ_S28X_QC_f	gtctatggaaacggacattgtctagctggatgaccggctac
PrgJ_S28X_QC_r	gtagccggtcatccagctagacaatgtccgtttccatagac
PrgJ_QC_890_L29X_f	gaaacggacattgtctcgtaggatgaccggctactc
PrgJ_QC_890_L29X_r	gagtagccggtcatcctacgagacaatgtccgtttc
PrgJ_L33X_QC_f	ctcgctggatgaccggtagctccaggctttttctgg
PrgJ_L33X_QC_r	ccagaaaaagcctggagctaccggtcatccagcgag

PrgJ_Q35X_QC_f	gatgaccggctactctaggctttttctggttcg
PrgJ_Q35X_QC_r	cgaaccagaaaaagcctagagtagccggtcatc
PrgJ_F37X_QC_f	ggctactccaggcttagtctggttcggcgattg
PrgJ_F37X_QC_r	caatcgccgaaccagactaagcctggagtagcc
PrgJ_S40X_QC_f	ctccaggctttttctggttaggcgattgccacggc
PrgJ_S40X_QC_r	gccgtggcaatcgcctaaccagaaaaagcctggag
PrgJ_A43X_QC_f	gctttttctggttcggcgatttagacggctgtggataaacagac
PrgJ_A43X_QC_r	gtctgtttatccacagccgtctaaatcgccgaaccagaaaaagc
PrgJ_V46X_QC_f	gcgattgccacggcttaggataaacagacgattaccaac
PrgJ_V46X_QC_r	gttggtaatcgtctgtttatcctaagccgtggcaatcgc
PrgJ_Q49X_QC_f	cacggctgtggataaatagacgattaccaacag
PrgJ_Q49X_QC_r	ctgttggtaatcgtctatttatccacagccgtg
PrgJ_T52X_QC_f	ggctgtggataaacagacgatttagaacaggattgaggaccctaatc
PrgJ_T52X_QC_r	gattagggtcctcaatcctgttctaaatcgtctgtttatccacagcc
PrgJ_I55X_QC_f	gataaacagacgattaccaacaggtaggaggaccctaatctggtg
PrgJ_I55X_QC_r	caccagattagggtcctcctacctgttggtaatcgtctgtttatc
PrgJ_D57X_QC_f	gacgattaccaacaggattgagtagcctaatctggtgacggatc
PrgJ_D57X_QC_r	gatccgtcaccagattaggctactcaatcctgttggtaatcgtc
PrgJ_L60_X_QC_f	caggattgaggaccctaattaggtgacggatcctaaagagc
PrgJ_L60_X_QC_r	gctctttaggatccgtcacctaattagggtcctcaatcctg
PrgJ_D63_X_QC_f	ccctaatctggtgacgtagcctaaagagctggctatttcg
PrgJ_D63_X_QC_r	cgaaatagccagctctttaggctacgtcaccagattaggg
PrgJ_QC_890_L67X_f	cggatcctaaagagtaggctatttcgcaagagatgatttc
PrgJ_QC_890_L67X_r	gaaatcatctcttgcgaaatagcctactctttaggatccg
PrgJ_QC_890_S70X_f	gatcctaaagagctggctatttagcaagagatgatttcagattataacctg
PrgJ_QC_890_S70X_r	caggttataatctgaaatcatctcttgctaaatagccagctctttaggatc
PrgJ_Q71_X_QC_f	cctaaagagctggctatttcgtaggagatgatttcagattataacctg
PrgJ_Q71_X_QC_r	caggttataatctgaaatcatctcctacgaaatagccagctcttagg
PrgJ_QC_890_I74X_f	ggctatttcgcaagagatgtagtcagattataacctgtatgtttctatgg
PrgJ_QC_890_I74X_r	ccatagaaacatacaggttataatctgactacatctcttgcgaaatagcc
PrgJ_QC_890_Y77X_f	ctatttcgcaagagatgatttcagattagaacctgtatgtttctatggtcag
PrgJ_QC_890_Y77X_r	ctgaccatagaaacatacaggttctaatctgaaatcatctcttgcgaaatag
PrgJ_QC_890_L79X_f	cgcaagagatgatttcagattataactagtatgtttctatggtcagtaccc

PrgJ_QC_890_L79X_r	gggtactgaccatagaaacatactagttataatctgaaatcatctcttgcg
PrgJ_Y80_x_QC_f	gatgatttcagattataacctgtaggtttctatggtcagtaccc
PrgJ_Y80_x_QC_r	gggtactgaccatagaaacctacaggttataatctgaaatcatc
PrgJ_V81_x_QC_f	caagagatgatttcagattataacctgtattagtctatggtcagtacccttac
PrgJ_V81_x_QC_r	gtaagggtactgaccatagactaatacaggttataatctgaaatcatctcttg
PrgJ_QC_890_M83X_f	gatttcagattataacctgtatgtttcttaggtcagtacccttactcgtaaag
PrgJ_QC_890_M83X_r	ctttacgagtaagggtactgacctaagaaacatacaggttataatctgaaatc
PrgJ_L87_x_QC_f	gtatgtttctatggtcagtacctagactcgtaaaggagtcgg
PrgJ_L87_x_QC_r	ccgactcctttacgagtctaggtactgaccatagaaacatac
PrgJ_V92_x_QC_f	cccttactcgtaaaggatagggggctgttgaaacgc
PrgJ_V92_x_QC_r	gcgtttcaacagccccctatcctttacgagtaaggg
PrgJ_QC_890_V95X_f	ctcgtaaaggagtcggggcttaggaaacgctattacgctcatg
PrgJ_QC_890_V95X_r	catgagcgtaatagcgtttcctaagccccgactcctttacgag
PrgJ_QC_890_L98X_f	gtcggggctgttgaaacgtagttacgctcatgattcgtcgatatc
PrgJ_QC_890_L98X_r	gatatcgacgaatcatgagcgtaactacgtttcaacagccccgac
PrgJ_QC_890_S101X_f	gttgaaacgctattacgctagtgattcgtcgatatctatatacttttctg
PrgJ_QC_890_S101X_r	cagaaaagtatatagatatcgacgaatcactagcgtaatagcgtttcaac
PrgJ_QC_E9A_f	gtcgattgcaactattgtccctgcgaatgccgttatagggcag
PrgJ_QC_E9A_r	ctgccctataacggcattcgcagggacaatagttgcaatcgac
PrgJ_QC_N10A_f	gtcgattgcaactattgtccctgaggcggccgttatagggcaggcggtcaatatcag
PrgJ_QC_N10A_r	ctgatattgaccgcctgccctataacggccgcctcagggacaatagttgcaatcgac
PrgJ_QC_Q15A_f	ctgagaatgccgttataggggcggcggtcaatatcaggtctatg
PrgJ_QC_Q15A_r	catagacctgatattgaccgccgcccctataacggcattctcag
PrgJ_QC_V17A_f	gttatagggcaggcggccaatatcaggtctatggaaacggac
PrgJ_QC_V17A_r	gtccgtttccatagacctgatattggccgcctgccctataac
PrgJ_QC_N18A_f	gttatagggcaggcggtcgcgatcaggtctatggaaacggac
PrgJ_QC_N18A_r	gtccgtttccatagacctgatcgcgaccgcctgccctataac
PrgJ_QC_T24A_f	caatatcaggtctatggaagcggacattgtctcgctg
PrgJ_QC_T24A_r	cagcgagacaatgtccgcttccatagacctgatattg
PrgJ_QC_L29A_f	gaaacggacattgtctcggcggatgaccggctactc
PrgJ_QC_L29A_r	gagtagccggtcatccgccgagacaatgtccgtttc
PrgJ_QC_D63A_f	cctaatctggtgacggctcctaaagagctggctatttc
PrgJ_QC_D63A_r	gaaatagccagctctttaggagccgtcaccagattagg

PrgJ_QC_Q71A_f	ctaaagagctggctatttcggcagagatgatttcagattataacctgtatg
PrgJ_QC_Q71A_r	catacaggttataatctgaaatcatctctgccgaaatagccagctctttag
PrgJ_QC_M83A_f	gatgatttcagattataacctgtatgtttctgcggtcagtacccttactcg
PrgJ_QC_M83A_r	cgagtaagggtactgaccgcagaaacatacaggttataatctgaaatcatc
PrgJ_QC_E96A_f	gagtcggggctgttgcgacgctattacgctcatgattc
PrgJ_QC_E96A_r	gaatcatgagcgtaatagcgtcgcaacagccccgactc
PrgJ_QC_T97A_f	gtcggggctgttgaagcgctattacgctcatgattc
PrgJ_QC_T97A_r	gaatcatgagcgtaatagcgcttcaacagccccgac
PrgJ_QC_L98A_f	gtcggggctgttgaaacggcgttacgctcatgattcgtcgatatc
PrgJ_QC_L98A_r	gatatcgacgaatcatgagcgtaacgccgtttcaacagccccgac
gib_uni_890_f	ggatcccccgggctgcagttc
gib_uni_890_r	actagttctagagcggccgccac
gib_uni_890_f2	caagctcaataaaaagccccac
gib_uni_890_r2	caagagggtcattatatttcgcg
gib_890_prgJ_a_f	gttattccgcgaaatataatgaccctcttgagatacgttgtgggctcgtc
gib_890_prgJ_d_r	caccgcggtggggctttttattgagcttgcgggtctgacaatcatttcc
prgI_seq_f	gcccgtcaatttgtcgatag
prgJ_seq_r	agcggtaaaatcaggctcag
gib_890_invJ_a_f	ccgcggtggggctttttattgagcttgaacgaaacaggttcctgacg
gib_890_invJ_d_r	gttattccgcgaaatataatgaccctcttggttatcccgcctccgtattc
invJ_1b_r	cattaaattatctcctctgactcgg
invJ_1bc336_r	ccgagtcagaggagataatttaatgtcattgcgtgtgagacagattgatc
invJ_seq_f	gcgcaaagaagggaactatc
invJ_seq_f	gaccaccgtttttctgcatc
invG_seq_f	gcaatcgctgctgaatagtg
invG_seq_r	tgttgtatttccgcctgttg
pBAD_seq_r	acggcgtttcacttctgagt
pBAD_seq_f	atcacggcagaaaagtccac
gib_avrA_araBAD_f	ctttactggcgttgaggaccaaagcagctcatcgatgcataatgtgcctgtc
gib_avrA_araBAD_f	agcaaaataacaatcaggcagttgttcacggatgcataatgtgcctgtc
gib_araBAD_spaS_f	tgggctagcaggaggaattcaccatgtcctcgaataaaacagaaaaacc
gib_malint_araBAD_r	ggttaatatctttcgataccaccacgtcacggtgaattcctcctgctagccca
gib_malint_araBAD_f	ggataatgcgaggatgcctatctagacatcgatgcataatgtgcctgtc

gib_araBAD_prgK_f	tgggctagcaggaggaattcaccatgattcgtcgatatctatatacttttc
pBAD_seq_r	acggcgtttcacttctgagt
gib_pT10_OrgB_f	cgtaatgaaattcaggaggaattcaccatgtcattgcgtgtgagacag
gib_pT10_OrgB_r	catccgccaaaacagccaagctcaccttataacctccgcttg
gib_pT12_OrgA_f	gaaattcaggaggaattcaccatgataaggcgaaatcgtcaaatg
gib_pT10_OrgA_r	catccgccaaaacagccaagctcaacaggcgaaagcgggg
gib_pT10n_invI_f	cgctttttagactggtcgtaatgaacatcctttgatgacacgttgag
gib_pT10n_invI_r	catccgccaaaacagccaagcttaaattatctcctctgactcggcc
SipD_seq_f	cgcgcttaatctgaaaggtc
SipD_seq_r	ggcctttaatttcccctgac
gib_890_sipD_c_f	tggcgaactggggatattatgcttaatattctgcaaggataacagaagag
gib_890_sipD_b_r	aatattaagcataatatccccagttcgcca
gib_uni_SipD275_r	tcccggcgcgcctaaacc
gib_uni_SipD275_r	aaagactcaaaactcgaaatggataac
gib_SipD276_myc_r	gttatccatttcgagttttgagtctttagagcctaaatcttcttcgctaatcagtttc
gib_SipD275_NL_f	ggtttaggcgcgccgggaggttctatggtcttcacactcgaagatttc

3.4 Site directed mutagenesis

Site directed mutagenesis was used to introduce point mutations in genes cloned either in expression or suicide plasmids, being the last ones utilized to generate *S.* Typhimurium mutant strains. The mutagenesis was performed according to the Quick Change instruction manual (https://www.agilent.com/cs/library/usermanuals/Public/200523.pdf) using KOD polymerase (Thermo Fisher). Comprehensive lists of the plasmids generated with this methodology and the mutagenic oligonucleotides used (Eurofins) can be found in Tables 2 and 3, respectively. All constructs were verified by plasmid DNA sequencing (Eurofins).

3.5 Allelic exchange

All genomic DNA modifications were made in *Salmonella enterica* serovar Typhimurium strain SL1344 (Hoiseth and Stocker, 1981) using the allelic exchange method described by Kaniga and co-workers (Kaniga et al., 1994).

Salmonella mutants were screened by colony PCR performed with Taq DNA polymerase (New England Biolabs) and further verified by genomic DNA sequencing (Eurofins). Suicide plasmids and sequencing oligonucleotides used for mutant generation are shown in Tables 2 and 3, respectively.

3.6 SPI-1 secretion assay

Secretion assays were carried out following previously published protocols with minimal modifications (Monjarás Feria et al., 2015; Torres-Vargas et al., 2019; Kuhlen et al., 2020). *S.* Typhimurium strains were grown overnight with low aeration in LB broth supplemented with 0.3 M NaCl and the required antibiotics at 37°C and 180 r.p.m. The day after, cultures were diluted to A_{600}= 0.1 into 3 ml of the same media and cultured under the same conditions for 5 h. Then, A_{600} of each culture was measured and the obtained values were used to normalize the volume of SDS PAGE loading buffer volume required to resuspend whole cell and supernatant samples to avoid uneven sample loading. Bacterial suspensions were harvested and centrifuged at 10,000 x *g* for 2 minutes and 4°C to separate whole cells and supernatants. Whole cells were resuspended in the corresponding calculated volumes of SDS PAGE loading buffer. Supernatants were passed through 0.2 µm pore size filters and 0.1 % (m/v) Na-desoxycholic acid was added as co-precipitant. Secreted proteins into the culture supernatant were precipitated with 10 % (v/v) tricholoacetic acid (TCA) for 30 minutes at 4°C and pelleted via centrifugation at 20,000 x *g* for 20 minutes and 4 °C. Pellets containing precipitated proteins were washed with acetone, air dried and resuspended in the corresponding volumes of SDS PAGE loading buffer supplemented with 10 % (v/v) of Tris-HCl 1 M pH 7 to neutralize remaining TCA. Whole cell samples and secreted proteins were subjected to SDS PAGE analysis, Western blotting, and immunodetection.

3.7 *in vivo* photocrosslinking

Protein-protein interactions between the *Salmonella* SPI-1 T3SS components were identified via a site-directed *in vivo* photocrosslinking approach. The

experimental procedure used in this study was based on previously published methodologies (Dietsche et al., 2016; Farrell et al., 2005), which requires the enhanced expression of SPI-1 T3SS. To achieve this, *S*. Typhimurium strains expressed the master transcriptional regulator of SPI-1 T3SS, HilA, from a high-copy plasmid under the control of the L-arabinose-inducible promoter P_{araBAD}. Bacteria were routinely grown for 5 h at 37 °C and low aeration in LB broth supplemented with 0.3 M NaCl, 100 µg ampicillin, 1 mM *p*Bpa and 0.05 % L-arabinose. 5 ODU of bacterial cells were harvested, washed with 5 mL of chilled 1 fold phosphate buffered saline solution (PBS) and centrifuged for 3 minutes at 4 000 x *g* and 4°C. The resulting pellets were resuspended in 1 mL of chilled 1 fold PBS and transferred into 6-well plates. Samples were placed on a UV transilluminator table (UVP) and irradiated (λ=365 nm) for 30 minutes. Finally, bacterial cells were centrifuged at 10, 000 x *g* and 4°C for 2 minutes and stored at -80°C until use for further analysis.

3.8 Bacterial crude membrane purification

In this study, bacterial crude membranes were purified as previously described (Dietsche et al., 2016; Torres-Vargas et al., 2019; Kuhlen et al., 2020). 5 ODU of bacterial cell were harvested, resuspended in 750 µl of chilled lysis buffer (250 mM sucrose, 50 mM triethanolamine, pH 7.5, 1 mM EDTA, 1 mM MgCl2, 10 µg/ml DNAse, 1:100 protease inhibitor cocktail [Roche] and 2 mg/ml lysozyme) and kept on ice for 30 minutes. Cell suspensions were lysed by bead milling and lysates were clarified from beads, intact cells and debris by centrifugation for 10 minutes at 10, 000 x *g* and 4°C. Subsequently, supernatants were transferred to fresh ultracentrifuge microtubes and bacterial membranes were pelleted by centrifugation for 50 minutes at 52, 000 rpm and 4°C in a Beckman TLA55 rotor. Samples were stored at -20°C until use for further analysis by SDS PAGE, western blotting and immunodetection.

3.9 SDS PAGE, Western blotting and immunodetection

Protein samples were loaded into the wells of 8-16 % SERVAGel™ TG PRiME precast gels, along with the molecular weight marker All Blue Prestained Protein Standards (Bio-Rad), as formerly described (Monjarás Feria et al., 2016; Torres-Vargas et al., 2019; Kuhlen et al., 2020). Gels were run for 15 minutes at 100 V and then the voltage was increased to 210 V to finish the run in about 1.5 h. Proteins were then transferred on PVDF membranes (Bio-Rad) at 4°C for 2 h at 35 V. Blots were blocked in 5 % (m/v) skimmed milk in 1 fold Tris-buffered saline solution (TBS) at room temperature for 1 h and rinsed 3 times for 15 minutes with 3 % Tween in 1 fold TBS (TBS-T). For the immunodetection the following antibodies were used: primary antibodies anti SctE (1:1000), anti SctP (1:2000) (Monjarás Feria et al., 2015), anti Myc (1:1000) (Roche), anti SctI (1:2000) (Marlovits et al., 2006), anti NC base (Wagner et al., 2010) and M2 anti FLAG (1:10,000) (Sigma-Aldrich). Secondary antibodies (Thermo Fisher) were goat anti mouse IgG Dylight 800 conjugate (1:5000) and goat anti rabbit IgG Dylight 680 (1:5000). Scanning of the PVDF membranes and image analysis was performed with a Li-Cor Odyssey system and Image Studio 3.1 (Li-Cor).

3.10 BN PAGE

Blue Native (BN) polyacrylamide gel electrophoresis (PAGE) was performed according to previously reported protocols with minimal changes (Wagner et al., 2010; Zilkenat et al., 2016). Purified bacterial crude membranes were resuspended in 1 fold PBS and the protein concentration was quantified with the Pierce bicinchoninic acid (BCA) Protein Assay kit (Thermo Fisher). Afterwards 10 µg of membrane proteins were solubilized with 10 % n-dodecyl-β-D-maltopyranoside (DDM) for 1 h at 4°C. Non solubilized material was pelleted down by centrifugation for 20 minutes at 20, 000 x *g* and 4°C. Supernatant containing the extracted proteins was transferred to a fresh microtube, subsequently 10 fold BN loading dye (5 % [w/v] Serva Blue G [Serva Electrophoresis], 250 mM aminocaproic acid, 50 % glycerol) was added and samples were gently mixed and kept on ice. Finally, samples were loaded on a NativePAGE 4-16 % Novex Bis-Trisgel system (Thermo Fisher), the

electrophoresis was run at 4°C for 50 minutes at 130 V and 250 V and 300 mA for 2 h. Once the electrophoresis was finished, the BN gel was incubated in 1 fold running buffer (25 mM Tris, 192 mM glycine, 0.1 % [w/v] SDS) for 20 minutes at room temperature and then proteins were transferred on PVDF membranes (Bio-Rad) and immunodetected using standard procedures.

3.11 Purification of SPI-1 needle complexes

Purification of needle complexes (NCs) from *S*. Typhimurium strains was carried out using reported protocols with minimal modifications (Dietsche et al., 2016; Kubori et al., 1998; Monjarás Feria et al., 2015). Bacterial cultures were grown routinely for 5 h at 37°C and constant shacking (150 rpm) in LB broth supplemented with 0.3 M NaCl and the required antibiotics. Bacteria were centrifuged for 15 minutes at 3 000 x *g* and 4°C and resuspended in chilled resuspension buffer (150 mM Tris [pH 7.4], 0.5 M sucrose, 1 mg/ml lysozyme, and 7 mM EDTA). Bacterial slurries were incubated on ice for 45 minutes with continuous stirring. Afterwards cell suspensions were shifted to a water bath at 37°C for 20 minutes and then 10 % DDM was added to lyse the cells, 5 minutes later lysates were placed back in the ice bucket and supplemented with 450 mM NaCl and 12 mM MgCl2, slurries wee incubated on ice for 1 h more. Lysates were clarified from debris and intact cells by centrifugation for 30 minutes at 15, 000 x *g* and 4°C. Supernatants were centrifuged for 2.5 h at 264, 900 x *g* and 4°C to pellet NCs. Subsequently, pellets containing NCs were resuspended in a gradient buffer (0.4 % DDM, 1 fold PBS, 375 mM NaCl and 5 mM EDTA) and adjusted to 27.5 % ClCs as final concentration. Samples were centrifuged for 16 h at 286, 000 x *g*. 0.5 ml aliquots were collected using a Biocomp gradient station and selected fractions were pooled and centrifuged for 2 h at 121,19 x *g* to pellet the NCs. Pellets containing NCs were resuspended in the final buffer (0.1% DDM, 1 fold PBS, 375 mM NaCl, and 5 mM EDTA). Samples by transmission electron microscopy.

3.12 Transmission Electron microscopy

Electron microscopy analysis of purified NCs was performed by Dr. York-Dieter Stierhof and colleagues in the Centre for Plant Molecular Biology (ZMBP) of the University of Tübingen. Samples were negatively stained and visualized as previously described (Monjarás Feria et al., 2015; Zilkenat et al., 2016; Dietsche et al., 2016).

3.13 Detection of effector-NLuc proteins in bacterial cultures

Detection of proteins secreted through the *Salmonella* SPI-1 T3SS in the bacterial culture was carried out as formerly described (Westerhausen et al., 2020). Separation of whole cells from the culture supernatant after incubation of *Salmonella* strains under SPI-1 inducing conditions was carried out as described in the **Secretion assay** section. The Nano-Glo® Luciferase Assay Reagent (Promega) was freshly reconstituted before use following the instructions provided by the manufacturer. 25 µl of bacterial culture supernatant were transferred to a 384-well plate and an equal amount of reconstituted reagent was added to each well. Luminescence was measured in a multimode microplate reader (Tecan Spark) using the following settings: attenuation: auto, settle time: 0 ms, integration time: 100 ms.

3.14 Luciferase-based time course secretion assay

Secreted proteins through the *Salmonella* SPI-1 T3SS were detected in the culture media via a luciferase-based assay (Westerhausen et al., 2020). Secretion deficient *S.* Typhimurium strains used to perform time course secretion assays harboured individual in-frame deletions of *sctK*, *sctL*, *sctN*, *sctO* or *sctQ* (T3SS cytoplasmic components) from the chromosome and had as common denominator expression of SipA fused to the luciferase Nanoluc (NLuc) from the *sipA* native locus. To restore T3 protein secretion, SctK, SctL, SctN, SctO and SctQ were individually expressed in the corresponding *Salmonella* mutant from a low-copy plasmid under the control of a rhamnose-inducible promoter P_{rha}. Bacterial strains were routinely grown overnight in LB broth supplemented with

0.3 M NaCl and the required antibiotics. The day after cultures were inoculated to A_{600}=0.1 and incubated at 37°C and 150 rpm for ~2.5 h until A_{600}=1.0 was reached. The Nano-Glo® HiBiT Extracellular Reagent (Promega) was freshly reconstituted before use, as suggested by the manufacturer. 50 µl of bacterial culture were transferred to a 96-well plate and an equal amount of reconstituted reagent was added to each well along with 0.5 mM rhamnose to induce protein expression. Luminescence was measured at 37°C during 1 h every 3 minutes in a multimode microplate reader (Tecan Spark) using the following settings: attenuation: auto, settle time: 0 ms, integration time: 100 ms.

3.15 Synchronization of T3SS bases assembly

Salmonella strains (secretion deficient background Δ*sctN*) were cultured overnight under standard conditions (see previous sections). The next day cultures were diluted to A_{600}= 0.1 in LB supplemented with 0.3 M NaCl and antibiotics when needed and incubated under SPI-1 inducing conditions for ~2.5 h or until A_{600}=1.0. Expression of the gene of interest (SctT, SctR or SctJ) under the control of an L-arabinose-inducible promoter P_{araBAD} was induced by addition of 0.05 % L-arabinose, cultures continued incubating for 1 h under the same conditions. Afterwards 0.1 % fucose was added to repress P_{araBAD} promoter and allow completion of NC basal body assembly. Fully assembled NCs turned secretion competent by addition of 0.5 mM rhamnose to the media to express SctN from a low-copy plasmid under the control of a rhamnose-inducible promoter P_{rha}. Time course secretion of SctA fused to NLuc was performed as described in the previous section.

4 Results

4.1 Development of a genetic system to synchronize assembly of the T3SS base

In *Salmonella* bacterial populations the processes involved in the injectisome biogenesis occur asynchronously due to its intrinsic modular design and multistep assembly. This chapter describes the development of a genetic system that allows to synchronize assembly of the T3SS and secretion of proteins. Such a system could potentially to improve the resolution of the analysis of relevant processes such as inner rod assembly, needle length control and secretion specificity switch. Results presented in this chapter are not published.

4.1.1 Identification of T3SS components suitable to regulate NC base assembly

Efficient assembly of the NC base relies on the highly coordinated association of the fully assembled export apparatus with the IM ring structures, the stable location of cytoplasmic components in the cytoplasmic side of the T3SS and the later recruitment of the OM-embedded secretin ring. Genetic analyses have evidenced that elimination of structural components of the NC base results in assembly of non-functional intermediate subcomplexes. Thus, controlled assembly of NC can be achieved by fine tuning expression of key base elements (Wagner et al., 2010; Kaniga et al., 1994). Five *S.* Typhimurium mutants (Δ*sctC*, Δ*sctD*, Δ*sctJ*, Δ*sctR*, and Δ*sctU*) (Fig. 8A) were used to identify the NC base component that more efficiently restored T3SS functionality and assembly when expressed from a low-copy plasmid (pT10) under the control of the L-rhamnose inducible promoter P_{rha}. Bacterial strains were cultured for 5 h under SPI-1 T3SS inducing conditions in the presence of L-rhamnose, and secretion of proteins in the culture supernatant was assessed by SDS PAGE, Western blotting and immunodetection. Individual deletion of *sctC*, *sctD*, *sctJ*, *sctR*, or *sctU* from the *Salmonella* chromosome lead to complete abrogation of type 3-dependent secretion of substrates and affected NC assembly to different extents. While the Δ*sctC* and Δ*sctD* mutants failed to assemble NCs, the Δ*sctR*, Δ*sctU* and Δ*sctJ* strains only presented reduced efficiency in NC production (Fig. 8B and 8C),

consistent with previous reports (Wagner et al., 2010; Kaniga et al., 1994). No difference between the secretion profile displayed by the wild type strain and all five complemented mutants was observed, as both early (SctP) and intermediate (SctE) substrates were detected at similar levels, except for the Δ*sctC* and Δ*sctD* strains, which secreted slightly reduced amounts proteins (Fig. 8B). A similar effect on NC assembly was obtained: pT10-based expression of SctJ, SctR, and SctU yielded wild type amounts of complexes, while P_{rha}-driven expression of SctC and SctD partially restored NC assembly (Fig 8C).

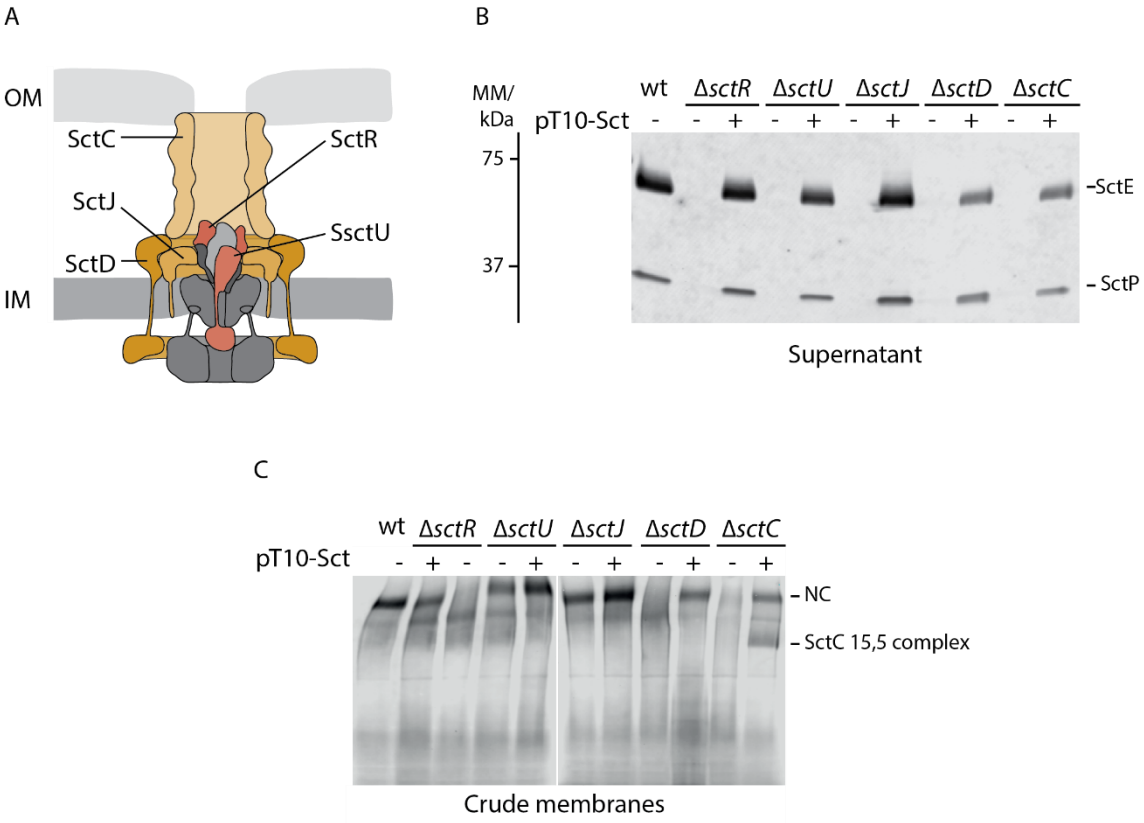

Fig. 8 Type 3 secretion functionality of NC base mutants.
A. Illustration of the T3SS base, with core components highlighted in orange and red shades. **B.** Immunodetection of SctP and SctE on Western blot of SDS PAGE-separated culture supernatants from *S.* Typhimurium mutants expressing (+) or not (-) T3SS core components from plasmids (pT10-Sct). **C.** Immunoblotting analysis of BN PAGE-resolved NCs isolated from indicated strains lacking base components. pT10-based complementation is indicated with a + mark. Shown are immunoblots representative of three independent experiments.

Although pT10-based expression of the five selected NC base components restored NC assembly and type 3 secretion functionality, only three structural elements SctR, SctU and SctJ, were included in the implemented expression system thoroughly described below. The two remaining components SctC and

SctD were excluded due to the observed poor complementation of Δ*sctC* and Δ*sctD* mutants, likely caused by inefficient formation of the IM and OM ring structures SctC and SctD, respectively.

4.1.2 Construction of the *araC-P*$_{araBAD}$ promoter-based expression system

Synchronization of NC base assembly entailed a genetic system that enabled to induce expression of NC core components and rapidly shut it off in order to restrict full assembly of bases to a defined time frame. In this manner, further assembly depends on the availability of such core components. Since *sctR*, *sctU* and *sctJ* proved to be suitable targets of controllable gene expression to modulate NC base assembly, we generated a genetic system consisting of the *araC-P*$_{araBAD}$ expression cassette (*P*$_{araBAD}$ promoter and its regulatory gene, *araC*) obtained from the vector pBAD24 (Guzman et al., 1995) and *sctR*, *sctU* or *sctJ* as target gene. Expression of target genes downstream the *P*$_{araBAD}$ promoter of the arabinose operon is controlled by AraC, a transcriptional regulator which in absence of L-arabinose forms a dimer that binds to the regulatory elements O_2 and I_1, creating a DNA loop and repressing transcription from *P*$_{araBAD}$ (Fig. 9A). In the presence of L-arabinose, the AraC dimer, instead, changes its binding sites to the regulatory elements I_1 and I_2 and releases the DNA loop allowing transcription from *P*$_{araBAD}$ (Fig. 9B) (Schleif, 2000a).

Attempting to preserve native gene dosage, a single copy of the genetic system was integrated into the chromosome of the *Salmonella* Δ*sctR*, Δ*sctU* and Δ*sctJ* strains at a neutral site within two nonessential operons of the maltose transport system that are transcribed in opposite directions. Earlier studies have shown that expression cassettes inserted into this maltose integration site (MIS) permitted uncoupled expression of T3SS components and did not have detrimental effects on bacterial cells (Wagner et al., 2010; Monjarás Feria et al., 2015).

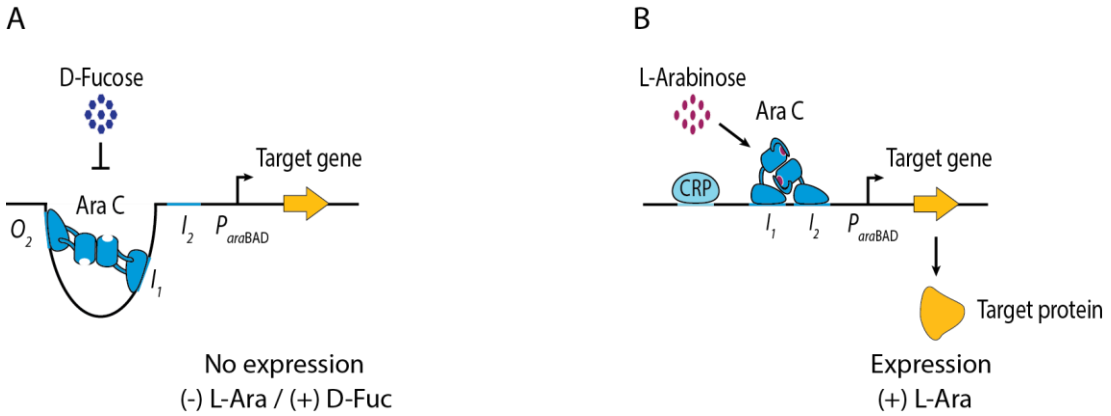

Fig. 9 Organization of the P_{araBAD} promoter-based expression system.
A. Representation of the *araC*-P_{araBAD} expression cassette containing the L-arabinose inducible P_{araBAD} promoter of the arabinose operon and its regulatory gene *araC*. Expression of *araC* is under the control of the cAMP receptor protein (CRP), also required for induction of P_{araBAD}-driven expression. In the absence of L-arabinose or presence of D-fucose, the transcriptional regulator AraC forms a dimer and binds to the regulatory elements O_2 and I_1 creating a DNA loop and repressing transcription from P_{araBAD}. **B.** In the presence of L-arabinose, the AraC dimer changes its binding positions to the regulatory elements I_1 and I_2 and releases the DNA loop, allowing expression from P_{araBAD}.

4.1.3 Modulation and repression of the *araC*-P_{araBAD} promoter-based expression cassette

The P_{araBAD} promoter-based expression systems offers the possibility to finely tune gene expression rate by partially inducing the promoter, and to efficiently repress expression (Guzman et al., 1995). Different concentrations of L-arabinose were used to activate expression of *sctR*, *sctU* and *sctJ* from the P_{araBAD} promoter and assess the extent of type 3 secretion recovery. *S.* Typhimurium strains were cultured for 5 h under SPI-1 inducing conditions in the presence of 0.02, 0.05 and 0.1 % (m/v) L-arabinose and a standard secretion assay was performed. The proteins secreted into the culture supernatant in a type 3-dependent manner were analyzed by SDS PAGE and immunodetection with polyclonal antibodies against SctP and SctE. Figure 10A shows that P_{araBAD}-driven expression of *sctR* restored secretion of SctP and SctE, early and intermediate substrates, respectively, in a dose dependent-manner, but failed to restore secretion to wild type levels even when the highest concentration of inducer was used. In contrast, supplementing the media with 0.05 % L-arabinose sufficed to restore secretion to wild type levels in the case of *sctU* and *sctJ*, while 0.1 % had a general negative effect on secretion. Based on such effects, the optimal concentration of inducer used in the following experiments was fixed to

0.05 % (m/v). To evaluate the effectiveness of repression of P_{araBAD}-driven gene expression, the nonmetabolizable analog of L-arabinose, D-fucose, was employed to antagonize the effect of L-arabinose. For this purpose, bacterial cultures were supplemented with sugars as indicated in figure 10B and secretion of substrates was monitored using standard procedures. As previously observed, L-arabinose-dependent expression of *sctR*, *sctU* and *sctJ* rescued the secretion deficient phenotype of the three null mutants, since both early and intermediate substrates were detected into the culture supernatant. In contrast, simultaneous addition of 0.05 % L-arabinose and 0.1 % D-fucose to the media resulted in repression of P_{araBAD}-driven gene expression and, thus, type 3-dependent secretion was not restored (Fig. 10B).

As a next step, time course analysis of *sctJ* expression was performed under two different conditions; the first of them allowed determining how fast the P_{araBAD} promoter was induced while the second permitted to assess the repressing effect of D-fucose on gene expression. Two individual cultures of the selected *Salmonella* strains were cultured under standard SPI-1 inducing conditions for 2.5 h and then both cultures were supplemented with 0.05 % L-arabinose to induce SctJ expression. Ninety minutes later, 0.1 % D-fucose was added to one culture to repress P_{araBAD} promoter and halt expression, whereas SctJ expression proceeded uninterrupted in the other culture. Samples were harvested at the indicated time points and subjected to SDS PAGE followed by immunodetection with polyclonal antibodies against SctJ. As seen in figure 10C and 10D, in the repressed state, P_{araBAD}-driven SctJ expression was tightly regulated and therefore SctJ was detected only 15 minutes after L-arabinose addition. Maximum level of expression was achieved within 30 minutes upon induction and the amount of produced SctJ remained stable over the following 120 minutes regardless of the presence of D-fucose. The SctJ signal changed little over the time following D-fucose addition, thus indicating it had no impact on SctJ stability (Fig. 10D).

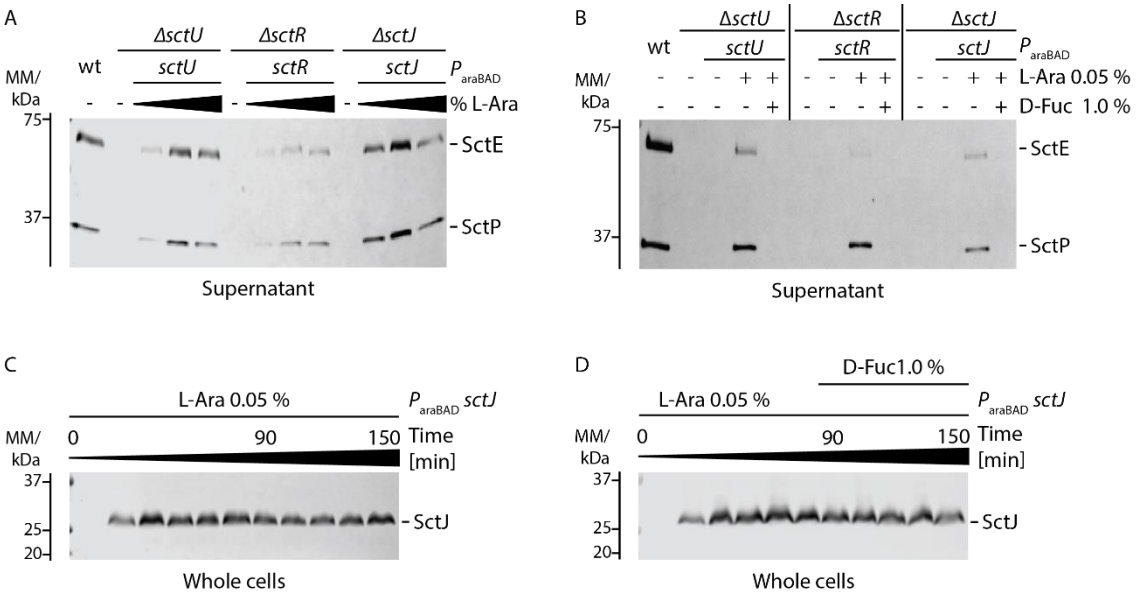

Fig. 10 Modulation of P_{araBAD}-driven expression of NC base components *sctR*, *sctU* and *sctJ*.
A. Immunoblotting analysis of SDS-resolved culture supernatants from *S.* Thyphimurium strains expressing *sctR*, *sctU* and *sctJ* from P_{araBAD} in a L-arabinose dose-dependent manner. The concentrations of inducer tested were 0.02 %, 0.05 % and 0.1 % (w/v). Presence of early and intermediate substrates SctP and SctE, repsectively was detected with polyclonal α-SctP and α-SctE antibodies. **B.** Immunodetection as in (A) but showing the effect of D-fucose repression of P_{araBAD}-driven *sctR*, *sctU* and *sctJ* expression on type 3-dependent secretion of SctP and SctE. **C.** Immunodetection of SctJ on western blots of whole cells lysates of a *Salmonella* strain expressing *sctJ* from P_{araBAD} analyzed by SDS PAGE. **D.** Immunodetection as in C but presenting repression of *sctJ* expression by D-fucose. Shown are immunoblots representative of three independent experiments.

Considering these results, both induction and repression periods were narrowed down to 60 minutes each. This implied more than enough time to guarantee maximal protein production/maturation and supply of the missing T3SS component required for full assembly of the NCs bases, which will be assessed in the following sections of this chapter.

Altogether, these results indicated that uncoupled expression of T3SS core components from the P_{araBAD} promoter-based expression system i) was susceptible to modulation over a comparatively wide range of inducer concentrations, ii) effectively complemented the respective knockout mutation in the chromosome, iii) did not present leaky expression in the repressed state and iv) was efficiently shut off upon addition of D-fucose.

4.1.4 Analysis of sorting platform mutants to activate and monitor type 3 secretion

Stable linkage between the IM substructure and the cytoplasmic components (SctK, SctL, SctN, SctO, and SctQ) is a crucial event that enables the NC to secrete proteins in a type 3-dependent fashion and to finalize its assembly by means of secretion and subsequent formation of the inner rod, needle and translocation pore (Hu et al., 2015, 2017). In *Salmonella*, the presence of all cytoplasmic components is essential for their recruitment to the NC base and therefore regulation of the expression of individual components provides a convenient tool to control the onset of secretion (Zhang et al., 2017).

A quick and sensitive luciferase-based secretion assay was combined with a plasmid-based expression system to activate and monitor secretion in *Salmonella* strains individually lacking the cytoplasmic components (Fig. 11A). Illustration of the experimental setup is shown in figure 11C, standard secretion assays were performed to assess SPI-1 T3SS functionality of mutants individually lacking the cytoplasmic components and expressing the respective component from a L-rhamnose-inducible promoter, P_{rhaBAD}, on pT10-based plasmid. Proteins secreted to the extracellular medium were detected by SDS PAGE, Western blotting and immunodetection. L-rhamnose-dependent expression of the five sorting platform components efficiently restored secretion of early, intermediate and late substrates, except for the *sctK* complemented strain, which failed to secrete middle and late substrates (Fig. 11B and D). Furthermore, to characterize the secretion kinetics of substrates, a transcriptional fusion of the luciferase Nanoluc (NLuc) to the effector protein SipA was integrated into the chromosome of the five *Salmonella* null mutants and time course luciferase-based secretion assays were carried out (Westerhausen et al., 2020). As seen in figure 11D, all five sorting platform mutants were secretion deficient, as previously reported, therefore, no luciferase activity was detected in the extracellular medium. In contrast, the pattern of SipA-NLuc secretion exhibited by the five complemented strains presented an initial lag phase during which the luminescent signal was low and remained constant, followed by a phase during which, 20 minutes upon

L-rhamnose addition the extracellular signal from SipA-NLuc rapidly increased over the time. Sole exception was the *sctK* complemented strains in which the signal changed little over time; observation consistent with the displayed secretion profile. A clear third phase was exhibited by strains expressing SctL and SctO and, to a lesser extent, by those expressing SctN and SctQ, in which the luminescent signal flattened, presumably due to high luciferase activity and consequent substrate depletion. In general, strains expressing SctL, SctN, SctO and SctQ showed similar SipA-NLuc secretion kinetics and secretion profiles. Hence the most suitable component to activate secretion of substrates and to be included in the synchronization system was identified by means of practical considerations: SctK, SctL and SctO were excluded to avoid disturbances in cytoplasmic subcomplexes formation since they are core components of the sorting platform proved to interact with one another forming a stable subcomplex that recruits SctN and SctO to complete the cytoplasmic substructure (Zhang et al., 2017). In addition, SctK was ruled out due to its plausible role in secretion specificity regulation. SctO was discarded since its absence only slightly decreased the formation of sorting platform subcomplexes (Zhang et al., 2017).

As a proof of concept, SctN was selected to determine whether upon its induction by L-rhamnose the secreted substrates could assemble into extracellular needle structures in wild type and Δ*sctP* (needle length regulator) genetic backgrounds. To this end, bacterial cells were cultured as described in figure 11C and two hours after onset of secretion, samples were harvested to purify NCs and visualize them by TEM. Electron micrographs showed basal bodies structures and fully assembled NCs attached to needles of regular length in the wild type strain, whereas deletion of the needle length regulator, SctP, resulted in the distinctive abnormally long needle filaments detached from the base (Fig. 11E).

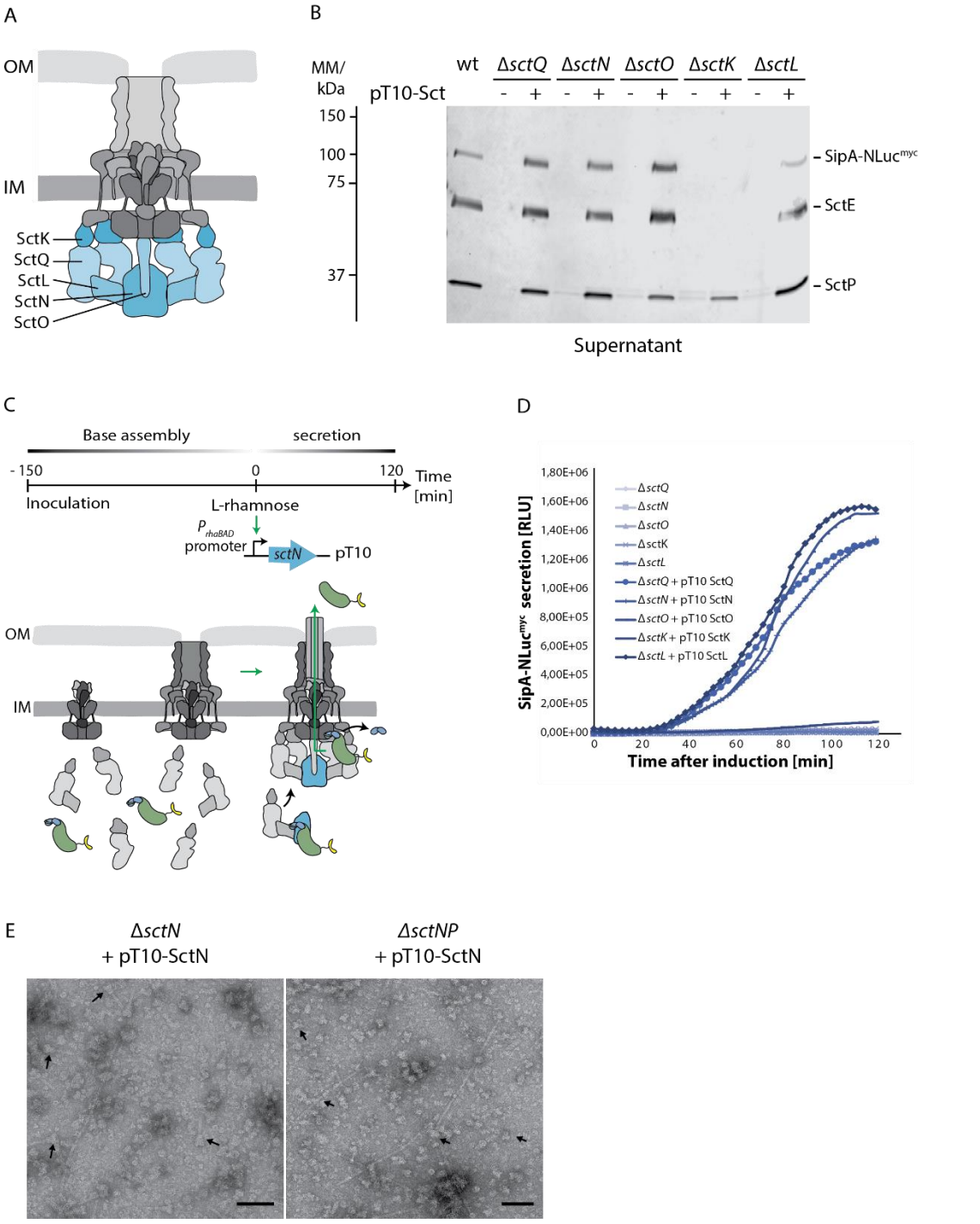

Fig. 11 Type 3 secretion functionality of sorting platform mutants.
A. Illustration of the T3SS sorting platform components depicted in blue shades. **B.** Immunodetection of SctP, SctE and SipA-NLuc^{myc} in SDS PAGE and Western blot analysed culture supernatants from indicated *S.* Typhimurium strains. pT10-based complementation is indicated with a + mark. **C.** Schematic overview of the experimental setup followed to monitor secretion over time: *Salmonella* mutants were cultured for 2.5 h under standard SPI-1 inducing conditions to allow NC base assembly, then pT10-based expression of *sctK*, *sctL*, *sctN*, *sctO* and *sctQ* was induced by addition of L-rhamnose to trigger secretion of SipA-NLuc^{myc}. **D.** Time course secretion of SipA-NLuc^{myc}, luciferase activity was quantified in the culture supernatant at different time points after L-rhamnose addition. **E.** Transmission electron micrographs of purified NCs. Single Δ*sctN* and double Δ*sctN,* Δ*sctP Salmonella* strains were grown as described in C and 2 h after L-rhamnose addition bacterial cells were harvested to isolate NCs and visualize them by TEM. Bar 100 nm. Shown are immunoblots and luciferase assays representative of three independent experiments.

4.1.5 Synchronization system setup and proof of concept

With the purpose of constructing the genetic synchronization system, a collection of *Salmonella* strains by sequential allelic exchanges. The resulting genetic backgrounds enabled to exploit the compatibility of the P_{araBAD} and P_{rhaBAD} promoters to uncouple expression of the T3SS elements and achieve coordinated formation of NCs bases and secretion of substrates. As a first step, the *araC*-P_{araBAD} expression system was inserted into the chromosome of *Salmonella* mutants lacking *sctN* and *sctR*, *sctU* or *sctJ*. Then, a transcriptional fusion of NLuc to SctA was introduced. Considering that unlike the effector protein SipA, the needle tip protein SctA is a T3SS structural component and its secretion is independent of host cell contact, it seemed rather convenient using SctA to monitor type 3 secretion in a synchronized scenario (Lunelli et al., 2011; Rathinavelan et al., 2014).

Deletion of *sctN* from the chromosome was complemented in trans from a low-copy plasmid (pT10). Figure 12 illustrates the synchronization system: bacterial cultures were inoculated and grown under SPI-1 inducing conditions for 2.5 h, during which all T3SS elements were produced and formation of intermediate subcomplexes occurred. Once A_{600}=1.0 was reached, P_{araBAD}-driven expression of the missing component (SctR, SctU or SctJ) was induced with L-arabinose. Of note, this newly produced component could not be incorporated in pre-existing subcomplexes, but rather was incorporated into *de novo* assembled NC bases (Wagner et al., 2010). Media was then supplemented with D-fucose to repress gene expression from the P_{araBAD} promoter and to cut off the component supply, which in turn hindered further assembly of complete bases and brought the assembly pathway back to production of non-functional subcomplexes. Addition of L-rhamnose induced P_{rhaBAD}-driven expression of *sctN* to complete the sorting platform and triggered type 3-dependent secretion of SctA-NLuc, which was monitored via the luciferase-based secretion assay.

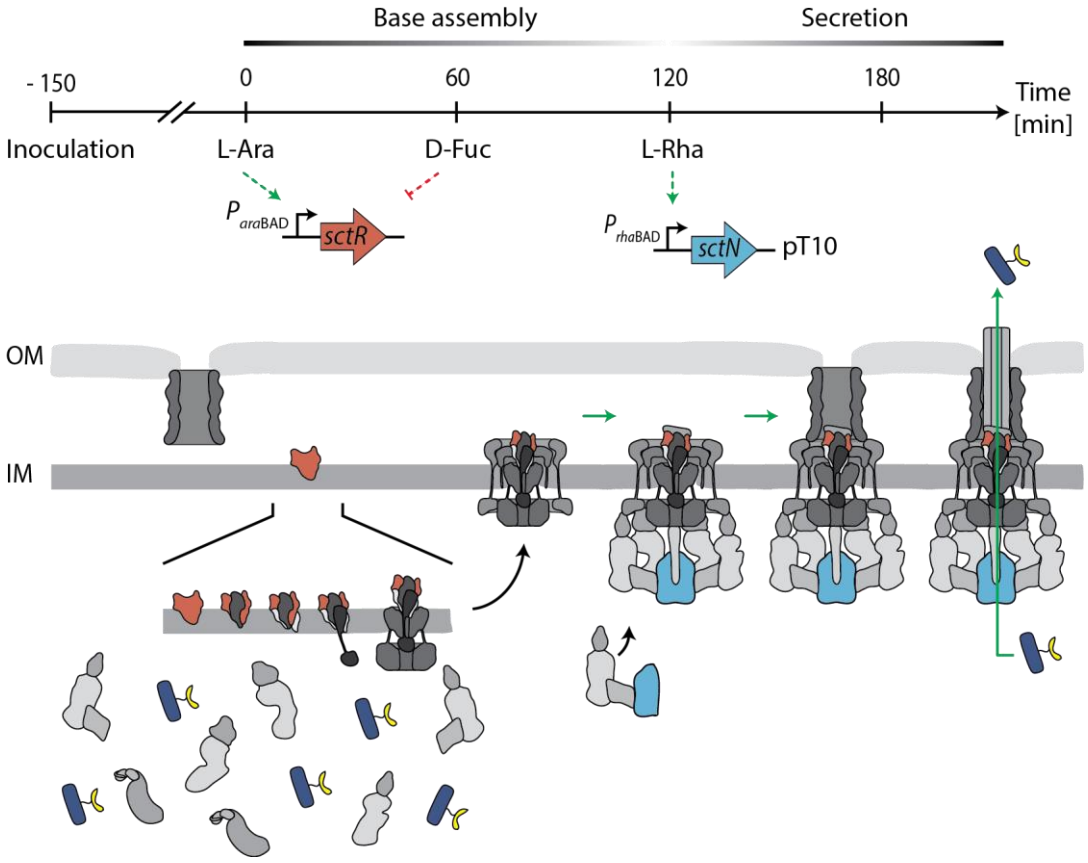

Fig. 12 Synchronization system.
Schematic overview of the synchronization system setup. Bacterial cultures are grown under SPI-1 inducing conditions for 2.5 h, during which formation of intermediate T3SS substructures occurs. Once A_{600}=1.0 is reached, P_{araBAD}-driven expression of the missing component, in this case SctU, is induced with L-arabinose and the newly produced component is incorporated into de novo assembled bases. Supplementation of the media with D-fucose represses gene expression from the P_{araBAD} promoter and stops further assembly of complete bases. L-rhamnose-induced expression of SctN from P_{rhaBAD} enables completion of the sorting platform and onset of type 3-dependent secretion of SctA-NLuc^{myc} into the culture supernatant, which is monitored via the luciferase-based secretion assay.

Following the experimental setups illustrated in figure 12, a series of synchronization assays were conducted to evaluate efficiency of *de novo* assembly of NCs and their functionality under different conditions. To this end, *Salmonella* strains were grown under SPI-1 inducing conditions to an A_{600}=1.0, then bacterial cultures were supplemented as follows: i) no addition of sugars to keep P_{araBAD} and P_{rhaBAD} in repressed state, under which scenario neither efficient NC assembly nor protein secretion was permitted (Fig. 13A), ii) sequential addition within two hours gap of L-arabinose and L-rhamnose to induce P_{araBAD}/P_{rhaBAD}-driven gene expression, respectively. This allowed uninterrupted assembly of complete NC bases and later onset of secretion (Fig. 13B), and iii) addition of L-arabinose and D-fucose to narrow down gene expression from

P_{rhaBAD} and NC base assembly, followed by later addition of L-rhamnose to induce *sctN* P_{araBAD}-driven expression and render NCs competent for secretion of substrates (Fig. 13C). Samples were harvested at the indicated time points and subsequently NC bases-containing membranes were purified. NC base assembly and composition was analyzed by BN and SDS PAGE, followed by immunodetection with polyclonal antibodies raised against SctJ and SctD (Fig. 13D). After L-rhamnose addition, secreted SctA-NLuc^{myc} into the culture supernatant was detected and tracked over time employing the luciferase-based secretion assay (Fig. 13E).

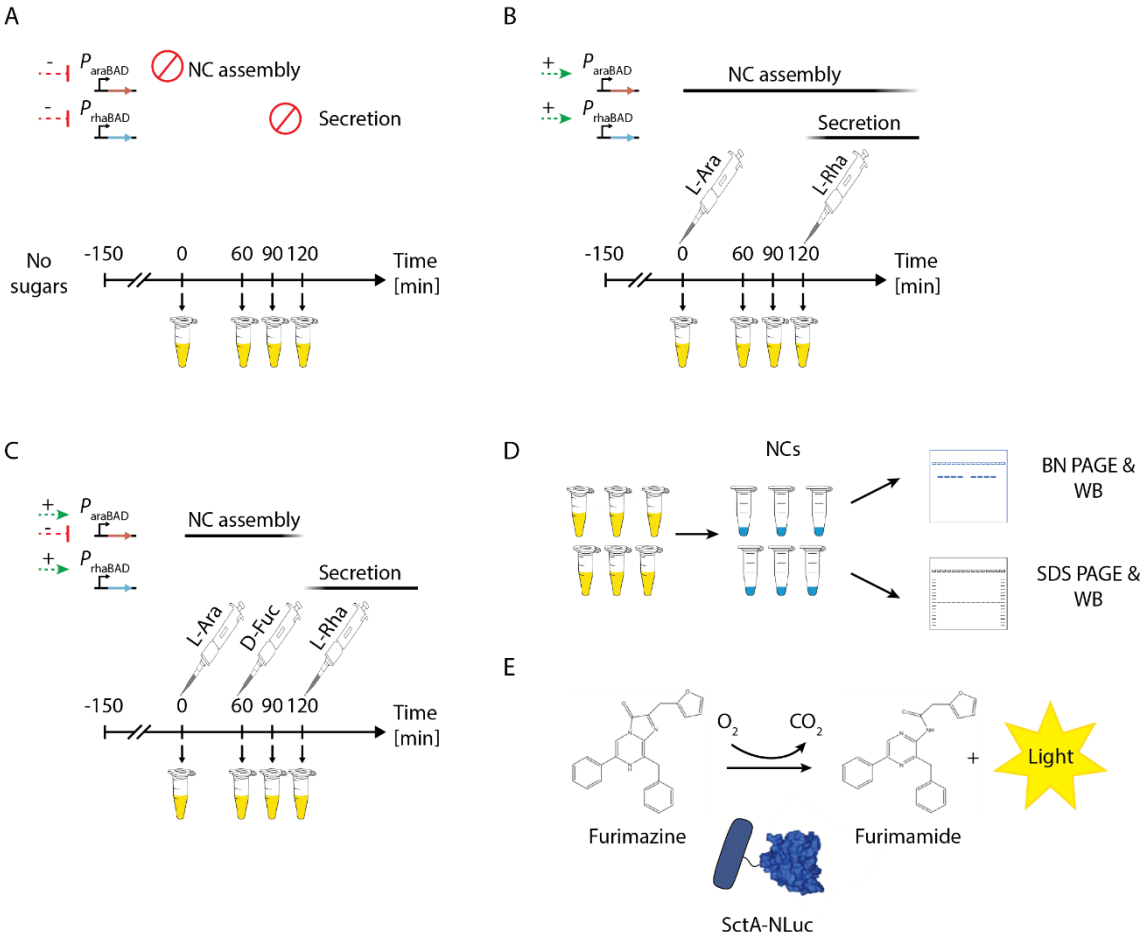

Fig. 13 Schematic overview of the synchronization assays performed under different conditions. **A.** *S.* Typhimurium strains are grown under SPI-1 inducing conditions to an A_{600}=1.0. Then, bacterial cultures are let grow in the absence of any sugar to keep P_{araBAD} and P_{rhaBAD} in a repressed state, which results in neither base assembly nor type 3 secretion **B.** Sequential addition of L-arabinose and L-rhamnose to induce P_{araBAD}/P_{rhaBAD}-driven gene expression, respectively, allows uninterrupted base assembly and later onset of type 3 secretion. **C.** Addition of L-arabinose and D-fucose narrows down gene expression from P_{rhaBAD} and base assembly. Later addition of L-rhamnose induces *sctN* P_{araBAD}-driven expression and turns NCs competent for type 3-dependent secretion of substrates. **D.** Samples are harvested at the indicated time points and NC bases are purified to be analyzed by BN and SDS PAGE, followed by immunodetection. **E** After L-rhamnose addition, secreted SctA-NLuc^{myc} into the culture supernatant is detected and tracked over time via the luciferase-based secretion assay.

Deletion of *sctR* and *sctU* led to a drastic reduction in assembly of NC bases, but did not abrogate it completely, since small amounts of bases were detected under native conditions in the P_{araBAD} repressed state, and accumulated over time (Fig. 14A), in agreement with previous reports (Wagner et al., 2010). P_{araBAD}-driven production of SctR, SctU and SctJ, efficiently promoted de novo assembly of NC bases and generated the largest amounts within 60 min after L-arabinose addition and persisted over the time at similar levels in both P_{araBAD} *sctU* and *sctJ* strains, but slightly decayed in the *sctR* mutant (Fig. 14A). Further resolution of the assembled bases into their individual components by denaturing SDS PAGE and immunodetection revealed the presence of SctJ and SctD (IM ring structures subunits). Under all tested conditions, the amounts of SctD subunits (outer IM ring) in crude membrane preparations were proportional to the amounts of bases assembled, which confirmed the multiprotein character of the observed NCs bases (Fig. 14A).

Fully assembled NC bases resulting from P_{araBAD}-driven expression of *sctR*, *sctU* and *sctJ,* enabled the secretion of proteins into the culture supernatant only after L-rhamnose-induced expression of the ATPase SctN, as in absence of the P_{rhaBAD} inducer the luminescent signal was negligible and remained steady (Fig. 14B left plot). The luminescence increased in a time-dependent manner after induction of SctN expression, indicating secretion of SctA-NLuc (Fig. 14B). Significant increase in the luminescent signal was observed 15 min after L-rhamnose addition in both *sctR* and *sctU* mutants, whilst in the *sctJ* background the increase was delayed and occurred 10 min later (Fig. 14B left plot). Comparable results were obtained with the luciferase-based secretion assay when gene expression from P_{araBAD} was restricted to 1 h by supplementing bacterial cultures with D-fucose. However, the detected luciferase activity was 10 times lower when than the one observed when P_{araBAD} was continuously induced (Fig. 14B right plot).

To corroborate that the conditions used to achieve synchronized base assembly and secretion onset generated complete NCs, a large scale synchronization assay was performed following the experimental setup showed in figure 14C. 60

minutes after onset of secretion, bacterial cells were harvested and assembled NCs were isolated and visualized by TEM. As seen in figure 14C, despite the fact that it was possible to obtain fully assembled NCs, a generalized low yield of complexes was obtained from the three P_{araBAD} strains in the wild type background, and even lower in the context of deregulated needle length, i.e. Δ*sctP* strain, where only one base attached to an abnormally long needle filament was observed (Fig. 14C indicated with black arrows).

Altogether, these results proved the synchronization system suitable for studying secretion regulatory processes involved in T3SS biogenesis such as secretion specificity switching, but not for structural analysis that require large amount of complexes.

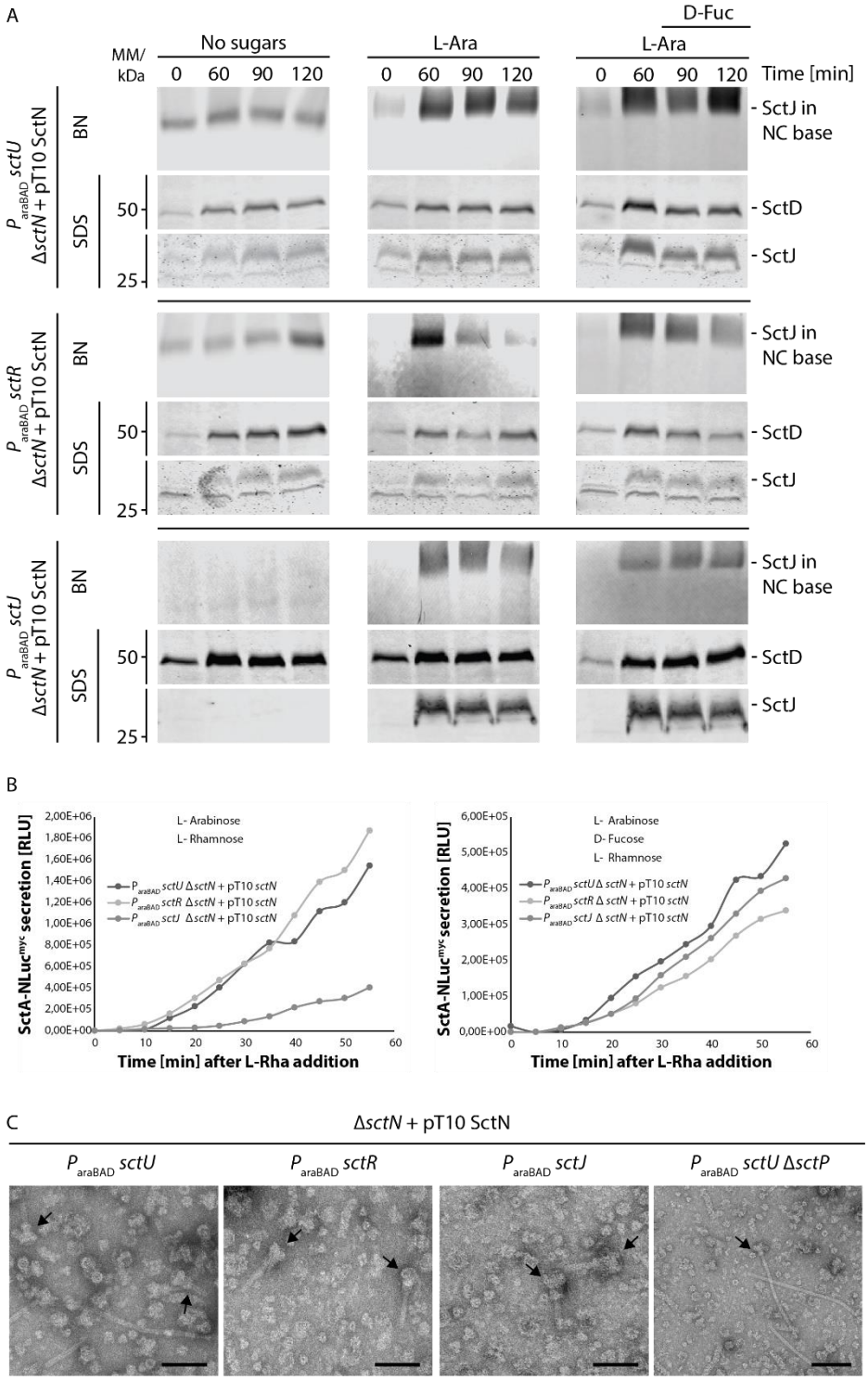

Fig. 14 Synchronized assembly of NC bases and onset of secretion in strains harbouring the *P*araBAD expression cassette within the MIS.
A. Immunodetection of SctJ and SctD in Western blots of SDS and BN PAGE-resolved NC bases isolated from the indicated *P*araBAD, Δ*sctN S.* Typhimurium strains cultured under different conditions. **B.** Secretion functionality of the same strains as in A. SctA-NLuc^{myc} secretion was monitored via quantification of luciferase activity in the culture supernatant over time after L-rhamnose-induced SctN expression. **C.** Transmission electron micrographs of NCs purified from indicated the strains indicated in A and the double mutant Δ*sctN,* Δ*sctP P*araBAD *sctU*. Bar 100 nm. Shown are immunoblots and luciferase assays representative of three independent experiments.

4.2 Optimization of the P_{araBAD}-based synchronization system

As an extension of the first chapter, this second section of results thoroughly describes the strategy developed to optimize the formerly implemented P_{araBAD}-based synchronization system. In the previous proof of principle experiments TEM analysis revealed that low yield of fully assembled NCs was the biggest shortcoming of the synchronization system, limiting its use in structural analyses. Therefore, a number of optimization steps were performed with the purpose of increasing the number of NC obtained with this approach. Results presented in this chapter are not published.

4.2.1 Expression of NC components from the P_{araBAD}-based expression cassette contained within the SPI-1 insertion site

All structural components of the T3SS are encoded within the *S.* Typhimurium SPI-1 and are expressed simultaneously in response to environmental conditions that resemble the host intestinal lumen (de Nisco et al., 2018). Analysis of the genetic organization of SPI-1 revealed the presence of several operons in which functionally related genes are clustered in order to coordinate their expression (Collazo and Galán, 1996). The T3SS components SctR, SctS, SctT and SctU are encoded within a single operon. This gene organization presumably mediates their temporally and spatially coordinated expression, which in turn facilitates their simultaneous targeting to the IM, where they interact with one another to assemble the export apparatus (Collazo and Galán, 1996). Hence, we hypothesized that the low yield of injectisomes obtained via the synchronization system was due to the different IM localization of the export apparatus components encoded within the SPI-1 and the MIS, respectively, which hindered their association and recruitment into the IM complex.

In an attempt to test this hypothesis and to increase the likelihood of encounter of all five export apparatus components, the first optimization step consisted in transferring the P_{araBAD}-based expression cassette along with its target gene from the MIS to an integration site withing the SPI-1 (SPI-1 IS). The extent of complementation of secretion functionality achieved via P_{araBAD}-based SctU and

SctR expression from the SPI-1 IS was evaluated and compared to the MIS. Standard secretion assays were performed growing the four P_{araBAD} mutants in the presence of increasing concentrations of L-arabinose (0.02 %, 0.05 % and 0.1 % [w/v]) to induce P_{araBAD}-driven gene expression. In agreement with the aforementioned results, L-arabinose-dependent expression of *sctU* and *sctR* from the SPI-1 IS restored secretion of early (SctP) and intermediate substrates (SctE and SctA-NLuc^{myc}) in a dose-dependent manner, reaching the highest level of secretion when bacterial cultures were supplemented with 0.1 % L-arabinose (Fig. 15A). No substantial difference was observed between the level of complementation achieved with P_{araBAD}-driven expression of *sctU* and *sctR* from the SPI-1 IS and the MIS (Fig. 15A). Considering these results, 0.05 % was selected as the optimal concentration of L-arabinose to be used in further experiments.

In order to confirm that the P_{araBAD} promoter located within the SPI-1 IS was susceptible to negative regulation by D-fucose, the four *S.* Typhimurium mutants harbouring the P_{araBAD}-based expression cassette were cultured under SPI-1 inducing conditions in the presence or absence of L-arabinose and D-fucose as indicated in figure 15B. The secretion of proteins into the culture supernatant was detected following standard procedures. As seen in figure 14B, *sctR* expression from P_{araBAD} was efficiently repressed by D-fucose irrespectively of the locus were the expression cassette was inserted. In contrast, small amounts of substrates were present in the culture supernatants of both P_{araBAD} *sctU* mutants even when the promoter was in the repressed state (presence of D-fucose), indicating leaky expression from the L-arabinose inducible promoter (Fig. 15A and 15B).

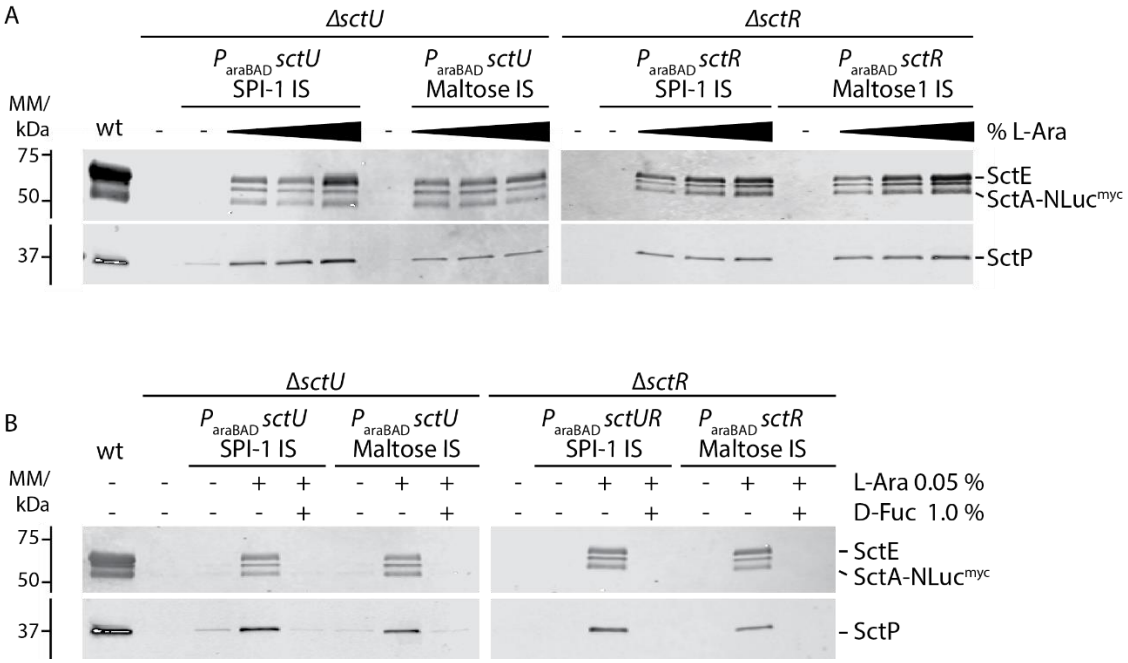

Fig. 15 Modulated expression of NC base components from the P_{araBAD} expression cassette contained within the SPI-1 insertion site.
A. Immunoblotting analysis of SDS-resolved culture supernatants from the indicated *S.* Thyphimurium P_{araBAD} strains. Expression of *sctU* and *sctR* was induced with increasing concentrations of L-arabinose (0.02 %, 0.05 % and 0.1 % [w/v]). Presence of early, intermediate and late substrates SctP, SctE and SctA-NLuc^{myc}, respectively, was detected with anti SctP, anti SctE and anti myc antibodies. **B.** Immunodetection as in A but showing D-fucose negative regulation of P_{araBAD}-driven expression of *sctU* and *sctR*. Shown are immunoblots representative of four independent experiments.

4.2.2 Onset of type 3 secretion in NC bases assembled in a synchronized fashion

With the aim of assessing whether shifting the integration site of P_{araBAD}-based expression cassette positively affected the yield of fully assembled NCs, the two recently generated P_{araBAD} *sctU* and *sctR* mutants were devoid of *sctN* and complemented *in trans* via expression of SctN from a pT10-based construct. Regular synchronization assays were performed following the experimental procedures described in figure 13, where assembly of NC bases in the P_{araBAD} mutants was examined under three different conditions i) absence of inducers to determine basal assembly, ii) sequential induction of P_{araBAD} and P_{rhaBAD}-driven gene expression to allow uninterrupted assembly and onset of type 3 secretion, and iii) controlled P_{araBAD}-based gene expression to mediate synchronized assembly and later activation of P_{rhaBAD} to initiate secretion of substrates. Samples were harvested at indicated the time points to purify crude membranes

and immunodetect assembled NCs bases in their native configuration. Subsequently, type 3-dependent secretion of SctA-NLuc^{myc} was activated and monitored for 1 h. Under the first tested condition in which the L-arabinose inducible promoter remained in the repressed state and resembled the Δ*sctU* and Δ*sctR* genetic backgrounds, NC bases were assembled with low efficiency and accumulated over the time at similar levels in all strains (Fig. 16A left side). On the contrary, P_{araBAD}-driven expression of *sctU* from the SPI-1 IS resulted in enhanced *de novo* assembly of bases when compared to the original strain (Fig. 16A centre and left side). However, this improvement had no impact on secretion as the curves that described SctA-NLuc^{myc} secretion in both *sctU* mutants were virtually indistinguishable (Fig. 16B left plot). Interestingly, in the new *sctR* mutant neither NC base assembly nor secretion functionality was enhanced but rather slightly diminished (Fig. 16A and 16B right plot).

Finally, large scale synchronization assays were carried out to investigate how transferring the P_{araBAD}-based expression cassette to the SPI-1 affected NCs assembly. As mentioned before, the synchronization system was developed with the aim of providing insight into the mechanistic details of needle length regulation and secretion specificity switching, thus the needle length regulator *sctP* was deleted in both *sctU* Δ*sctN* and *sctR* Δ*sctN* mutants to prove the feasibility of the system. TEM analysis of complexes purified from both *sctN* null mutants revealed the presence of few NCs completely assembled and some bases lacking an attached needle filament (Fig. 16C). Unfortunately, in the Δ*sctP* backgrounds no NC with abnormally long needle were observed. Overall, no relevant improvement in neither yield of NC nor in secretion functionality was obtained with this first step of optimization.

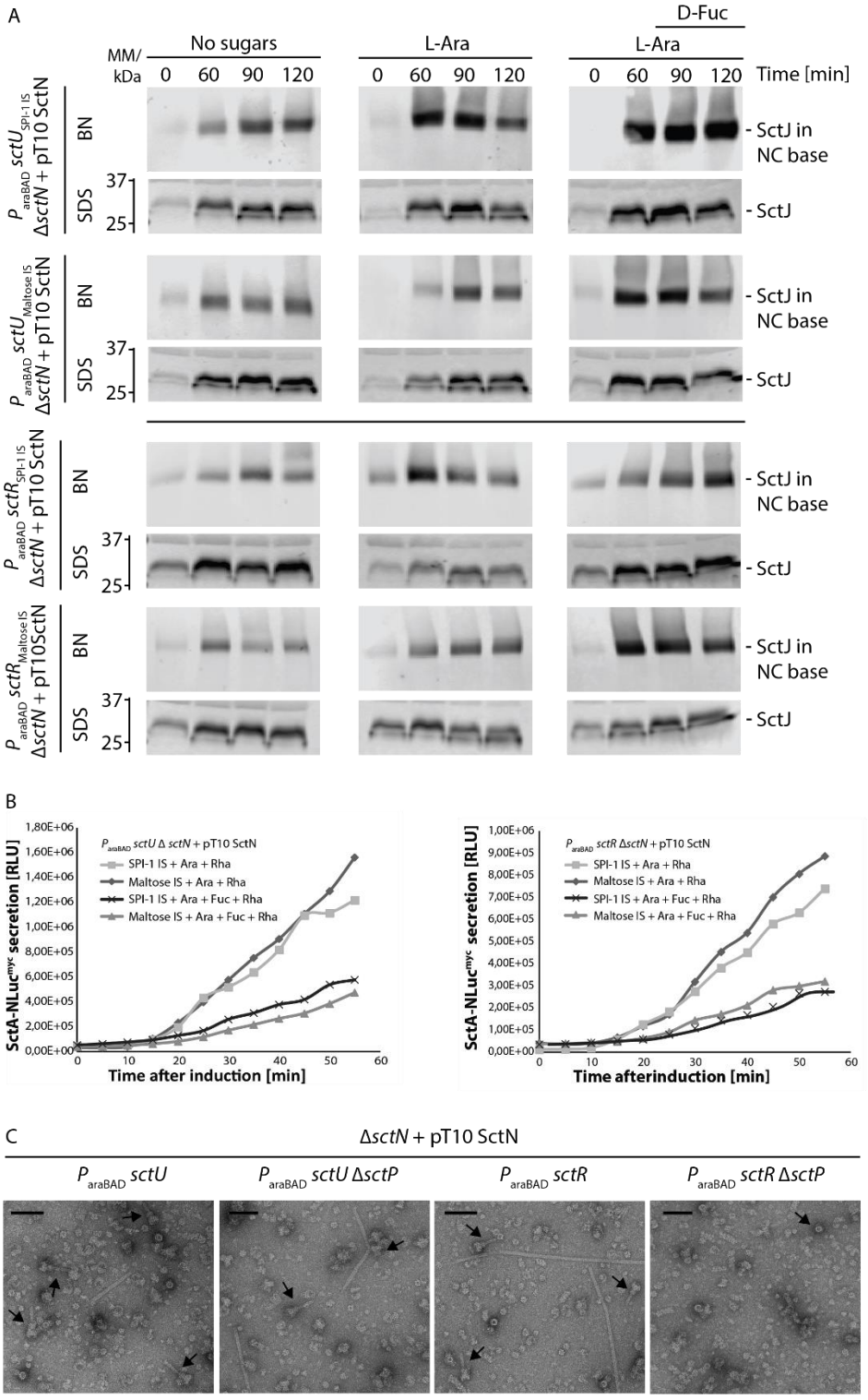

Fig. 16 Synchronized assembly of NC bases and onset of secretion in strains containing the *P*araBAD expression cassette within the SPI-1 and maltose insertion sites.
A. Immunodetection of SctJ in Western blots of SDS and BN PAGE-resolved NC bases isolated from the indicated *P*araBAD, Δ*sctN S.* Typhimurium. strains cultured under different conditions. **B.** Secretion functionality of the same strains as in A. SctA-NLuc^{myc} secretion was monitored via quantification of luciferase activity in the culture supernatant over time after induction of rhamnose-dependent expression of SctN. **C.** Transmission electron micrographs of NCs purified from the strains indicated in A and the double mutant Δ*sctN,* Δ*sctP P*araBAD *sctU*. Arrows indicate fully assembled NCs and NC bases. Bar 100 nm. Shown are immunoblots and luciferase assays representative of three independent experiments.

4.2.3 Coupling of SctC assembly with onset of type 3 secretion

Recent cryo-EM studies elucidated the atomic structure of the injectisome OM secretin ring revealing discrete structural changes of the SctC periplasmic gate in response to the assembly of the inner rod and needle structures (Hu et al., 2018; Hu et al., 2019). These observations gave rise to a two-stage model to explain the mechanism of substrate-mediated opening of the SctC periplasmic gate (Fig. 17). In an early stage, prior to type 3-dependent secretion of substrates, the periplasmic gate is in a closed conformation (Fig. 17 I). Initial secretion and assembly of the inner rod and the needle within the secretin lumen induce conformational changes in SctC and allosterically unlock the gate (Fig. 17 II). Further polymerization of SctI protomers into the needle filament provides supplementary energy to sterically push the gate open (Fig. 17 III). The fully open periplasmic gate accommodates the needle filament to anchor it and to give continuity to the secretion conduit (Fig. 17 IV).

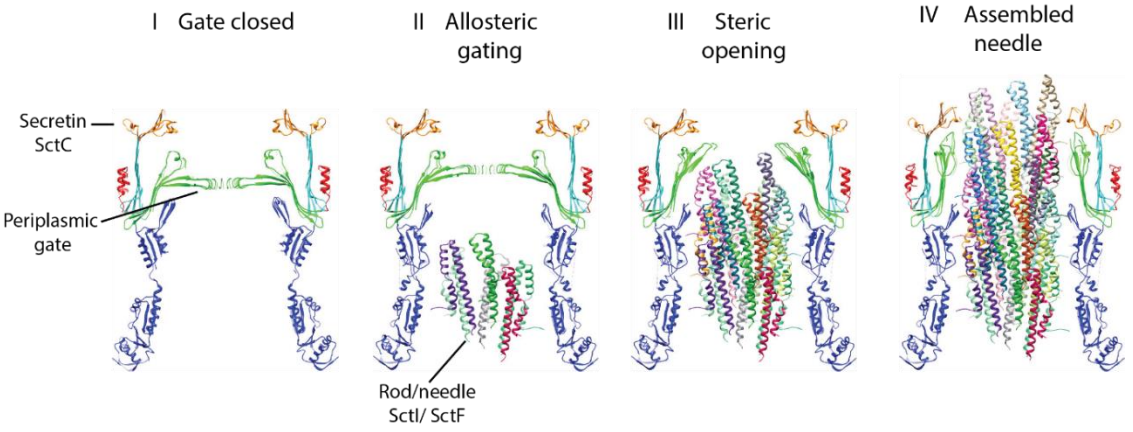

Fig. 17. Simplified illustration of the mechanism of substrate-mediated SctC periplasmic gate opening[5].
I. Prior to activation of secretion of substrates the periplasmic gate is in a closed conformation. **II.** Initial secretion and assembly of the inner rod and needle filament SctI and SctF, respectively, induce conformational changes in SctC, which in turn trigger an allosteric transition that unlock the gate. **III.** Further assembly of the needle filament within SctC sterically pushes the periplasmic gate open. **IV.** The fully open gate accommodates the needle filament in the SctC lumen to continue the secretion conduct.

According to this model, completion of the NC base is a prerequisite for active secretion of proteins in a type 3-dependent manner. However, during the development of this study secretion and assembly of the inner rod protein SctI were proven to occur independently of the secretin (Fig. 26), in the synchronize

[5] Fig. 17 has been published in Nat. Microbiol. by Hu et al., 2018, and adapted for its use in this thesis.

scenario this is likely to occur if fully assembled IM substructures of the base become secretion competent before recruitment of the secretin ring, hence the question arises, is assembly of the secretin and opening of its periplasmic gate hindered by prior assembly of inner rod/needle structures? In order to address this question, a collection of four pT10-based tricistronic constructs encoding the ATPase SctN, the secretin SctC and the pilotin InvH, which aids assembly of SctC in the OM, was generated to complement *in trans* the *sctC sctN* double deletion mutant carrying P_{araBAD} *sctU* or P_{araBAD} *sctR*. A separate list containing detailed description of the tricistronic constructs used in this section is provided in table 4. The difference between these four constructs lies on the gene order and the sort of Shine-Dalgarno (SD) sequence located upstream of each gene; this strategy allowed increasing the odds of optimal expression of SctC and its efficient insertion in the OM.

Table 4. pT10-based tricistronic constructs encoding *sctN*, *sctC* and *invH*

ID	Inserts order	Description
pMIB7105	SctC, InvH, SctN	Native SD* (nSD) sequence upstream *sctC* and *invH* and optimized SD (oSD) sequence upstream *sctN*
pMIB7106	SctC, InvH, SctN	Optimized SD (oSD) sequence upstream *sctC*, *invH* and *sctN*
pMIB7107	SctN, SctC, InvH	Optimized SD (oSD) sequence upstream *sctN* and native SD (nSD) sequence upstream *sctC* and *invH*
pMIB7108	SctN, SctC, InvH	Optimized SD (oSD) sequence upstream *sctN, sctC* and *invH*

*SD (Shine-Dalgarno) sequences correspond to the ribosome binding sequences (RBS) either taken from the *S.* Typhimurium genome (native) or contained in the pT10 vector (optimized).

The four newly generated variants of the tricistronic pT10-based construct listed in table 4 were individually introduced into the double *sctC sctN* deletion mutants to investigate the extent of complementation of secretion functionality. For this purpose, standard synchronization assays were performed in accordance to the experimental setup illustrated in figure 18.

Once the IM substructure of the NC base is synchronously assembled, L-rhamnose is added to induce P_{rhaBAD}-driven coexpression of *sctN*, *sctC* and *invH* to coordinately activate secretion and initiate assembly of the secretin ring in the OM, respectively. Encounter of the IM and OM substructures completes assembly of the base and recruits SctN along with the rest of cytoplasmic components to initiate secretion of inner rod and needle subunits that assemble within the SctC lumen and initiate opening of the periplasmic gate. When fully open, the periplasmic gate lodges the needle filament, through which intermediate and late substrates can effectively travel. Secretion of SctA-NLuc^{myc} in a type 3-dependent fashion is monitored over the time the via luciferase-based secretion assay.

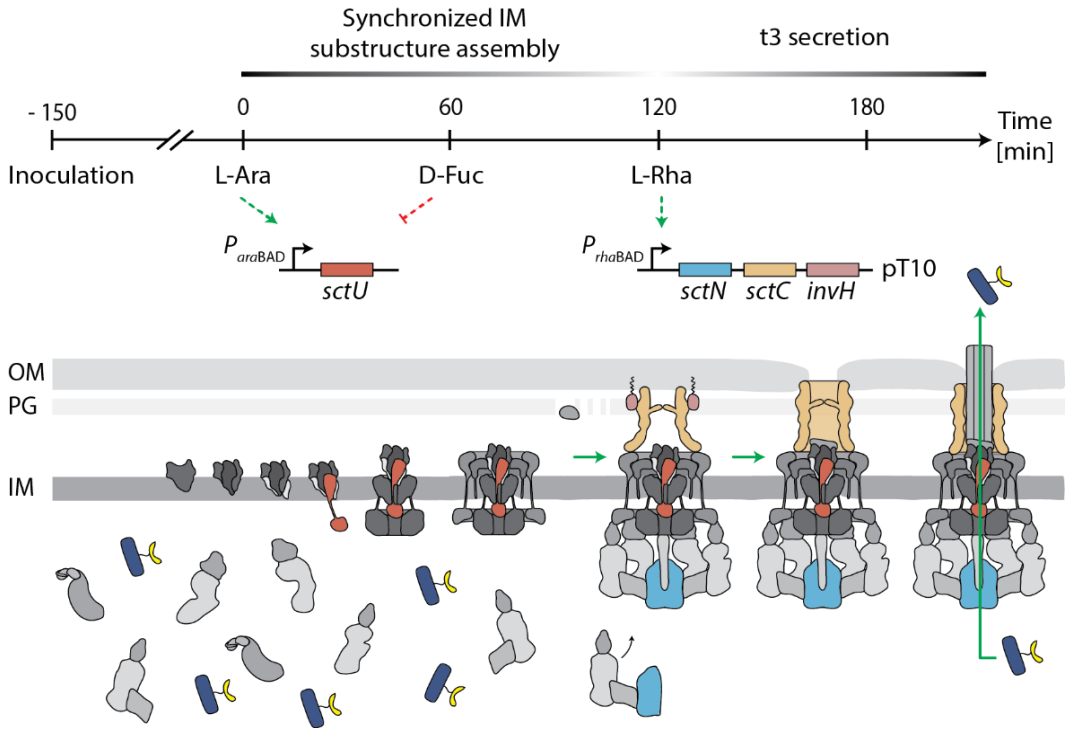

Fig. 18 Overview of the experimental setup for the synchronization assay.
S. Typhimurium Δ*sctC* Δ*sctN* P_{araBAD} *sctU* (or *sctR*) mutant strains each carrying one of the four tricistronic constructs encoding the ATPase *sctN*, the secretin *sctC* and the pilotin *invH*, is grown under SPI-1 inducing conditions for 2.5 h. In this initial stage formation of intermediate substructures takes place. Once A_{600}=1.0 is reached, P_{araBAD}-driven expression of *sctU* (or *sctR*) is induced with L-arabinose and the newly produced component is incorporated into *de novo* assembled IM subcomplexes. Supplementation of the media with D-fucose inactivates *sctU* expression and stops further assembly of IM subcomplexes. Addition of L-rhamnose induces expression of SctN, SctC and InvH from P_{rhaBAD}. This mediates formation of the secretin ring in the OM and enables completion of the sorting platform. Encounter of the IM and OM substructures finalizes NC base assembly and recruits SctN along with the rest of cytoplasmic components to initiate secretion of early substrates (inner rod and needle) that assemble within the SctC lumen and initiate opening of the periplasmic gate. Once fully open, the periplasmic gate lodges the needle filament to facilitate the transit of intermediate and late substrates. Secretion of SctA-NLuc^{myc} into the culture supernatant is monitored for 2 h via the luciferase-based secretion assay.

Efficient substrate-mediated opening of the SctC periplasmic gate and, consequently, complete assembly of injectisomes are expected to be accomplished via sctN and sctC co-expression.

In the wild type P_{araBAD} strains the curve that describes SctA-NLuc^{myc} secretion presented a lag phase (~6 minutes) after which the luminescent signal rapidly increased and flattened after 90 and 110 minutes in the *sctU* and *sctR* mutant respectively, owing to depletion of the luciferase substrate (Fig 19A and 19B). In contrast, in both single Δ*sctN* mutants, the luminescent signal exhibited an extended lag phase of approximately 20 minutes before the signal increased exponentially (Fig 19A and 19B). Surprisingly, pT10-based complementation of the *sctN sctC* double deletion mutants poorly restored the secretion functionality when compared to wild-type and complemented *sctN* null strains. Moreover, it was not possible to discern the levels of complementation achieved with the four tested constructs, therefore the boxed areas in figure 19A and 19B were magnified. As shown in figures 19C and 19D, the luminescent signal of SctA-NLuc^{myc} into the culture supernatant remained steady during 30 minutes after P_{rhaBAD}-driven expression of *sctN* and *sctC* was induced. This time frame was ~50 % longer than that of the single *sctN* mutant and represented the time required for assembly of the secretin ring in the OM and, its association with the IM substructure to complete the NC base. Similar results were obtained from all four tested constructs.

In summary, rather than improving secretion functionality, coupled assembly of secretin ring and initiation of secretion significantly reduced the levels of secretion and noticeable extended the lag of its activation.

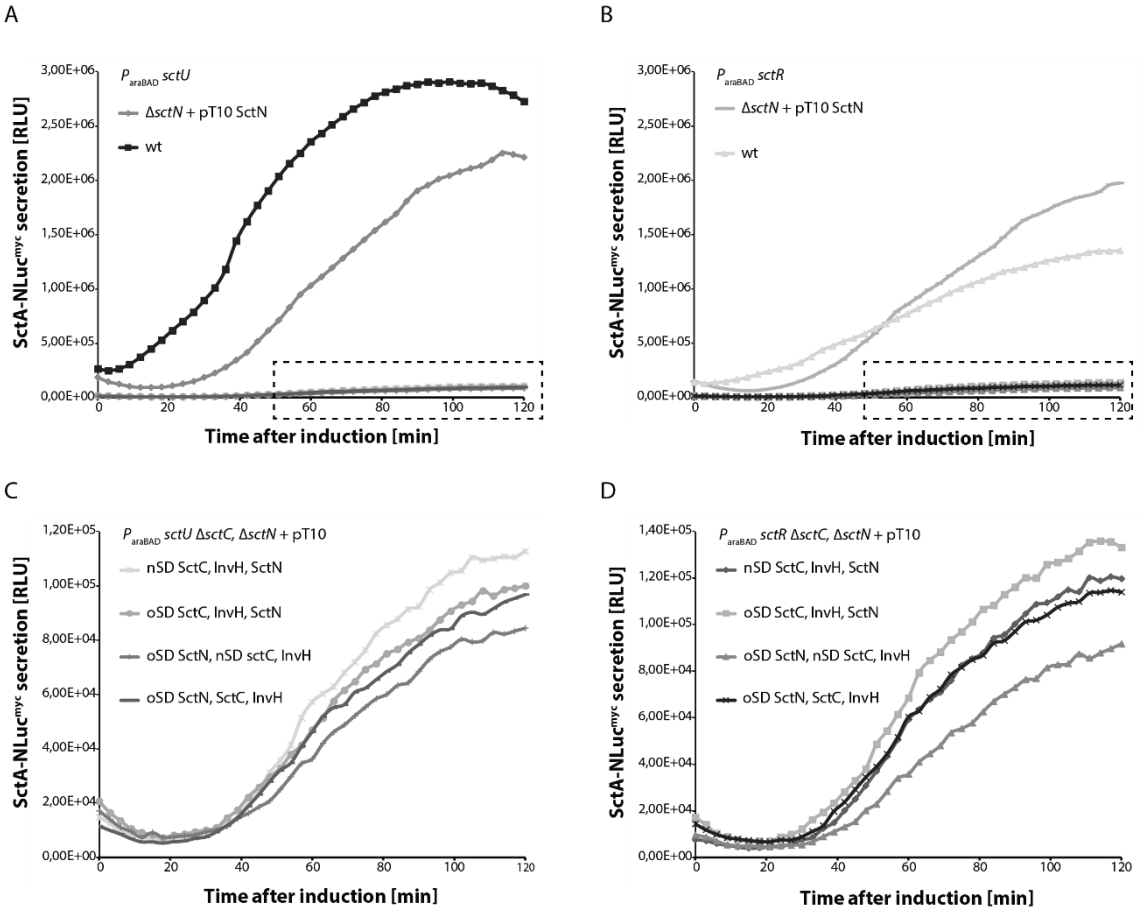

Fig. 19 Secretion functionality of *S.* Typhimurium Δ*sctN* Δ*sctC* P_{araBAD} double mutants.
A. SctA-NLuc^{myc} secretion into the culture supernatant of the P_{araBAD} *sctU* and the secretion deficient Δ*sctN* mutant expressing SctN from a pT10-based plasmid. Type 3-dependent secretion was activated via the induction of L-rhamnose-dependent expression of SctN. **B.** As in A but monitoring secretion functionality of the P_{araBAD} *sctR* strains. **C.** Zoom of the boxed area in A showing plasmid-based complementation of the Δ*sctN* Δ*sctC* P_{araBAD} *sctU* double mutant. Four tricistronic pT10-based constructs containing either native or optimized Shine Dalgarno (SD) sequences were used. SctA-NLuc^{myc} secretion was monitored via quantification of luciferase activity over time after L-rhamnose addition. **D.** As in C but zoom of the boxed area in B showing plasmid-based complementation of the Δ*sctN* Δ*sctC* P_{araBAD} *sctR* double mutant with the four tricistronic pT10-based constructs as indicated in C. Shown are luciferase assays representative of three independent experiments.

4.2.4 Deletion of the L-arabinose AraE transporting system

The several advantageous features of the P_{araBAD}-based expression system have been emphasized throughout this chapter; however, this expression system is fallible, and being prone to heterogeneous expression is its main shortcoming (Siegele and Hu, 1997). The uptake of the inducer L-arabinose occurs via both the low-affinity uptake system AraE and the high-affinity AraFGH transporter, the expression of which is under the control of the L-arabinose-inducible promoters P_E and P_{FGH}, respectively (Fig. 20A) (Binder et al., 2016; Schleif, 2000). The autocatalytic behaviour of the L-arabinose transporters is responsible for the

observed heterogeneous expression, termed all-or-none expression, in which a portion of cells in the bacterial population is fully induced while the rest is non-induced. The concentration of L-arabinose in the medium does not change the level of gene expression in the induced cells, instead it affects the portion of the population that is fully induced (Siegele and Hu, 1997). With the purpose of determining whether the inefficient assembly of the injectisomes and the low secretion activity observed in the synchronization assays were due to intermediate expression levels from the P_{araBAD} promoter, *araE* was deleted from the chromosome of the P_{araBAD} *sctU* and P_{araBAD} *sctR* strains. The most commonly used strategy to eliminate the all-or-none phenomenon is expressing the low-affinity uptake system encoded by *araE* from an arabinose-independent promoter (Khlebnikov et al., 2000, 2001). Unfortunately, this approach was not feasible for the complex genetic organization of the synchronization system that already exploits two compatible inducible promoters.

Following the experimental procedure illustrated in figure 20B, the assembly of NCs bases was synchronized in all P_{araBAD} *sctU* and P_{araBAD} *sctR* strains: the wil type, the Δ*sctN* and the Δ*sctN* Δ*araE*. Once type 3 secretion was activated via L-rhamnose-dependent expression of *sctN*, secretion of the intermediate substrate SctA-NLuc^{myc} was monitored via the luciferase-based secretion assay. Comparison of the luminescent signal detected into the culture supernatant of the P_{araBAD} *sctU* (or *sctR*) wild type strains and those devoid of *araE*, revealed that the signals differed in one order of magnitude with the Δ*araE* mutants exhibiting the highest levels of SctA-NLuc^{myc} secretion (Fig. 20C and 20D). Comparable results were observed in the complemented Δ*sctN* strains: deletion of *araE* resulted in a slightly higher luminescent signal but the increment was negligible (Fig. 20C and 20D).

These data show that overall elimination of the low-affinity AraE transporter positively affected the yield of fully assembled and functional injectisomes, as reflected by the improved secretion functionality.

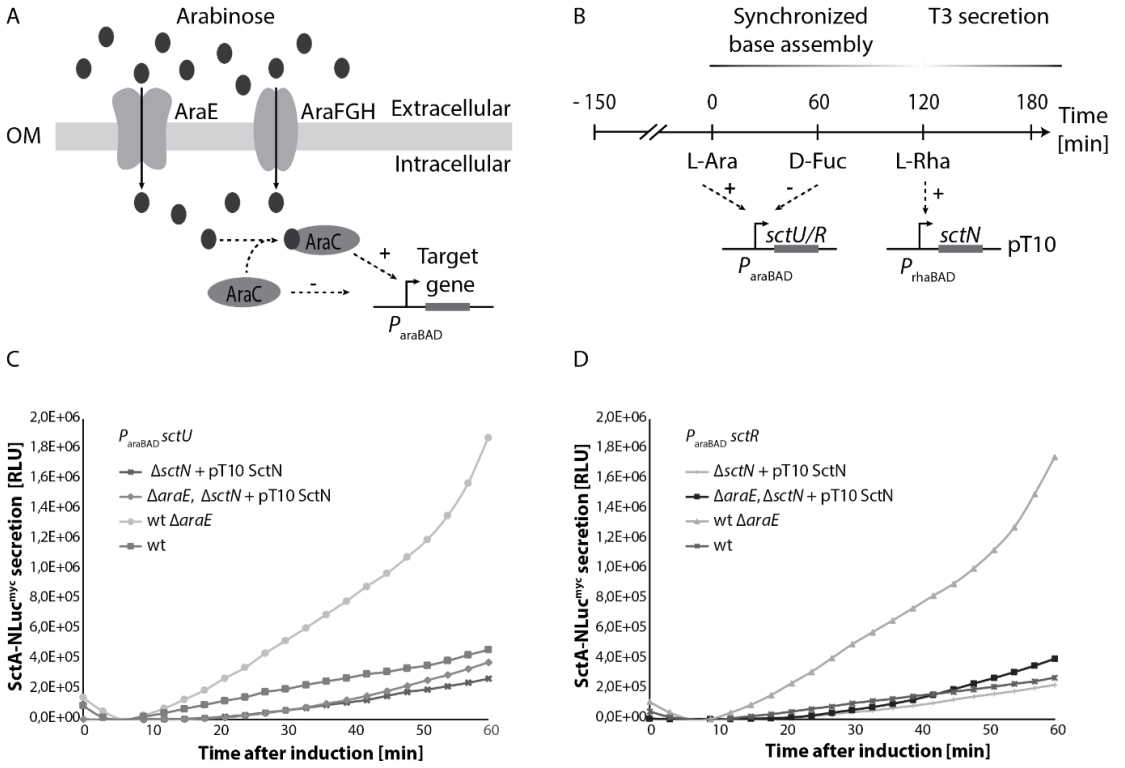

Fig. 20 Secretion functionality of *S.* Typhimurium P_{araBAD} strains devoid of the AraE transporter[6].
A. Simplified cartoon depicting the mechanism of active L-arabinose intake via the AraE and the AraFGH transport proteins, and regulation of P_{araBAD}-driven expression of the target gene. In the presence of L-arabinose AraC positively regulates expression from P_{araBAD}, while in the absence of inducer AraC tightly represses expression of the target gene. **B.** Schematic illustration of the experimental setup. *S.* Typhimurium P_{araBAD} strains lacking the AraE transport system are grown under SPI-1 inducing conditions for 2.5 h. Then, the bacterial cultures are supplemented with L-arabinose to activate *sctU* or *sctR* expression from P_{araBAD} and consequently initiate efficient NC base assembly. One hour later D-fucose is added to stop further assembly, type 3-dependent secretion of SctA-NLuc^{myc} is initiated after L-rhamnose-induced expression of SctN. **C.** SctA-NLuc^{myc} secretion into the culture supernatant of the P_{araBAD} *sctU* strain was monitored via quantification of luciferase activity over time after L-rhamnose addition. **D.** As in C but monitoring secretion functionality of P_{araBAD} *sctR* strains. Shown are luciferase assays representative of three independent experiments.

4.2.5 Proof of concept of synchronization assays coupled with *in vivo* photocrosslinking

In an attempt to prove the assumption that in the absence of the AraE transporter the yield of fully assembled injectisomes is more efficient, the synchronization system was coupled to the *in vivo* photocrosslinking technic (Farrell et al., 2005). This approach is based on an aminoacyl tRNA synthetase-tRNA pair that mediates *in vivo* site-specific incorporation of the photoreactive amino acid *p*-benzoyl-L-phenylalanine (*p*Bpa) into peptide chains in response to the amber codon TAG. Due to properties such as low reactivity in aqueous solution, site specificity, chemical stability and amenability to be manipulated in ambient *p*Bpa is the preferred photoreactive group for analysis of protein-protein interactions

[6] Fig. 20 A Has been published in PLoS One by Binder et al., 2016, and adapted for its use in this thesis

(Kauer et al., 1986). Irradiation with UV light (λ=365 nm) excites the benzophenone group of *p*Bpa and facilitates its interaction with C-H bonds within ~3-8 Å, the wavelength for activation has no detrimental effects on proteins or bacterial cells (Fig. 21) (Farrell et al., 2005; Stanley et al., 2011).

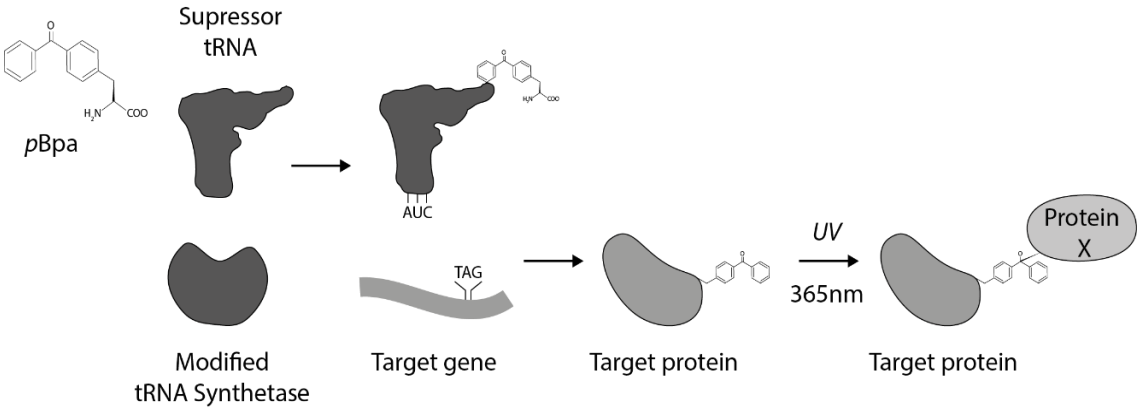

Fig. 22 Principle of the *in vivo* photocrosslinking approach[7].
Cartoon depicting the genetic incorporation of *p*Bpa into a target protein. In the sequence of a target gene the codon for any selected amino acid is mutated to the amber codon TAG. The pair aminoacyl-tRNA synthetase/tRNA supresses the TAG codon and incorporates *p*Bpa at the mutated position. Upon UV irradiation (λ= 365 nm) the *p*Bpa-containing target protein crosslinks proteins in the proximity.

The *in vivo* photo approach has proven effective in detecting *p*Bpa-mediated protein-protein interactions between export apparatus components responsible for nucleation of the injectisome assembly (Dietsche et al 2016; Kuhlen et al 2017). For the coupling, two *sctR*-FLAG-tag *p*Bpa alleles (T15X and V170X) were individually introduced into the chromosome of the P_{araBAD} *sctU* strain using allelic exchange. The resulting strains were grown under SPI-1 conditions in the presence of *p*Bpa, synchronization of NC base assembly was performed according to the standard procedure, and then bacterial cultures were irradiated with UV light to induce the covalent formation of proteins complexes. Subsequently, bacterial membranes were purified and subjected to BN and SDS PAGE followed by Western blot to immunodetect the presence of protein complexes with an anti-FLAG antibody. Upon UV irradiation, both the expected distinctive crosslinks $SctR^{FLAG}$-$SctR^{FLAG}$ and $SctR^{FLAG}$-SctT were efficiently yielded by the *p*Bpa mutants T15X and V170, respectively (Fig. 22A). Further BN analysis of the observed crosslinks confirmed their occurrence in fully assembled

[7] Fig. 22 has been published in FEBS Lett. by Stanley et al., 2011, and adapted for its use in this thesis.

injectisomes as previously reported (Fig. 22B) (Dietsche et al., 2016). Moreover, the SctR^{FLAG}-SctT subcomplex was readily detected, thus indicating its assembly took place efficiently as did the downstream steps in the assembly pathway neither (Fig. 22B).

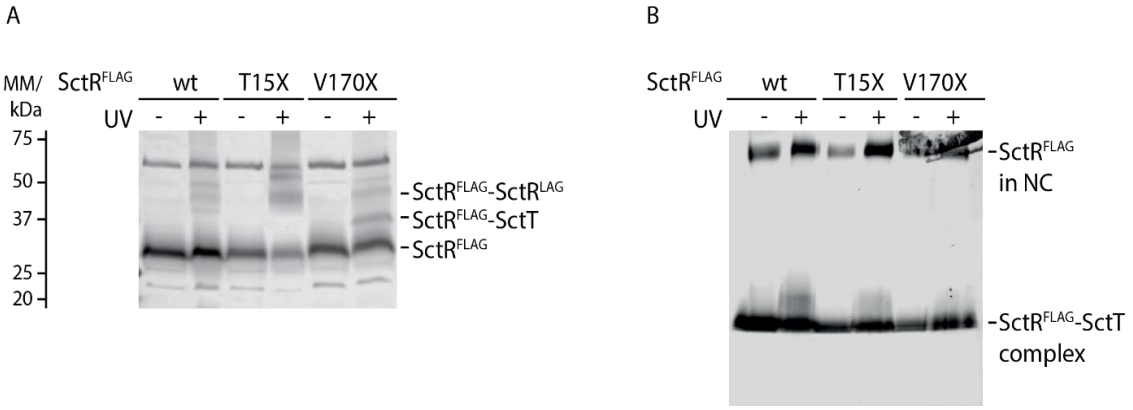

Fig. 22 Assembly of export apparatus subcomplexes in the *S.* Typhimurium P_{araBAD} *sctU* strain.
A. Immunoblotting analysis of crude membranes purified from *S.* Typhimurium P_{araBAD} *sctU* strains expressing the indicated SctR *p*Bpa mutants from the chromosome. Equal amounts of each sample were left untreated (-) or exposed to UV light (+) to induce distinctive SctR-SctR and SctR-SctT photocrosslinks, which were detected via immunodetection of SctR^{FLAG} with an anti FLAG antibody. **B.** Immunodetection of SctR^{FLAG} in crude membranes separated on BN PAGE and SDS PAGE obtained from the same bacterial strains as in A. Shown immunoblots are representative of two independent experiments.

4.3 Characterization of the needle adaptor protein SctI

This third chapter of results focuses on the biochemical characterization of the interaction network of the inner rod SctI and export apparatus components via *in vivo* photocrosslinking (Fig. 22). By evaluating the occurrence of crosslinks between SctI and export apparatus components in different genetic backgrounds, this study aimed to improve the understanding of SctI assembly and structure, as well as its role in needle length control and secretion specificity switching. This third chapter encompasses results published in Molecular Microbiology by Torres-Vargas et al., 2019, and additional complementary findings.

I performed the experiments and analysed the data. I contributed to the data curation and writing the original draft of the paper.

Table 5. Contribution of co-authors to the included publication. Claudia Edith Torres-Vargas, Thales Kronenberger, Nora Roos, Tobias Dietsche, Antti Poso and Samuel Wagner. 2019. The inner rod of virulence-associated type III secretion systems constitutes a needle adapter of one helical turn that is deeply integrated into the system´s export apparatus. Mol Microbiol. 2019 Sep;112(3):918-931. doi: 10.1111/mmi.14327. Epub 2019 Jun 26. PMID: 31183905.

Author	Author position	Scientific ideas %	Data generation %	Analysis and interpretation %	Paper writing %
Claudia Edith Torres-Vargas	1	30	50	30	10
Thales Kronenberger	2	5	20	5	5
Nora Roos	3	10	10	10	0
Tobias Dietsche	4	10	10	10	0
Antti Poso	5	5	0	5	0
Samuel Wagner	6	40	0	40	85
Title of paper	The inner rod of virulence-associated type III secretion systems constitutes a needle adapter of one helical turn that is deeply integrated into the system´s export apparatus				
Status in publication process	The publication was accepted on 07 June 2019 in Molecular Microbiology, and published on 10 September 2019 in the Volume 112, Issue 3, Pages 918-931				

4.3.1 Complete map of protein-protein interactions of SctI with the export apparatus components SctR and SctT[8]

To map protein-protein interactions of SctI with the export apparatus components SctR and SctT via *in vivo* photocrosslinking, 38 amino acids were individually replaced with *p*Bpa (represented by X) throughout the length of SctI. To maintain wild type gene dosage and to avoid multi-copy effects, the 38 single amber mutations were introduced into the chromosome of three *Salmonella* strains: one expressing a FLAG-tagged version of SctR, one expressing FLAG-tagged SctT and a third strain without any FLAG-tagged component. The resulting *p*Bpa SctI mutants were cultured under SPI-1 inducing conditions for 5 h and their ability to secrete the early and middle substrates SctP and SctE, respectively, was examined by secretion assay.

Although the majority of SctI *p*Bpa mutants retained their capacity to secrete both SctP and SctE at levels similar to the wild type strain, introduction of *p*Bpa at several positions (N10X, L29X, L33X, D57X, D63X, Y80X, V95X, and S101X) led to drastic reduction in secretion (Fig. 23). The severity of this negative effect varied among strains, with the $SctR^{FLAG}$ strain being the most affected followed by the $SctT^{FLAG}$ strain. Three mutants (L67X, V81X and L98X) exhibited a consistent abrogation of secretion in all genetic backgrounds, most likely due to the presence of highly charged 3XFLAG tags in the $SctR_5S_1T_1$ complex, namely five in the $SctT^{FLAG}$ strain and three in the $SctT^{FLAG}$ strains. This in conjunction with *p*Bpa, might alter the conformation of the complex rendering it unsuited for the transit of SctP and SctE during secretion (Fig. 23). In agreement with this, mutants T5X, S28X, Y77X and V92X presented substantial reduction in protein secretion in the wild type strain and the defect gradually worsened in the $SctR^{FLAG}$ and $SctT^{FLAG}$ strains. Surprisingly, the opposite effect was observed upon replacement of S40 and T52 with *p*Bpa, which resulted in loss of secretion functionality in the wild type strain, whilst in both the $SctT^{FLAG}$ and $SctT^{FLAG}$ backgrounds secretion was restored (Fig. 23).

[8] Section 4.3.1 contains information published in Mol. Microbiol. by Torres-Vargas et al., 2019, and adapted for its use in this thesis.

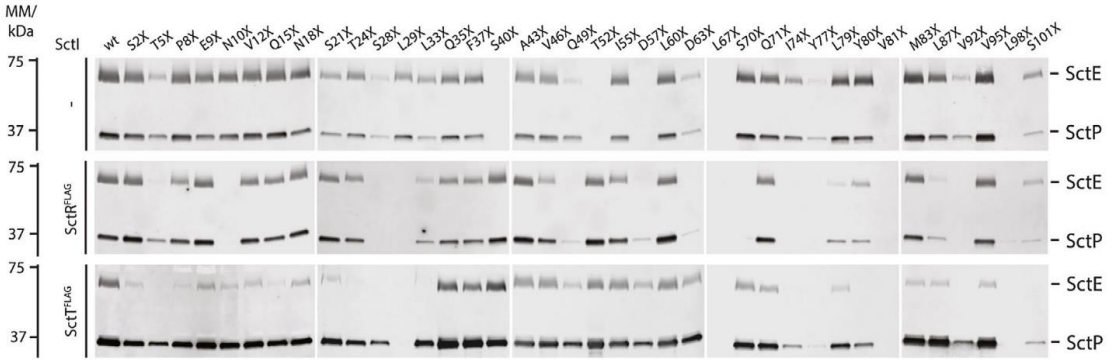

Fig. 23 Secretion profile of chromosomal SctI *p*Bpa mutants[9].
SDS PAGE and Western blot analysis of culture supernatants from *S.* Typhimurium SctI *p*Bpa mutants (represented by X) in the three indicated backgrounds: no FLAG (top), SctR^{FLAG} (centre) and SctT^{FLAG} (bottom). Presence of SctP and SctE, early and middle substrate, respectively, was immunodetected with polyclonal antibodies anti SctP and anti SctE. Shown are immunoblots representative of three independent experiments.

Interestingly, none of the analysed mutants showed a differential secretion profile i.e. in which only secretion of the middle substrate SctE was impaired. A general defect was observed instead, suggesting unaltered secretion specificity regulation when secretion was not compromised (Fig. 23). Since it was impossible to detect SctI either in culture supernatants or in whole cell lysates, the possibility that the defects on secretion were caused by reduced SctI expression or stability cannot be ruled out.

To monitor *p*Bpa-mediated protein-protein interactions, bacterial cells were harvested after 5 h of growth under SPI-1 inducing conditions, and directly exposed to UV light. Then crude membranes were purified and analysed by SDS PAGE and, subsequently, the resolved proteins were transferred to nitrocellulose membranes. Blots were probed with an anti FLAG antibody to detect shifts in the molecular weight of SctRFLAG and SctTFLAG that are indicative of covalently crosslinked protein complexes. Strong SctI-SctRFLAG and SctI-SctTFLAG crosslinks were detected at positions located within the central and C-terminal part or SctI (F37X-V95X) except for S2X and S21X (Fig. 24A and 24B).

[9] Fig. 23 and the displayed information have been published in Mol. Microbiol. by Torres-Vargas et al., 2019, and adapted for their use in this thesis.

The composition of the observed crosslinks was revealed by re-probing a selected subset of blots with an α-SctI antibodie, as seen in the overlay of signals from $SctR^{FLAG}$ (green) and SctI (red) which confirmed their interaction at positions Y77X and M83X (Fig. 24A). Strikingly, immunodetection of SctI in western blots containing crude membranes isolated from the $SctR^{FLAG}$ strain confirmed interaction of untagged SctT and SctI at positions S2, F37, T52, I55, Y77, L79, M83 and V95, discarding any influence of the FLAG-tag in promoting unspecific interactions (Fig. 24B). It is noteworthy mentioning that no SctI-SctI interactions were detected and the reported SctI polymerization pattern showed by the M83X *p*Bpa mutant was not reproducible in this study, rather a strong crosslink to $SctR^{FLAG}$ was observed (Fig. 24A) (Lefebre and Gálan, 2014).

Notice that some of the SctI *p*Bpa mutants exhibiting substantial reduction in secretion (D57X, D63X, I74X, Y77X and V81X), presented as well prominent crosslinks to SctT and SctR, indicating assembly of SctI in non-native configurations that obstruct the secretion channel and, consequently, impeding the passage of substrates. The relevance of the SctI central and C-terminal regions encompassing residues 52-57 and 80-95 for its assembly and function is emphasised by the occurrence of strong crosslinks and severe defects in secretion (Fig. 23 and 24). Altogether these results proved that the *in vivo* photocrosslinking approach is a suitable tool to further investigate SctI function and to monitor its assembly in the context of relevant genetic backgrounds. Thus, the SctI-SctR and SctI-SctT signature crosslinks mediated by functional SctI *p*Bpa mutants, for instance S21X, S40X, M83X and V95X, were chosen as ideal reporters of SctI native assembly in the following experiments.

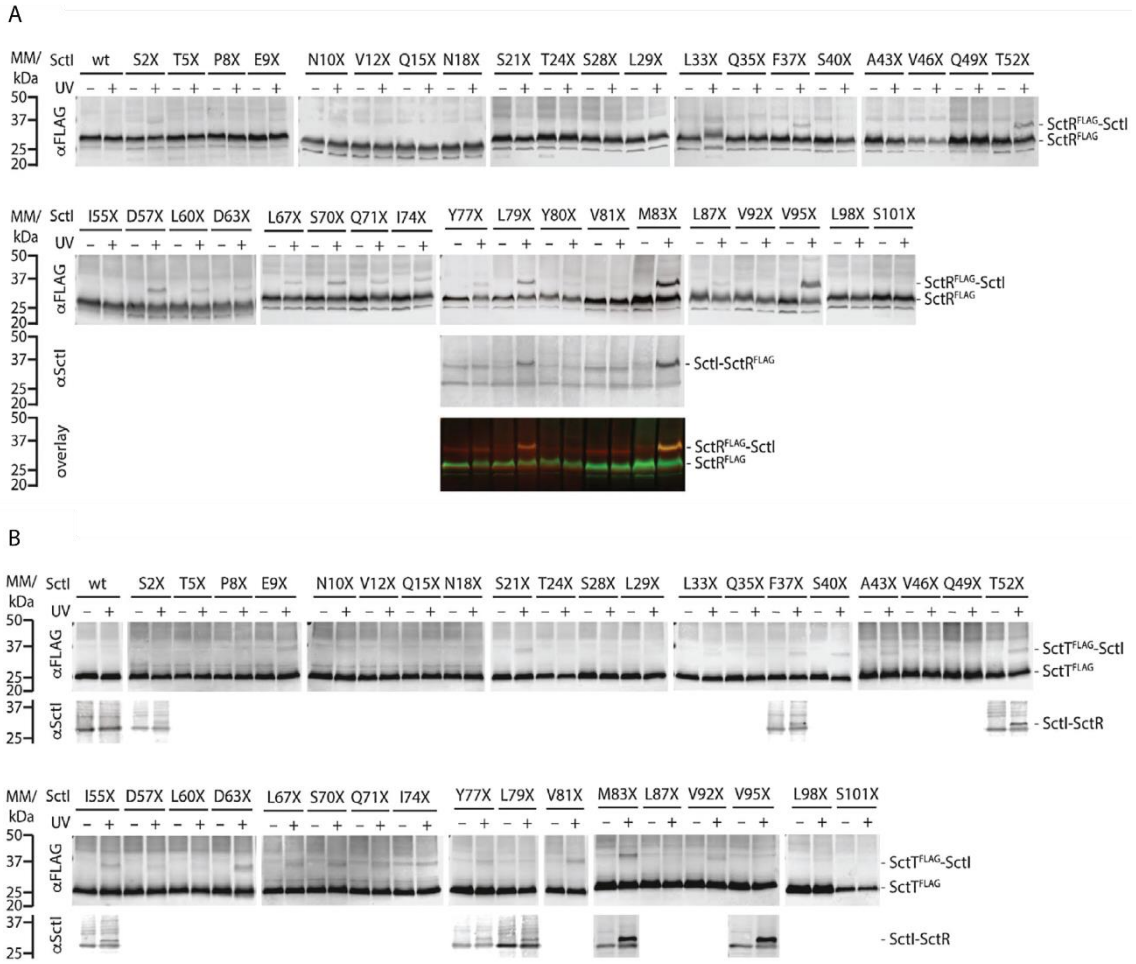

Fig. 24 Interaction network of chromosomal SctI *p*Bpa mutants and the export apparatus components SctT and SctR[10].
A. SDS PAGE and Western blot analysis of crude membranes purified from *S.* Typhimurium SctI *p*Bpa mutants (represented by X). Equal amounts of each sample were left untreated (-) or exposed to UV light (+) to induce photocrosslinks of *p*Bpa to nearby interacting partners. Occurrence of SctR^{FLAG}-SctI crosslinks was shown by immunodetection with an anti FLAG antibody. The estern blot containing samples Y77X-M83X was reprobed with an anti SctI antibody to corroborate its presence in the observed protein complexes. Detection of both SctR^{FLAG} and SctI in the same band is showed in the overlay of the signals for SctR^{FLAG} (green, scanned in the 800 nm channel) and SctI (red, scanned in the 700 nm channel). **B.** Immunodetection as in A but detecting SctT^{FLAG}-SctI interactions. A subset of Western blots was reprobed with anti SctI antibody and neither SctR^{FLAG}-SctI nor SctI-SctI crosslinks were detected, but SctT-SctI interactions were observed instead. Shown immunoblots are representative of three independent experiments.

4.3.2 Interactions of SctI with the export apparatus components SctR and SctT occur in fully assembled and functional NCs[11]

With the purpose of assessing the occurrence of the identified SctI crosslinks between SctI and the export apparatus components in the context of disrupted injectisome assembly and type 3 secretion, a separated set of *Salmonella* strains was generated using allelic exchange. The SctI *p*Bpa mutants M83X and S40X

[10] Fig. 24 with the displayed information have been published in Mol. Microbiol. by Torres-Vargas et al., 2019, and adapted for their use in this thesis.

[11] Section 4.3.2 contains unpublished information.

were individually devoid of their chromosomal copy of *sctN* and *sctJ*, genes encoding the T3SS ATPase and the outer IM ring, respectively. As expected, neither SctI-SctR nor SctI-SctT crosslink was observed in the non-secreting Δ*sctN* background (Fig. 25A and 25B). These results evinced the requirement of SctI secretion for its subsequent interaction with the export apparatus and assembly within the NC base. Similarly, the characteristic $SctI_{M83X}$-SctR crosslink was no longer detected in the strain lacking SctJ (Fig. 25A). *sctJ* elimination impedes completion of the IM substructure and the downstream steps in the assembly pathway, which ultimately makes unfeasible to initiate secretion and assemble the inner rod and needle structures in a type 3-dependent manner (Fig. 4C).

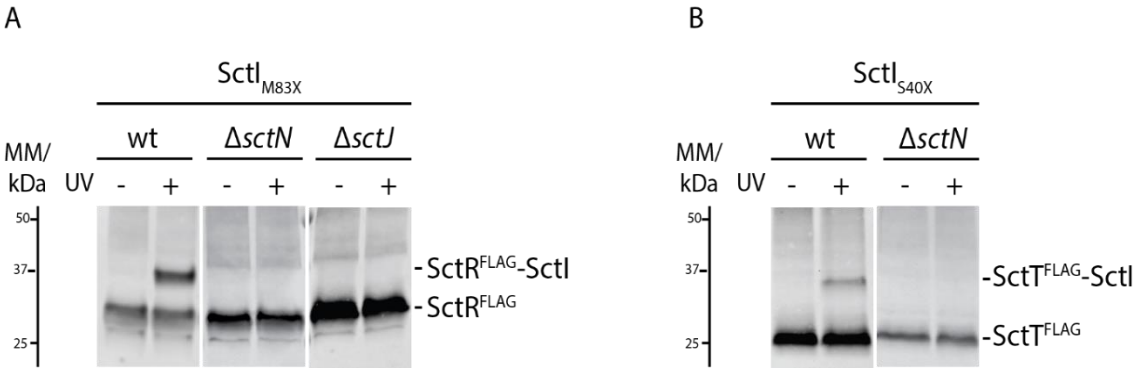

Fig. 25 Dependence of SctI-SctT^{FLAG} and SctI-SctR^{FLAG} crosslinks on fully assembled secretion competent NCs[12].
A. SDS PAGE and Western blot analysis of crude membranes purified from the indicated *S.* Typhimurium $SctI_{M83X}$ mutants. Equal amounts of each sample were left untreated (-) or exposed to UV light (+) to induce photocrosslinks of *p*Bpa to SctR^{FLAG}, and then immunodetection with an anti FLAG antibody. **B.** Immunodetection as in A but identifying SctT^{FLAG}-$SctI_{S40X}$ crosslinks. Shown are immunoblots representative of three independent experiments.

4.3.3 SctI assembly does not depend on the secretin SctC but entails the presence of the needle filament protein SctF[13]

According to the inside-out model of injectisome assembly (Fig. 4C), the export apparatus and secretin substructures independently nucleate assembly at the IM and OM, respectively. This model implies the possibility for cytoplasmic components to be recruited to the fully assembled IM subcomplex and, therefore, initiate secretion of early substrates prior to association with the OM secretin substructure to finalize injectisome assembly (Diepold and Wagner, 2014).

[12, 13] Fig 25 and section 4.3.3 with the displayed information have been published in Mol. Microbiol. by Torres-Vargas et al., 2019, and adapted for their use in this thesis.

In line with this premise, the inner rod protein was proved to enhance the activity of a T3SS-associated PG-lytic enzyme in the periplasmic space, presumably in order to spatially restrict PG-lytic activity above the IM substructure and facilitate assembly of the OM secretin ring (Burkinshaw et al., 2015). However, further studies are required to strengthen this notion. Using the functional SctI$_{M83X}$ mutant as reporter for inner rod assembly, the effect of *sctC* deletion on SctI assembly was assessed by probing the SctI-SctR crosslink (Fig. 26). The distinctive SctI$_{M83X}$-SctR^{FLAG} crosslink observed in the wild type background persisted in the absence of SctC but with diminished efficiency, implying that, although dispensable for SctI assembly, and hence, initiation of type 3-dependent secretion, the presence of the SctC ring structure is needed for proper assembly of the inner rod structure (Fig. 26).

In the Δ*sctC* background, substrates that have been secreted remain partially unfolded in the periplasmic space altering cell wall homeostasis and probably inducing stress. In an attempt to prevent such deleterious effects, the start codon of SctF was mutated (ATG to AAA) to completely abolish its expression. This allowed reassessing inner rod assembly in the absence SctF while preserving the native genetic context and avoiding polar effects on surrounding genes. Surprisingly, the SctI-SctR interaction was no longer observed either in the single mutant SctF$_{M1K}$ or in the double Δ*sctC*, SctF$_{M1K}$ strain, likely as result of compromised inner rod secretion or assembly (Fig. 26).

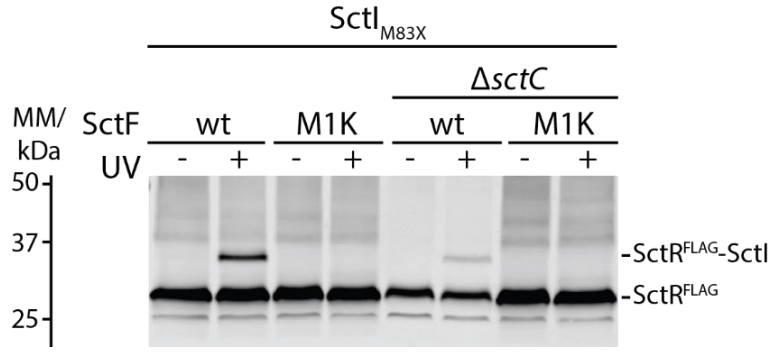

Fig. 26 Crosslinking of the SctI$_{M83X}$ mutant in the absence of the secretin and the needle filament[14]. Immunoblotting analysis of crude membranes purified from the Δ*sctC* and SctF$_{M1K}$ *S.* Typhimurium SctI$_{M83X}$ mutants. Equal amounts of each sample were left untreated (-) or exposed to UV light (+) to induce photocrosslinks of *p*Bpa to SctR^{FLAG}, which were detected immunodetected with an anti FLAG antibody. Shown are immunoblots representative of three independent experiments.

[14] Fig. 26 and the displayed information have been published in Mol. Microbiol. by Torres-Vargas et al., 2019, and adapted for their use in this thesis.

Cellular fractionations were performed in an attempt to elucidate whether the loss of inner rod assembly was due to defects in SctI secretion. Polyclonal antibodies against SctI were used to detect the inner rod protein in periplasmic fractions extracted from the same strains as in figure 26, including as negative control a *Salmonella* strain devoid of the whole SPI-1. SctI was detected neither in spheroplasts nor in the periplasmic fractions, rather one unspecific band with a mobility consistent with that of SctI (circa 10 kDa) was observed (Fig. 27). However, the $SctF_{M1K}$ mutant was observed to be unable to secrete the needle length regulator protein SctP into the periplasm (personal communication S. Westerhausen). Based on these findings, we assumed that deletion of SctF had a general negative effect on secretion.

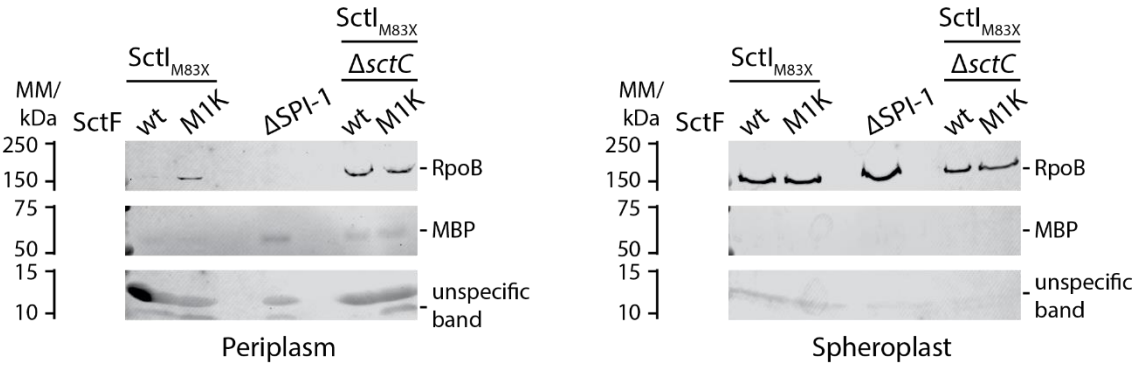

Fig. 27 Cell localization of SctI in the absence of the secretin and the needle filament[15].
Immunodetection of the inner protein SctI in periplasmic fractions and spheroplasts. The cytoplasmic and periplasmic markers RNA-polymerase B (RpoB) and maltose binding protein (MBP), respectively, were included as controls. Shown are immunoblots representative of three independent experiments.

4.3.4 Assembly of SctI does not depend on the needle-capping protein OrgC[16]

Assembly of the flagellar inner rod, hook and flagellin filament is assisted by specialized substrate-specific capping proteins that facilitate incorporation of new subunits at the growing end of the structure until it is completed (Hirano et al., 2005; Ohnishi et al., 1994). Capping proteins were long believed to be absent in virulence associated T3SSs and it was not before 2018 when Kato and colleagues reported experimental evidence for assisted assembly of the needle

[15] Fig. 27 and the displayed information are unpublished.

[16] Section 4.3.4 contains unpublished information.

filament by the capping protein OrgC in the SPI-1 injectisome (Kato et al., 2018). Remarkably, unlike flagellar cap proteins, OrgC is proposed to only promote initial polymerization of SctI subunits into the needle filament and not to participate in its subsequent elongation, suggesting that right after the assembly is initiated, OrgC is secreted into the culture supernatant and, hence, decarded. Despite being proved to be expendable for needle filament assembly, OrgC is required for optimal formation of needle filaments since *orgC* deletion from the wild type strain decreases the number of injectisomes harbouring an attached needle (Kato et al., 2018). This molecular mechanism suggests that, besides nucleating the polymerization of SctI protomers, OrgC might contribute to optimal anchoring of the needle filament to the NC base. To determine whether partial impairment of needle assembly influenced inner rod formation, *orgC* was deleted in three *p*Bpa $SctI_{M83X}$ mutants, one wild type, one lacking the secretin SctC, and one lacking both SctC and the needle length regulator SctP. Secretion functionality and occurrence of signature crosslinks to SctR were evaluated in the resulting strains.

As shown in figure 28A and 28B, *orgC* deletion in wild type *Salmonella* affected neither secretion functionality nor SctI assembly, as $SctI_{M83X}$-SctR crosslink was detected with identical efficiency than in the wild type strain. On the contrary, removing *orgC* from the Δ*sctC* and the Δ*sctCP* mutants resulted in less efficient assembly of SctI, as it was observed in the single mutant devoid of *sctC*. However, over secretion of SctI and other early substrates in the Δ*sctCP* strain appeared to somewhat compensate this effect (Fig. 27 and Fig. 28A). Moreover, in the Δ*sctC* and the Δ*sctCP* genetic backgrounds the inner rod seemed to adopt a non-native conformation that caused the $SctI_{M83X}$-SctR crosslink to migrate with an apparent molecular weight different from the one observed in the wild type strain (Fig. 28A). In summary these results revealed that the cap protein OrgC did not contribute to inner rod assembly, but nucleation of initial polymerization of SctI by OrgC influenced SctI native assembly.

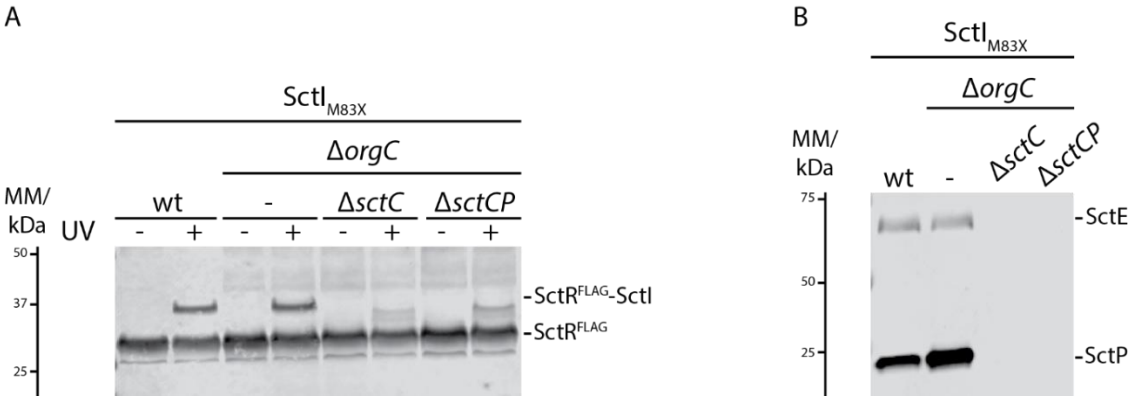

Fig. 28 Crosslinking of the SctI$_{M83X}$ mutant in the absence of the secretin SctC, the needle length regulator SctP and the needle filament cap protein OrgC[17].
A. Immunodetection of SctR^{FLAG} on SDS PAGE separated crude membranes isolated from the indicated *S.* Typhimurium strains. Equal amounts of each sample were left untreated (-) or exposed to UV light (+) to induce photocrosslinks of *p*Bpa to SctR^{FLAG}. **B.** SDS PAGE and Western blot analysis of culture supernatants from the same *S.* Typhimurium strains in A. Presence of SctP and SctE. early and middle substrate, respectively, was immunodetected with polyclonal antibodies anti SctP and anti SctE. Shown are immunoblots representative of three independent experiments.

4.3.5 Role of SctI assembly in needle length regulation and substrate specificity switching[18]

The detailed mechanism of needle length control in T3SSs remains to be elucidated as well as the existence of a molecular interplay between this regulatory process and inner rod assembly. A selection of ten amber mutations that yielded six SctI-SctR and four SctI-SctT distinctive crosslinks were individually introduced into the chromosome of a Δ*stcP S*. Typhimurium strain to monitor SctI assembly in the absence of the needle length regulator. The resulting SctI *p*Bpa mutants devoid of *sctP* exhibited crosslinks to both SctR and SctT with the same efficiency as their wild type counterpart (Fig. 29A and 29B), indicating no active role for the needle length regulator SctP in inner rod assembly.

[17] Fig. 28 and displayed information are unpublished.

[18] Section 4.3.5 contains information published in Mol. Microbiol. by Torres-Vargas et al., 2019, and adapted for its use in this thesis.

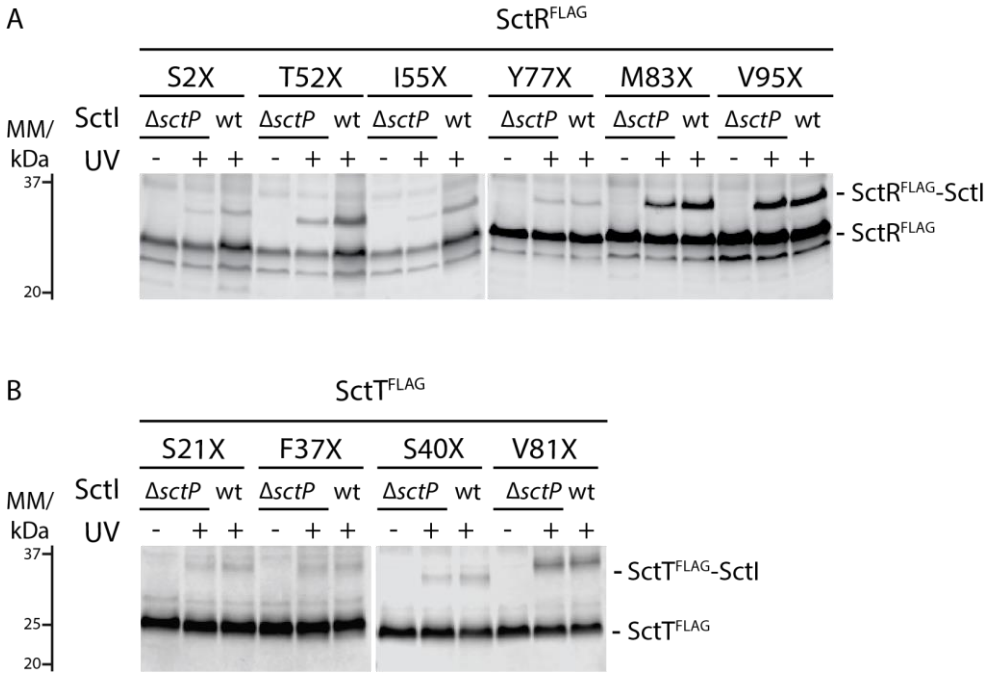

Fig. 29 Crosslinking of SctI pBpa mutants in the absence of the needle length regulator SctP[19].
A. Immunodetection of SctR^{FLAG} on SDS PAGE separated crude membranes isolated from either wild type or Δ*sctP S*. Typhimurium *p*Bpa SctI mutants. Equal amounts of each sample were left untreated (-) or exposed to UV light (+) to induce photocrosslinks of *p*Bpa to SctR^{FLAG}. **B.** Immunodetection as in A but detecting SctT^{FLAG}-SctI interactions. Shown are immunoblots representative of five independent experiments.

A comprehensive alanine scanning mutagenesis conducted by Lefebre and co-workers reported the contribution of numerous residues in SctI to needle length control, leading to the hypothesis that these effects were due to defective assembly of the inner rod (Lefebre and Galán, 2014). Unlike the aforementioned study, in which the SctI mutant variant were expressed from a high copy plasmid, we introduced a selection of six SctI alanine mutants onto the chromosome of a *S.* Typhimurium strain expressing SctR$_{G2X}^{FLAG}$ to assess whether the alanine mutations led to impaired inner rod assembly. Substitution of SctR$_{G2}$ with *p*Bpa was reported to mediate a strong photocrosslink to SctI (Dietsche et al., 2016). Hence, it represented a suitable alternative to track SctI assembly and allowed circumventing the disrupting effects on SctI caused by simultaneous introduction of alanine and amber mutations Five out of six tested SctI alanine mutants efficiently assembled into the inner rod (E9A, N10A, Q15A, D63A and Q71A), and only the M83A mutant presented a considerable reduction in SctI assembly

[19] Fig. 29 and displayed information have been published in Mol. Microbiol. by Torres-Vargas et al., 2019, and adapted for their use in this thesis.

efficiency (Fig. 30A). Comparison of the secretion profile exhibited by these SctI alanine mutants and the wild type strain revealed similar levels of the secretion of both SctP and SctE, early and middle substrates, respectively, with the exception of mutants D63A, Q71A and M83X, which presented reduced secretion of SctE (Fig. 30B).

The effect of systematic introduction of alanine mutations in SctI was not restricted to needle length control: likewise, significant alterations in secretion specificity switching were observed, leading to the involvement of SctI in the control of type 3 secretion hierarchy (Lefebre and Galán, 2014). A new battery of seven $SctR_{G2X}^{FLAG}$ strains harbouring SctI alanine mutant alleles implicated in secretion specificity switching was generated to examine their impact on inner rod assembly.

Every tested SctI alanine mutant produced characteristic SctI-SctR crosslinks, and the efficiency of these interactions was indistinguishable from the wild type (Fig. 30C). In contrast to the reported secretion profiles of mutants N17A, N18A and T24A, in this study all three strains displayed regular secretion of early (SctP) and middle (SctE) substrates. On the contrary, alanine mutations at positions L29 and L98 resulted in extremely reduced secretion of SctP and SctE, suggesting a general defect secretion (Fig. 30D). Interestingly, both strains E96A and T97A failed to secrete SctE but not SctP. To figure out whether the secretion defect was limited to middle substrates, secretion of two late substrates, SptP and SopE, was examined in these mutants. SctI E96A mutant showed diminished secretion of middle and late substrates, but the effect was more drastic for the middle substrate. In contrast, in the SctI T97A strain, a general severe defect in secretion functionality was observed, as the presence of secreted substrates was barely detected in the culture supernatant (Fig. 30E).

Altogether, these results demonstrated that assembly of the inner rod contributes neither to regulation of secretion specificity switching nor to needle length control.

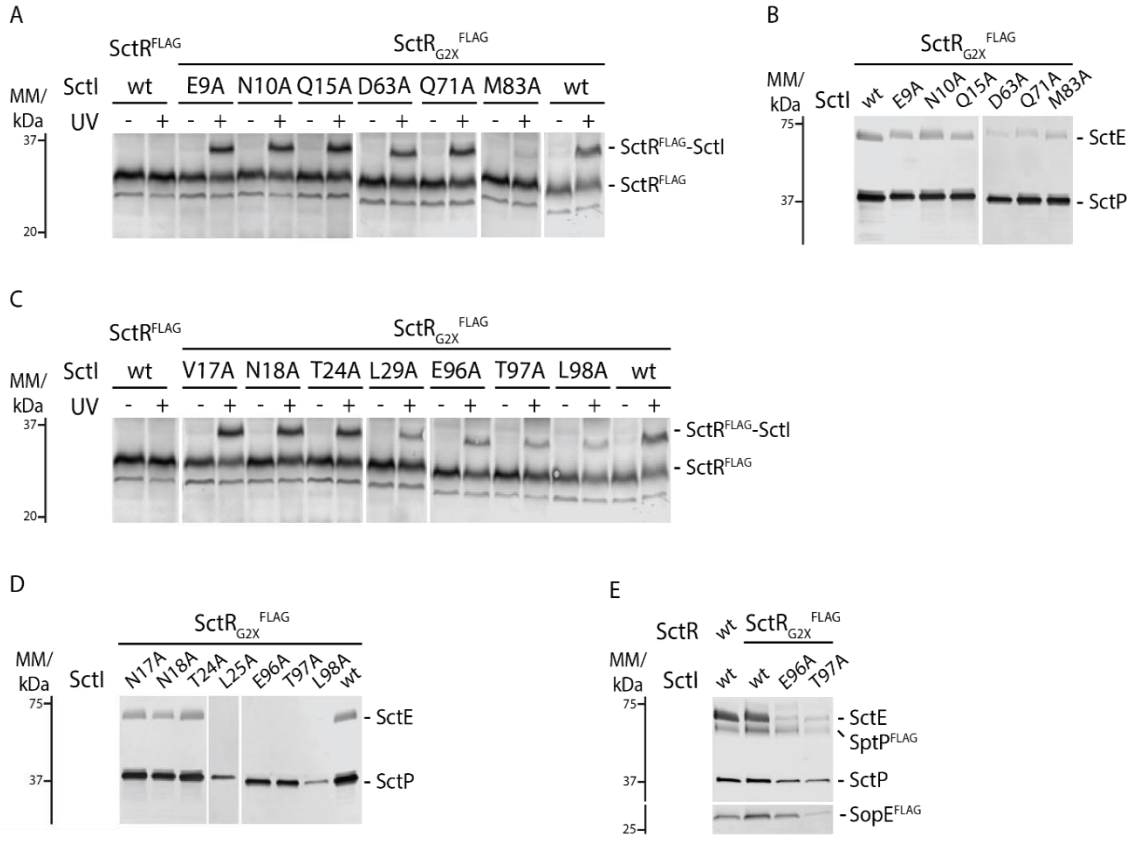

Fig. 30 Type 3 secretion functionality and crosslinking of SctI alanine mutants involved in needle length regulation and secretion specificity switching[20].
A. Immunoblotting analysis of crude membranes purified from *S.* Typhimurium SctI alanine mutants involved in needle length control. Equal amounts of each sample were left untreated (-) or exposed to UV light (+) to induce photocrosslinks of *p*Bpa to SctI, which were detected via immunodetection of $SctR_{G2X}^{FLAG}$ with an anti FLAG antibody. **B.** Secretion profile of the SctI alanine mutants indicated in A. Culture supernatants were SDS-separated and analysed by immunoblotting to detect the presence of SctP and SctE, early and middle substrate, respectively, with polyclonal antibodies anti-SctP and anti-SctE. **C.** Immunoblotting analysis as in A but identifying SctI- $SctR_{G2X}^{FLAG}$ crosslinks in the SctI alanine mutants. **D.** Secretion profile of alanine SctI mutants involved in secretion specificity switching as indicated in C. Analysis of culture supernatants was performed as in B. **E.** Secretion of late substrates $SptP^{FLAG}$ and $SopE^{FLAG}$ in the same SctI alanine mutants as in D. Shown are immunoblots representative of three independent experiments.

4.3.6 Kinetics of synchronized inner rod assembly within NC bases[21]

Based on the timer model of needle length regulation it has long been assumed that the inner rod traverses the entire periplasmic space connecting the export apparatus to the needle filament, which penetrates little into the NC base (Marlovits et al., 2006; Lefebre and Galán, 2014). In order to form a continuous secretion conduit, SctI monomers polymerize into the inner rod, and the time span of its assembly in turn times the duration of needle filament assembly, thus determining its length (Fig. 7). To get insight into the mechanisms of inner rod

[20] Fig. 30 and displayed information have been published in Mol. Microbiol. by Torres-Vargas et al., 2019, and adapted for their use in this thesis.

[21] Section 4.3.6 contains unpublished information.

assembly, the newly implemented P_{araBAD}-based synchronization system was combined with *in vivo* photocrosslinking to study the kinetics of occurrence of $SctI_X$-$SctR^{FLAG}$ interactions. To this end, four SctI *p*Bpa mutants (T52X, I55X, M83X and V95X) that produce distinctive crosslinks to the export apparatus protein SctR were individually introduced into the chromosome of both *S.* Typhimurium strains P_{araBAD} *sctU* Δ*sctN* and P_{araBAD} *sctU* Δ*sctN* Δ*sctP*.

Using the most representative SctI mutant, M83X, standard synchronization assays were performed and right after the coordinated assembly of NC bases was completed, secretion of substrates was activated via P_{rhaBAD}-driven expression of the ATPase SctN. Then, samples were collected at the indicated time points to track the rate of $SctI_{M83X}$-mediated crosslink to SctR. In parallel, secretion of the middle substrate SctA-$NLuc^{myc}$ was monitored over time to fully examine secretion functionality and its regulation (Fig. 31A). The characteristic $SctI_{M83X}$-SctR crosslink was absent in both Δ*sctN* and Δ*sctN*, Δ*sctP* genetic backgrounds even 30 minutes after L-rhamnose addition, time point at which SctA-$NLuc^{myc}$ secretion rapidly increased in the plasmid-complemented *sctN* null mutant, indicating that the secretion specificity switching had occurred, but only if both the inner rod and needle filament were completely assembled (Fig. 31B and 31C plot in the right). However, when compared to the strain harbouring a wild-type *sctI* allele, the $SctI_{M83X}$ mutant exhibited a drastically diminished secretion of SctA-$NLuc^{myc}$, which together with the unsuccessful detection of ScI-SctR interaction indicated a general defect in secretion (Fig. 31C).

To figure out whether it was possible at all to detect SctI assembly with this methodology, additional synchronization assays were performed following the procedure described in figure 31A but extending the time span of active secretion to 1 h before samples were harvested, and using the four Δ*scN* P_{araBAD} *sctU* SctI *p*Bpa mutants (denoted with S) along with regular SctI *p*Bpa strains as positive controls (Fig. 31D). In contrast to the prominent SctI-$SctR^{FLAG}$ crosslinks observed in all four regular strains, in the synchronized scenario only two mutants, T52X and V95X, successfully mediated SctI-$SctR^{FLAG}$ interactions

(indicated with an asterisk), although with lower efficiency (Fig. 31D). Note that the differences in the protein amount between regular and synchronized SctI *p*Bpa mutants were due to the enhanced expression of SPI-1 by its master transcriptional regulator, HilA expressed from a high-copy plasmid (Bajaj et al., 1995). This is a genetic tool routinely used in standard crosslinking assays but was not utilized in the synchronized mutants to preserve the native stoichiometry of the T3SS components encoded within the SPI-1 and *sctU* encoded within the maltose integration site.

In summary, it was not possible to study the kinetics of inner rod assembly with the newly implemented P_{araBAD}-based synchronization system mainly owing to the severe reduction of type 3-dependent secretion functionality that hindered the immunodetection of SctI-SctR interactions.

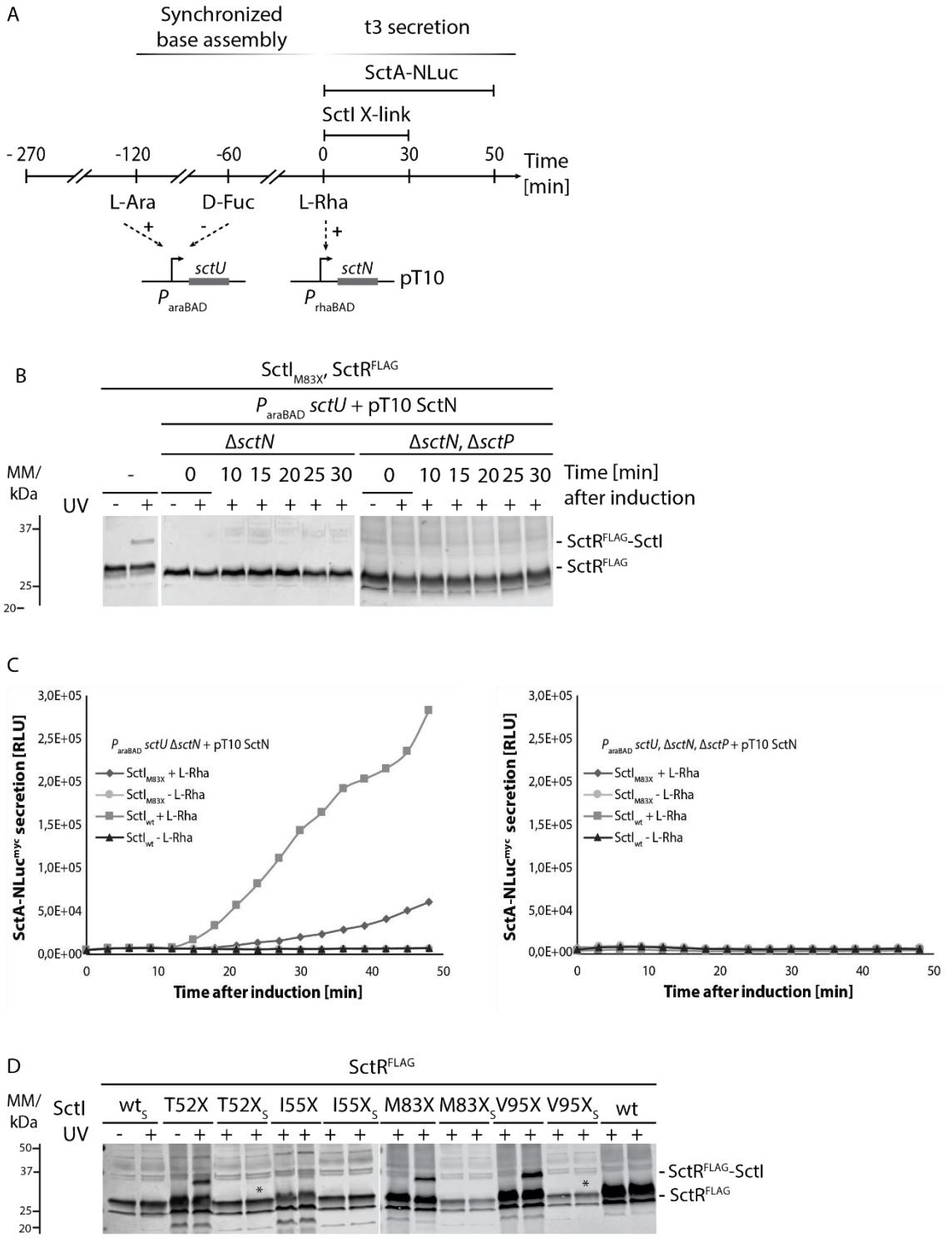

Fig. 31 Inner rod assembly in *S.* Typhimurium P_{araBAD} strains[22].
A. Schematic overview of the experimental setup. *S.* Typhimurium Δ*sctN* P_{araBAD} *sctU* and ΔsctN Δ*sctP* P_{araBAD} *sctU* mutants are grown under SPI-1 inducing conditions for 2.5 h. Then bacterial cultures are supplemented with L-arabinose to activate *sctU* expression from P_{araBAD} and, consequently, initiate efficient NC base assembly. 1h later D-fucose is added to stop further assembly, t3-dependent secretion of substrates initiated after L-rhamnose-induced expression of SctN. Then, assembly of the inner rod is monitored via *in vivo* photocrosslinking for 30 minutes, while secretion of the intermediate substrate SctA-$NLuc^{myc}$ is followed up via the luciferase-based secretion assay for 50 minutes. **B.** Kinetics of inner rod

[22] Fig. 31 and displayed information are unpublished.

assembly in *S.* Typhimurium Δ*sctN* P_{araBAD} *sctU* and ΔsctN, Δ*sctP* P_{araBAD} *sctU* mutants. Samples of bacterial cultures were harvested at the indicated time points after L-rhamnose addition, crude membranes were purified and subjected to SDS PAGE and Western blot analysis to detect the signature $SctI_{M83X}$-$SctR^{FLAG}$ crosslinking. **C.** SctA-$NLuc^{myc}$ secretion into the culture supernatant of the same strains as in B was monitored via quantification of luciferase activity over time after L-rhamnose addition. **D.** Immunoblotting analysis of crude membranes purified from *S.* Typhimurium SctI *p*Bpa mutants that produce signature crosslinks to $SctR^{FLAG}$. SctI-SctR interactions were probed in regular and synchronized Δ*sctN* P_{araBAD} *sctU* mutants (denoted with S). $T52X_S$ and $V95X_S$-mediated interaction to SctR is indicated with an asterisk. Equal amounts of each sample were left untreated (-) or exposed to UV light (+) to induce photocrosslinks of *p*Bpa to SctI, which were detected via immunodetection of $SctR^{FLAG}$ with anti FLAG antibody. Shown immunoblots and luciferase assays are representative of three independent experiments.

4.3.7 Model of SctI as an adapter between the export apparatus and the needle structure[23]

Longitudinal sections of the *S.* Typhimurium SPI-1 injectisome exhibit indistinguishable cylinder-shaped densities of the inner rod and needle filament within the NC, suggesting that these two components share structural similarity (Fig. 32A) (Marlovits et al., 2004, 2006; Worrall et al., 2016, 2018). Cryo-EM analysis of the export apparatus elucidated its helical assembly and parameters (5.7 subunits per turn and helical rise 4.0 Å), which are almost identical to those of the needle filament (5.6 subunits per turn and helical rise 4.3 Å) (Kuhlen et al 2018). In addition, specific residues of SctT and SctR contributing to their interaction with SctI were identified by *in vivo* photocrosslinking (Fig. 32B) (Dietsche et al., 2016; Kuhlen et al 2018). In conjunction, these observations implicated the helical array of the export apparatus in providing the structural foundation for assembly of the inner rod, which should adopt a similar topology to template helical assembly of the needle filament (Fig. 32C).

[23] Section 4.3.7contains information published in Mol. Microbiol. by Torres-Vargas et al., 2019, and adapted for their use in this thesis.

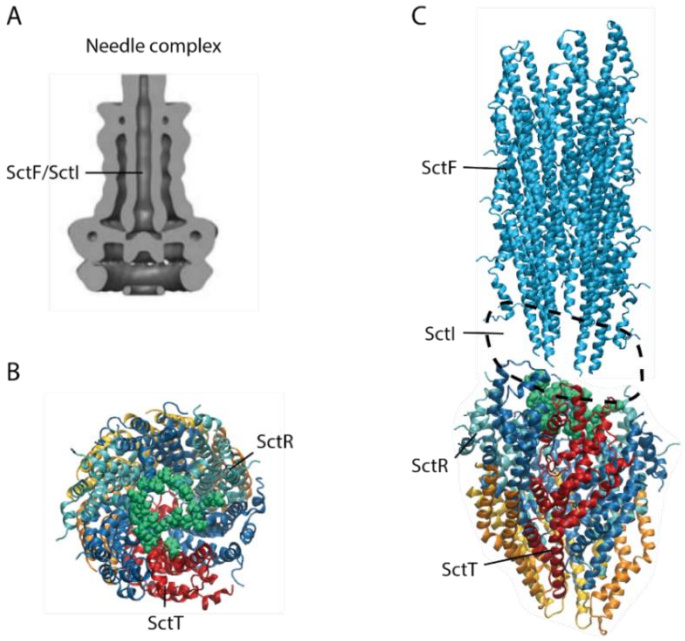

Fig. 32 Structures of the S. Typhimurium SPI-1 NC, export apparatus and needle filament[24].
A. Longitudinal section of the wild type SPI-1 injectisome reveals the helical density of the inner rod and needle structures. **B.** Top view of homology model of the *S.* Typhimurium $SctR_5S_1T_1$ complex (based on the *S. flexneri* $SctR_5S_1T_1$ structure, PDB 6R6B, SctR blue, SctS orange and SctT red). SctR and SctT positions that were previously observed to mediate *p*Bpa crosslinks to SctI are shown in green spheres. **C.** Side view of the structure of the *S.* Typhimurium SPI-1 injectisome needle filament (blue, PDB 6DWB) and homology model of the *Salmonella* $SctR_5S_1T_1$ complex as in B.

Considering the experimental evidence formerly mentioned, and the estimated stoichiometry of six SctI subunits per injectisome, the structure of the inner rod was modelled as the first helical turn of the needle filament (Fig. 33A). This filament homology model was validated by mapping onto it three conserved residues within the C-terminal domains of SctF and SctI ($SctF_{P41}$/$SctI_{P64}$, $SctF_{L44}$/$SctI_{L67}$ and $SctF_{Q48}$/$SctI_{Q71}$), which were located to the same subunit interface in SctI and SctF (Fig. 33B).

[24] Fig. 32A has been published in Nature by Marlovits et al., 2006, and adapted for its use in this thesis.
Fig. 32B has been published in Nat. Struct. Mol. Biol. by Kuhlen et al., 2018, and adapted for its use in this thesis.
Fig. 32C has been published in Mol. Microbiol. by Torres-Vargas et al., 2019, and adapted for their use in this thesis.

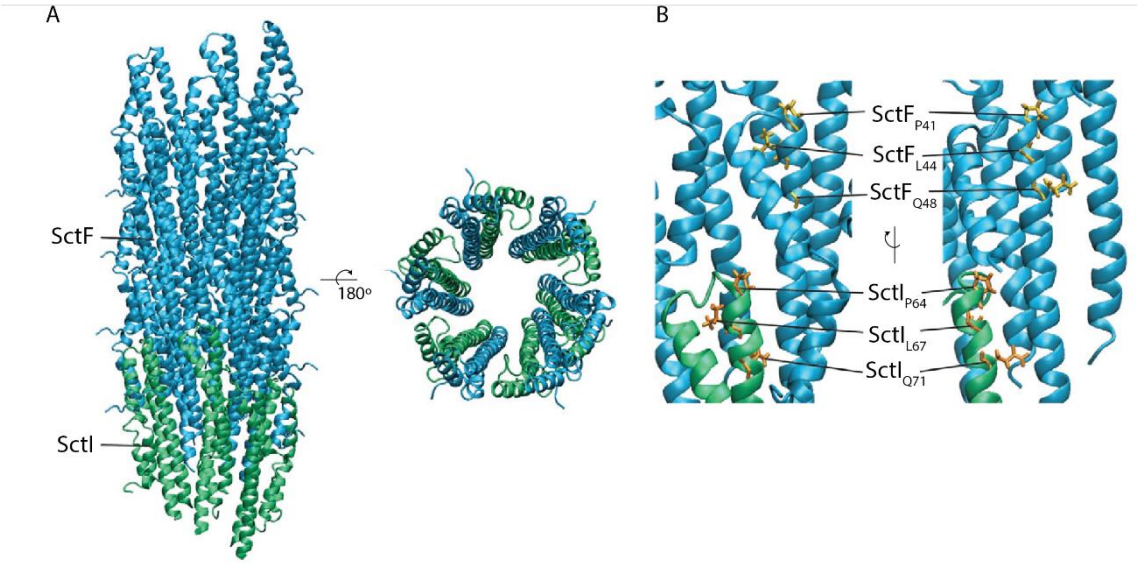

Fig. 33 Homology model of the inner rod structure[25].
A. Front and top view of the cartoon representation of modelled *S.* Typhimurium SPI-1 T3SS inner rod (in green, formed by 6 SctI subunits) and needle filament (in blue, formed by multiple SctF subunits, PDB 6DWB). $SctI_{22-101}$ homology model was created using SctF crystal structure as template and the assembled inner rod was modelled as the first helical turn of the needle filament. **B.** Closeup detail of the region encompassing conserved residues in SctF and SctI (showed as sticks) that mediate interaction between filament subunits.

Shortly after this work was published, the crystal structure of the entire *S.* Typhimurium SPI-1 injectisome was resolved including the long-time elusive inner rod structure (Hu et al., 2019). In agreement with the proposed SctI model (Fig. 34A) and reported stoichiometry (Zilkenat et al., 2016), the inner rod structure consists of six SctI subunits organized in a singled-turn helical array that connects the export apparatus to the needle filament (Fig. 34A). The first $SctI^{1}$ subunit exhibits an ordered C-terminal portion with a single helix, while the remaining of $SctI^{2-6}$ subunits show a N-terminal β-sheet followed by a helical hairpin (Fig. 34B).

[25] Fig. 33 and displayed information have been published in Nat. Microbiol. by Hu et al., 2019, and adapted for their use in this thesis.

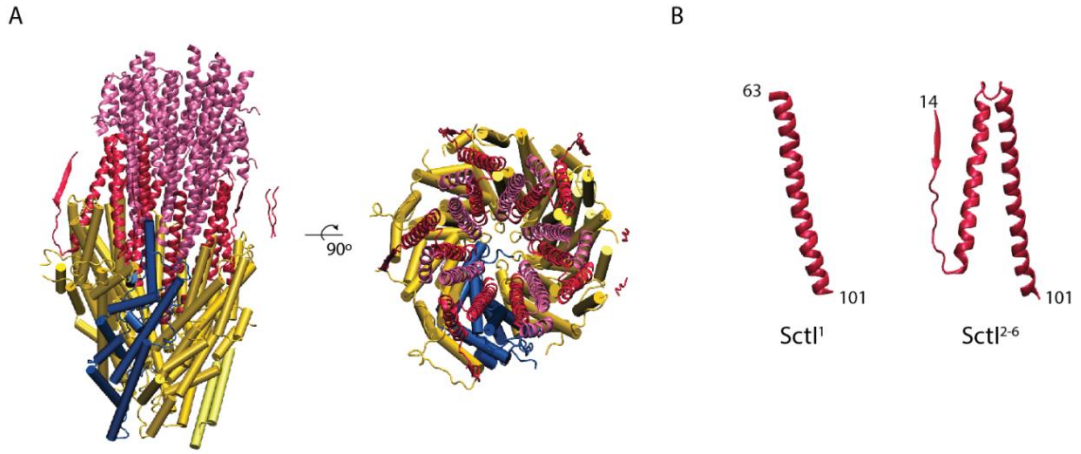

Fig. 34 Crystal structure of the *S.* Typhimurium SPI-1 injectisome inner rod[26].
A. Side and top view of the S. Typhimurium SPI-1 injectisome $SctT_5S_1R_1$ complex (SctT in orange, SctS in blue and SctR in yellow, PBD 6pep), inner rod (in red, PBD 6pep) and needle filament (in purple, PBD 6pep). **B.** Atomic model of SctI (in red, PBD 6pep) presenting the observed ordered states. $SctI^1$ exhibits a single C-terminal helix, whilst the subunits $SctI^{2-6}$ are ordered throughout their length.

With the objective of complementing the extensive functional data generated by this study, the location of relevant SctI residues was determined in both actual and modelled inner rod structure. Figure 35 highlights the SctI *p*Bpa mutants that were secretion deficient (in red) or significantly impaired in their secretion functionality (in orange), and SctI alanine mutants that selectively failed to secrete the middle substrate SctE (in purple). With the only exception of S101X, these *p*Bpa mutations were situated at the periphery of the secretion conduit and the interface between SctI or SctF subunits, in both modelled and crystal structure (Fig. 35A and 35B). It is likely that placing the voluminous *p*Bpa it at those positions perturbed either inner rod or needle assembly leading to a generalized loss of secretion functionality. Both E96A and T97A mutations, conversely, were located towards the central channel, altering its electrostatic properties, which in turn resulted in a differential effect on secretion (Fig. 35A and 35B). Interestingly, mutation of residue S101 in the actual structure was located towards the secretion conduit lumen and in close proximity to the export apparatus. Thus, its mutation to *p*Bpa led to drastic reduction of secretion, possibly owing to defective inner rod assembly rather than changes in its native electrostatic properties (Fig. 35B).

[26] Fig. 34 and displayed information have been published in Nat. Microbiol. by Hu et al., 2019, and adapted for their use in this thesis.

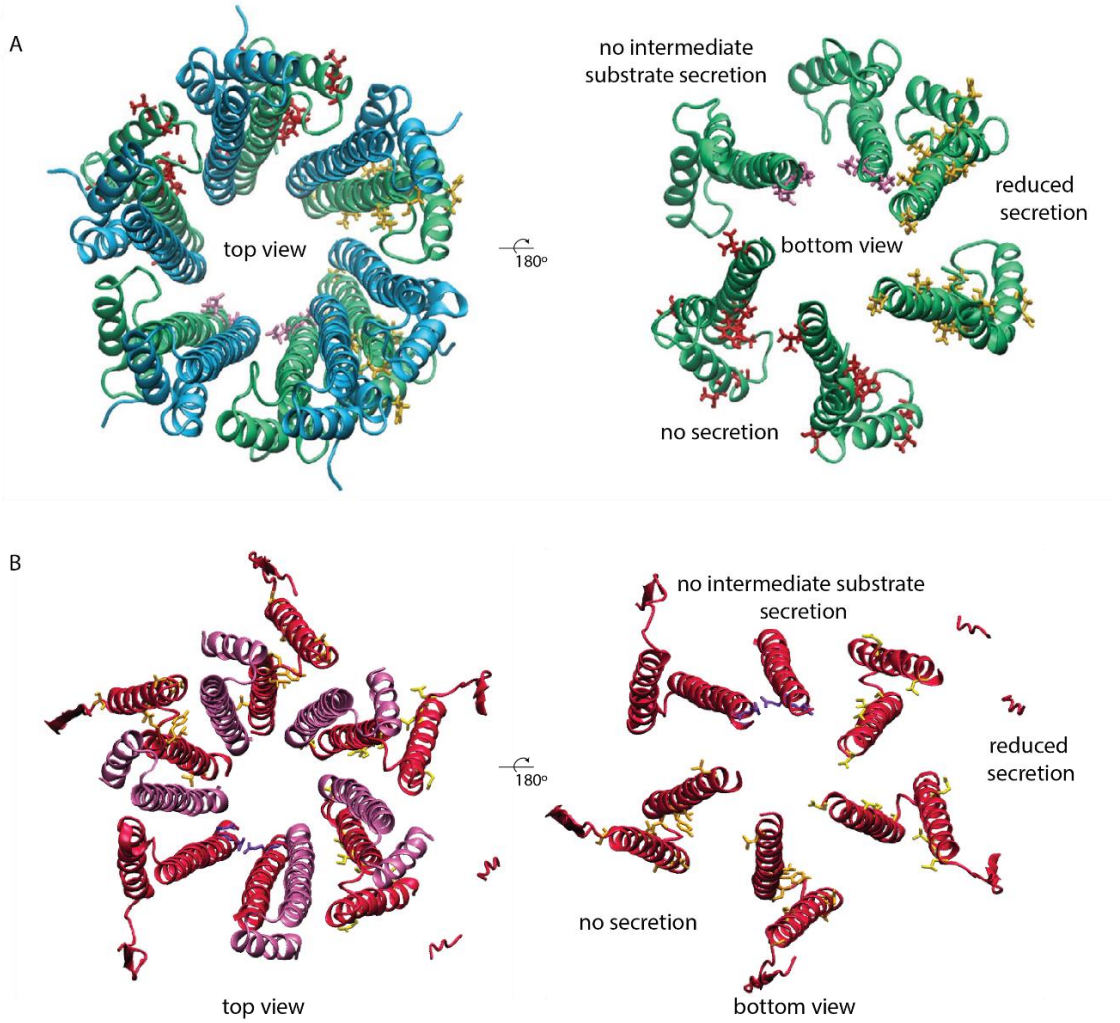

Fig. 35 Mapping of the secretion deficient SctI *p*Bpa and alanine mutants onto the SctI modelled and crystal structure[27].
A. Front and top view of the modelled SctI structure (Coloured as in figure 34). *p*Bpa mutations that abrogate or significantly reduce secretion in the wild-type background are shown in red. *p*Bpa mutants that exhibit considerably diminished secretion are shown in orange. E96A and T97A mutants that are defective for SctE secretion are shown in purple. **B.** Same as A but SctI *p*Bpa (in orange and yellow) and alanine (in purple) mutants were mapped onto the SctI crystal structure (Coloured as in figure 34, PDB 6pep).

Mapping SctI residues that, when mutated to *p*Bpa, yielded prominent crosslinks to SctR and SctT onto the SctI model and resolved structure revealed that with exception of Q71, these residues located toward the periphery of the inner rod and at the interface between SctI subunits (Fig. 36A and 36B). The C-terminal helix of SctI was oriented in the direction of the export apparatus, and therefore it was not surprising that this region encompassed two residues (M83 and V95) that mediated some of the strongest crosslinks to SctR (Fig. 36A and 36B).

[27] Fig. 35 and displayed information have been published in Mol. Microbiol. by Torres-Vargas et al., 2019, and adapted for their use in this thesis.

Surprisingly, other residues responsible for mediating SctI interactions with SctR and SctT (T52 and I55) were located in the distal end of the N-terminal helix of SctI (Fig. 36A and 36B). This observation suggested that the inner rod assembles deep within the export apparatus, an assumption supported by the resolved crystal structure, which revealed the exact SctI-SctRT interactions (Fig. 36A). Although some residues (S2 and E9) within the N-terminal portion of SctI were identified to facilitate its interaction with the export apparatus (Fig. 36A and 36B), indicating their close proximity, it was not possible to corroborate this notion since the first 13 residues of SctI did not exhibit any ordered structure (Fig. 36B) (Hu et al., 2019).

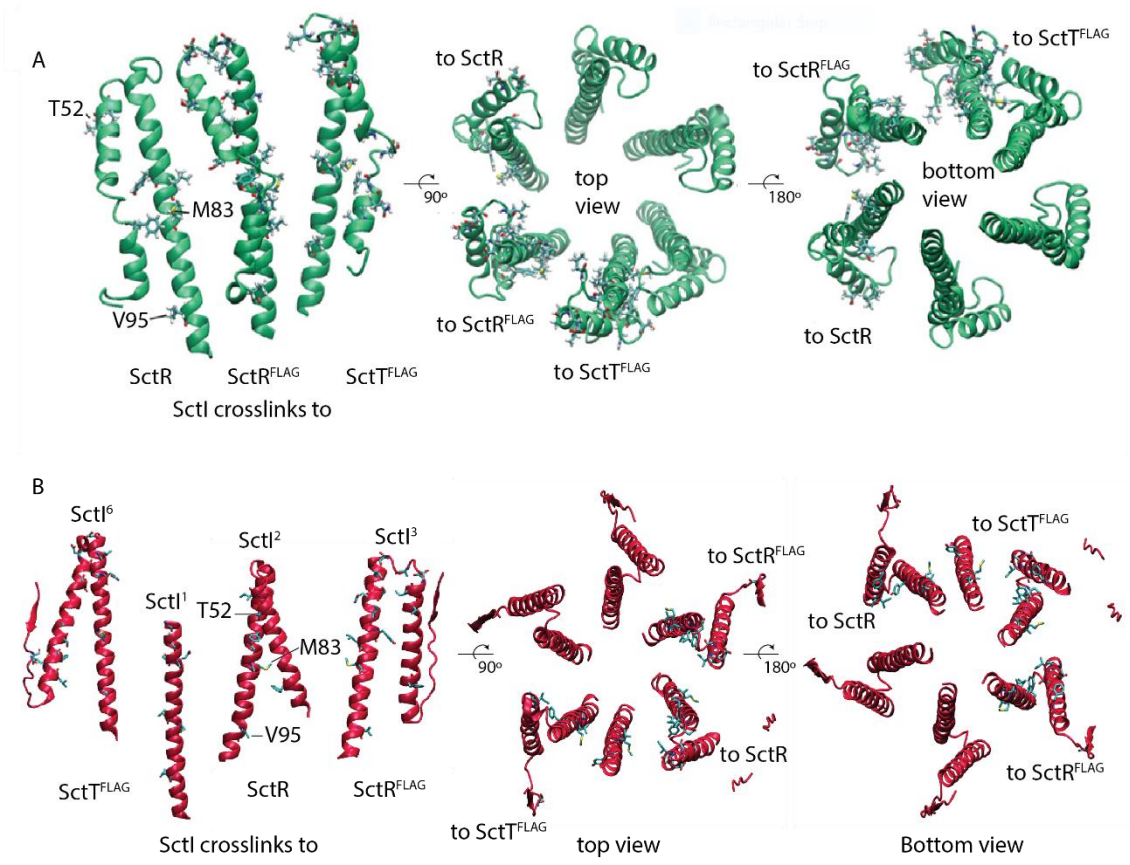

Fig. 36 Mapping of SctI-SctR and SctI-SctT crosslinks onto the modelled SctI structure and cartoon representation of SctI interactions with SctR and SctT[28].
A. Location of SctI residues that, when mutated to *p*Bpa, mediated crosslinks to SctR and SctT onto the SctI homology model (green). The position of residues T52, M83 and V95 that produced prominent crosslinks is indicated. **B.** As in A but residues were mapped onto the SctI crystal structure (red, PDB 6pep).

[28] Fig. 36 and displayed information have been published in Mol. Microbiol. by Torres-Vargas et al., 2019, and adapted for their use in this thesis.

Given the similar helical parameters of the inner rod/needle filament and the export apparatus, each SctI subunit was predicted to assemble onto one component of the SctR5SctT1 complex (Fig. 37A). The N-terminus of SctR and SctT were identified to contribute to their interaction with SctI. Therefore, the deep clefts exhibited by distal SctR N-terminus were thought to accommodate SctI (Fig. 37B). Even though it was difficult to locate precisely SctI-SctRT interactions, in this work the C-terminus of SctI was suggested to be placed in a space enclosed by helices 1 and 2 of contiguous SctR and SctT subunits (Fig. 37A). In agreement with the envisioned SctI-SctRT interactions, in the crystal structure the C-terminal helix of SctI[1] was bonded in a large groove at the interface of SctT-SctR[1], while SctI[2-6] and SctI[6] are bonded at SctR-SctR and SctR[5]-SctT interfaces, respectively (Fig. 37A) (Hu et al., 2019).

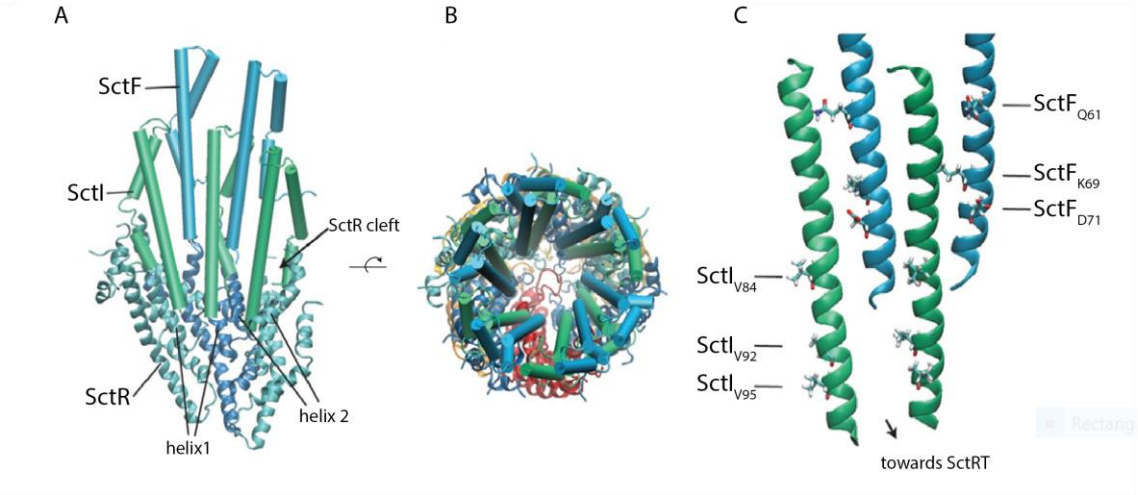

Fig. 37 Envisioned placement of one helical turn of the inner rod/needle filament on the $SctR_5S_1T_1$ complex[29].
A. Side view of the proposed placement of SctI onto the SctR complex. **B.** Top view of the proposed helical turn of SctI and SctF on top the $SctR_5S_1T_1$ complex. **C.** Closeup detail of SctI and SctF C-terminal domains entailing conserved residues among homologs. Residues that differ between SctI and SctF are shown as sticks.

[29] Fig. 37 and displayed information have been published in Mol. Microbiol. by Torres-Vargas et al., 2019, and adapted for their use in this thesis.

5 Discussion

A prerequisite for a molecular high resolution analysis of the injectisome biogenesis and regulation, is the circumvention of its heterogeneous assembly via the synchronization of the assembly pathway. Therefore, this study provides new insights into the regulatory processes that contribute to the assembly and function of the SPI-1 injectisome, which were obtained by means of a newly implemented P_{araBAD}-based synchronization system and an *in vivo* photocrosslinking approach.

5.1 Development of a P_{araBAD}-based system allows to synchronize T3SS assembly and secretion functionality

5.1.1 Plasmid-based expression of T3SS core components efficiently restores injectisome assembly and functionality

Efficient assembly of the injectisome depends on the coordinated association of IM and OM substructures. Deletion of structural components of the T3SS disrupts the formation of such substructures and the downstream steps in the assembly pathway (Kaniga et al., 1994; Wagner et al., 2010). In this study, the plasmid-based decoupled expression of five components of the NC base and export apparatus was shown to restore injectisome assembly and type 3 secretion functionality of the respective *S.* Typhimurium null mutants (Fig. 8B and 11C). The use of the low-copy plasmid, pT10, reduced possible toxic effects of overexpression of membrane-associated proteins while allowing the production of small amounts of proteins that suffice to rescue the mutant phenotypes. The levels of complementation ranged from intermediate to wild type and were comparable to previous reports in which such T3SS components were chromosomally encoded outside of the SPI-1 (Fig. 8B and 11C) (Wagner et al., 2010). There was a linear correlation between complementation efficiency and the number of copies of the components required to achieve it. Assuming the estimation that each *Salmonella* cell assembles circa 10-100 injectisomes (Kubori et al., 1998), it was not surprising that the best complementation level was accomplished in both *sctR* and *sctU* deletion mutants as solely 500 and 100 copies/cell are needed, respectively. Interestingly, assembly of the inner IM ring

SctJ, which requires 24 subunits per injectisome (2400 copies per cell) was likewise efficiently mediated by the plasmid-based expression of *sctJ*, in sharp contrast to the outer IM structure SctD, also present in 24-fold symmetry. In the particular case of the OM SctC secretin ring (15-fold symmetry), the intermediate level of complementation was attributed to prerequisites that influenced SctC membrane localization such as the essential assistance of the pilotin InvH and the efficient traversing of the IM barrier and periplasmic space facilitated by the Sec-pathway. Based on these observations, expression of *sctJ*, *sctR* and *sctU* was engineered to depend on the L-arabinose inducible promoter P_{araBAD} in order to synchronize assembly of NC bases. Numerous *araC-*P_{araBAD} plasmid-based expression systems have been extensively used to finely control gene expression due to the tight repression of P_{araBAD} in the absence of inducer, and its rapid responsiveness to medium composition (Fig. 9) (Guzmán et al., 1995; Beverin and Sheppard, 1971). These advantageous features of the *araC-*P_{araBAD} expression cassette were also exploited in this study. With the objective of preserving the native gene dosage, the cassette was introduced into the chromosome of *Salmonella* mutants in a neutral insertion site (MIS). L-arabinose-dependent expression of *sctJ*, *sctR* and *sctU* exhibited the distinctive behavior of P_{araBAD}-driven gene expression: i) it presented a linear response to the concentration of inducer (Fig. 10A), ii) it was tightly repressed in the absence of L-arabinose (Fig. 10A and 10B), iii) it was susceptible to be shut off by D-fucose (Fig. 10B and 10D), and iv) upon induction with L-arabinose, it responded within minutes (Fig. 10C and 10D). In line with the effect of plasmid-based expression of *sctJ* and *sctU* on secretion functionality, L-arabinose-dependent expression of these components effectively restored secretion to wild type levels (Fig. 10A). Consistently overexpression of *sctJ* or *sctR* has not been reported to have toxic effects or disturb type 3-dependent secretion. In contrast, *sctR* expression from the P_{araBAD} promoter poorly complemented the Δ*sctR* secretion deficient phenotype, even in the presence of a high concentration of inducer (0.1 % w/v) (Fig. 10A). This effect can be explained by the deleterious effects on bacterial cells that even moderate overexpression of SctR caused the formation of large permeable pores in the IM (Dietsche et al., 2016). In this study, although in single

chromosomal copy, *sctR* was overexpressed due to the strong P_{araBAD} promoter. However, only small variations in the viability of *Salmonella* strains was observed in the secretion assays (data not shown). Hence, additional immunodetection of cytoplasmic and periplasmic markers into the culture supernatant is required to confirm a lytic effect. Overexpression of *sctJ* or *sctU* has not been reported to have toxic effects or disrupt secretion.

5.1.2 Plasmid-based expression of T3SS cytoplasmic components effectively activates type 3 secretion

As for other protein complexes, stability, assembly and recruitment of T3SS cytoplasmic components to the NC base rely on the presence of all its constituents (Zhang et al., 2017; Lara-Tejero et al., 2019). Hence, their regulated expression provides an advantageous tool to control secretion. Here, the L-rhamnose-dependent expression of four T3SS cytoplasmic components, *sctL*, *sctN*, *sctO*, and *sctQ* coupled with a sensitive luciferase-based secretion assay was proved to be an amenable approach to activate and monitor secretion in similar fashion and extent, suggesting that all components are equally relevant for the function of this cytoplasmic structure (Fig. 11A and 11D). In agreement with this observation, the luciferase-based secretion and injection assays have been recently shown to provide highly sensitive and robust methods for the investigation of the molecular basis of protein secretion (Westerhausen et al., 2020). Moreover, activation of secretion after the complete assembly of the NC base yielded fully assembled injectisomes and even allowed the generation of long needle filaments in the absence of the needle length regulator SctP (Fig. 11C and 11E). The soluble protein SctK seemed to play a yet unreported role in the regulation of secretion specificity since its pT10-based expression differentially restored secretion of the early substrate SctP but not that of middle (SctE) and late substrates (SipA-NLuc) (Fig. 11A and 11D). Nonetheless, further experimental evidence is required to support this notion. These findings highlight the importance of SctK as a core component of the sorting platform.

5.1.3 A complex genetic system allows synchronizing T3SS assembly and secretion functionality

Combination of the implemented P_{araBAD}-based expression of T3SS core components, the pT10-based expression of the ATPase SctN and the sensitive luciferase-based secretion assay, resulted in a complex synchronization system. (Fig. 12). This system allowed coordinating Sec-dependent assembly of the NC base (Fig 14A) and initiating type 3-dependent secretion of proteins (Fig. 14B). Furthermore, with the use of this system it was possible to obtain fully assembled injectisomes with regular needle length and even replicate the typical phenotype of long needles produced by Δ*sctP* mutants (Fig. 14C). Even though in principle the system functioned as expected (Fig. 14A and 14B), it yielded a rather mixed population of complexes consisting of complete injectisomes and isolated bases (Fig. 14C), indicating defects in either assembly or secretion. The low yield of injectisomes restricted the use of the synchronization system for subsequent structural analyses that require a large number of particles e.g. cryo-EM.

5.2 Optimization of the P_{araBAD}-based synchronization system

The potential applications of the newly implemented synchronization system prompted the design of an optimization strategy to atone for its most relevant shortcomings.

Given the pivotal role of the export apparatus in nucleating injectisome assembly, it was hypothesized that decoupled expression of the export apparatus components *sctR* and *sctU* leads to their IM insertion in a position distant from the IM location where the remaining components encoded within the SPI-1 are inserted. To test this hypothesis, the P_{araBAD}-based expression cassette and the target gene (either *sctR* or *sctU*) were shifted to an insertion site within the SPI-1. Unfortunately, this approach did not improve secretion functionality (Fig. 15A and Fig. 16B), NC base assembly (Fig. 16A) or injectisome assembly (Fig. 16C). These results indicated that the pool of IM proteins was efficiently recruited by *sctR* and *sctU* for *de novo* assembly of complexes regardless of the genetic

location from which *sctR* and *sctU* were expressed. However, it is plausible that the obtained results are related to a particular topology adopted by the bacterial chromosome that brings the far apart SPI-1 and MIS in close proximity allowing the proteins to insert in neighboring locations in the IM and therefore, no evident difference between the SPI-1 IS and MIS is observed.

The second optimization step consisted of temporally coupling SctC assembly in the OM with activation of type 3-dependent secretion (Fig. 18). Rather than enhancing secretion functionality, this strategy extended its lag of activation and overall decreased its efficiency of one order of magnitude (Fig. 19). On the other hand, the lag of secretion onset is proposed to reflect the time required for *sctC* expression, insertion in the OM and polymerization into the secretin ring, which in turn mediates completion of the base (Fig. 19). In addition, owing to the absence of a complete NC, recruitment of the cytoplasmic components (among them SctN) to the IM was affected and consequently, secretion of proteins was inefficient (Fig. 19C and 19D). This observation is in line with reports of mislocalization of the cytoplasmic components to the bacterial poles in the absence of an intact NC base, suggesting that assembly of the base likely precedes assembly of the cytoplasmic sorting platform (Zhang et al., 2017).

A large body of experimental data has demonstrated that P_{araBAD}-based expression systems present a phenomenon called all-or-none expression, in which only a fraction of the population is induced while the rest remains non-induced and the response to variations of inducer concentration is observed in the size of the population that is induced, rather than in the levels of gene expression (Khlebnikov et al., 2001, 2002). To get rid of this unwanted effect, in this study, the low-affinity L-arabinose transporter *araE* was deleted from the genomic context of the *S*. Typhimurium strains harbouring the synchronization system. As expected, deletion of the *araE* transporter had a general positive effect on secretion functionality (Fig. 20C and 20D). Since a complete NC base is a prerequisite for recruitment of the cytoplasmic components (Zhang et al., 2017; Diepold et al., 2017), this effect on secretion functionality indicated a larger

number of fully assembled injectisomes. However, the positive effect was more notorious when assembly of the injectisome was solely dependent on the P_{araBAD}-driven expression of the export apparatus components *sctU* or *sctR* (Fig. 20C and 20D). In contrast, in a secretion deficient context (Δ*sctN*) the effect of *araE* deletion was not significant, indicating that increasing the number of complete NC bases was insufficient to improve the decoupled onset of secretion. All structural, regulatory and virulence proteins of the T3SS are expressed simultaneously. Thus, complex post-transcriptional mechanisms have evolved to coordinate in time and space the events involved in assembly and function of the injectisome. Chaperones, secretion substrates and cytoplasmic components are not required for the initial stages of assembly and must wait within the bacterial cytosol to be recruited to the NC base to be either secreted or recycled for the next cycle of secretion. Nevertheless, these findings underline the importance of the concurrent expression of every injectisome component for its efficient assembly and activation.

5.2.1 The P_{araBAD}-based synchronization system can be exploited to study injectisome assembly

Combination of the P_{araBAD}-based synchronization assay with the *in vivo* photocrosslinking approach proved to be a sensible strategy to detect protein-protein interactions of the export apparatus component SctR, that report on early assembly stages of the injectisome. Note that in order to efficiently detect protein-protein interactions, the regular *in vivo* photocrosslinking experimental setup requires boosted expression of the SPI-1 T3SS (See methodology section) (Lefebre and Galán, 2014; Dietsche et al., 2016). However, in order to maintain the native proportion of the T3SS components here, SPI-1 overexpression was omitted. Surprisingly, proof of principle experiments showed the occurrence of SctR-SctT and SctR-SctR crosslinks, even under native levels of SPI-1 expression (Fig. 21A). Moreover, these protein-protein interactions took place in fully assembled injectisomes as previously reported (Fig. 21B) (Dietsche et al., 2016; Kuhlen et al., 2018).

5.3 Characterization of the inner rod protein SctI

The T3SS inner rod is an essential structure responsible for anchoring the extracellular needle to the membrane-embedded NC base (Marlovits et al., 2006). Exhaustive mutational analyses of the inner rod protein SctI have shed light on novel roles in needle length control and secretion specificity switching. However, these observations have aroused controversies around SctI functions (Lefebre and Gálan, 2014; Marlovits et al., 2006; Wee and Hughes, 2015). Therefore, in order to gain further insight into the function and assembly of the inner rod, this study exploited the *in vivo* photocrosslinking approach to generate a comprehensive map of protein-protein interactions of SctI and two export apparatus components SctR and SctT (Fig. 24). The detected SctI-SctR and SctI-SctT interactions reported on SctI assembly and were conditioned by a secretion proficient NC base (Fig. 25A and 25B). Interestingly, some *p*Bpa SctI mutants (L67X, I74X, Y77X, V81X) that produced prominent crosslinks to SctR and SctT (Fig. 24), failed to secrete early and middle substrates, suggesting negative effects on SctI functionality (Fig. 23). Interestingly, these residues were located in the periphery of the inner rod and in the interface between SctI and SctF monomers (Fig. 35A and 35B), likely affecting their assembly rather than obstructing the secretion channel.

Since the inner rod is made up of six $SctI^{1-6}$ subunits and one needle subunit ($SctF^{1-5}$) is inserted in between every two SctI subunits (1 - 5), the only SctI-SctI interaction occurs among $SctI^{1}$ and $SctI^{6}$ (Fig. 36A and 36B). In line with this observation, no SctI-SctI interactions were detected in this study (data not shown). However, a former study reported the occurrence of SctI-SctI interactions upon UV irradiation of the plasmid-encoded SctI *p*Bpa mutant M83X (Lefebre and Galán, 2014). The observed $SctI_{M83X}$-SctI crosslinks were thought to represent polymerization of inner rod subunits and thus its assembly, while the loss of this characteristic crosslink in a Δ*sctP* background led to the proposal that SctI plays a role in needle length control (Fig. 7) (Lefebre and Galán, 2014). Here, instead of replicating the SctI-SctI interactions, chromosomally encoded $SctI_{M83X}$ mutant yielded the most prominent crosslink to SctR (Fig. 24). This discrepancy was attributed to plasmid-based overexpression of $SctI_{M83X}$ utilized in the

aforementioned work. It is plausible that $SctI_{M83X}$ overproduction led to artificial interactions between several SctI subunits which after UV irradiation were immunodetected as multiple bands and later on interpreted as inner rod polymerization pattern.

5.3.1 SctI assembly is independent of the OM secretin and needle filament

Although it has been observed that onset of secretion requires a complete NC base (Zhang et al., 2017; Diepold et al., 2017), in this work, assembly of the inner rod was found to be independent of the secretin SctC (Fig. 26), indicating activation of type 3 secretion prior to assembly and recruitment of the OM ring to the IM substructure. Surprisingly, assembly of inner rod seems to require the presence of the needle protein SctF (Fig. 26) and its efficient early polymerization into the needle filament (Fig. 28). In the absence of SctF, secretion of the needle length regulator SctP is abrogated. Thus, it is likely that SctI secretion and therefore assembly are affected too, suggesting a general defect in secretion functionality, rather than a specific effect on the inner rod. However, methods alternative to immunodetection are required to track down SctI and support this assumption.

5.3.2 SctI assembly plays a role neither in substrate specificity switching nor in needle length control

The timer model of needle length control proposes the protein SctP to exclusively function as a scaffold protein required to facilitate inner rod assembly (Marlovits et al., 2006; Lefebre and Galán, 2014). The results obtained in this work, revealed no dependence of SctI assembly on SctP action (Fig. 29). Furthermore, the SctI alanine mutants reported to disrupt needle length control and secretion specificity switching, exhibited optimal SctI assembly on top of the export apparatus, with exception of the SctI mutants M83A, L29A, E96A, T97A and L98A, the assembly of which was less efficient (Fig. 30A and 30C). Only two (E96 and T97A) of the examined mutants showed clear differential effects on secretion (Fig. 30D and

30E). Since both residues are located in the lumen of the secretion conduit, it is plausible that the observed alterations in secretion hierarchy are due to changes in electrostatic properties of the secretion channel (Fig. 35A and 36B). Similarly, discrete mutations in SctI and SctF positioned in the secretion channel have been reported to modify its surface properties and alter secretion of middle and late substrates (Guo et al., 2019; Hu et al., 2019). We attribute the discrepancies between the reported and observed phenotypes of SctI alanine mutants to differences in SctI expression methods, i.e. chromosomal single copy versus high-copy plasmid expression. Plasmid-based overexpression of SctI used in the aforementioned studies has been demonstrated to result in artifacts (Wee and Hughes, 2015).

5.3.3 Model of SctI as a needle adapter

Discovery of the export apparatus helical array and its transmembrane location laid the foundation for the requirement of a short helical adapter to connect and anchor the needle filament to the NC base. Based on the estimated SctI stoichiometry and homology between SctI and SctF, in this work the inner rod structure was modelled as the first helical turn of the needle filament consisting of 6 SctI subunits (Fig. 33). This model is supported by the recently resolved crystal structure of the *S*. Typhimurium SPI-1 injectisome, which reveals that certainly six monomers of SctI form a helical assembly located between the export apparatus and needle (PBD 6pep) (Fig. 34A) (Hu et al., 2019). SctI monomers display two distinctive topologies: $SctI^{1}$ consists of a single C-terminal α-helix, while the $SctI^{2-6}$ subunits adopt a N-terminal β-sheet followed by an ordered hairpin (Fig. 34B) (Hu et al., 2019). In our modelled SctI structure, three conserved hydrophobic residues (V84, V92 and V95) within SctI C-terminal region are suggested to facilitate its adapter role by mediating interactions with SctR and SctT (Fig. 37). Mapping these residues onto the crystal structure of SctI confirms their contribution to anchor the needle structure to the export apparatus as they are located towards the $SctI^{2-5}$-SctR and $SctI^{1,6}$-SctT interfaces. Likewise, three corresponding polar and charged residues (Q61, K69 and D72) at the

C-terminus of SctF are placed in the interfaces between SctI and $SctF^{1-5}$, and the contiguous $SctF^{6+}$ subunits. The pivotal role of C-terminus of SctI in its assembly is supported by numerous mutational analyses conducted in SctI homologs (Cao et al., 2017; Lefebre and Gálan, 2014; Monlezun et al., 2015).

The fact that the inner rod consists of six SctI subunits arrayed in a single helical turn has relevant implications for the timer model of needle length control (Fig. 7) (Marlovits et al., 2006; Lefebre and Galán, 2014). Assembly of six inner rod subunits might occur within a really short time span, which is unlike to provide the required resolution in time to dictate needle length (Fig. 31B). In addition, SctI furnishes the needle filament with the appropriate surface for its helical assembly. Therefore, both structures are unlikely to assemble simultaneously. Altogether, the data generated in this study contribute to put an end to the time-hollowed controversy around needle length control in the *S.* Typhimurium SPI-1 injectisome and point towards the ruler model as the molecular mechanism that governs needle length (Fig. 6) (Erhardt et al., 2010, 2011; Journet et al., 2003; Wee and Hughes, 2015).

5.4 Concluding remarks

This study provides a complex genetic system that allows synchronizing assembly of the *S.* Typhimurium SPI-1 injectisome. Moreover, this newly implemented synchronization system comprises a highly sensitive luciferase-based secretion assay, which would be a resourceful tool to investigate relevant biological processes involved in the regulation of type 3-dependent secretion. Although extremely elaborate, the synchronization system is yet amenable to integration of further approaches e. g. *in vivo* photocrosslinking, expanding the scope of its application.

Additionally, the herein presented characterization and *in silico* model of SctI provide a large body of experimental evidence that the T3SS inner rod functions as a helical adapter between the export apparatus and the needle structure. This model is confirmed by the recently resolved crystal structure of the whole SPI-1

injectisome. The actual inner rod configuration has important functional repercussions and reveals no active role of SctI in needle length control, thus proving the conserved molecular ruler mechanism responsible for regulating needle length control in the SPI-1 T3SS. Furthermore, the inner rod is demonstrated to be involved in substrate specificity by contributing to the electrostatic properties of the secretion conduit´s surface. Considering the new insights into the structure and function of SctI, we propose to rename the inner rod as “needle adapter”.

References

Abby, S. S., & Rocha, E. P. C. (2012). The Non-Flagellar Type III Secretion System Evolved from the Bacterial Flagellum and Diversified into Host-Cell Adapted Systems. *PLoS Genet*, *8*(9), 1002983. https://doi.org/10.1371/journal.pgen.1002983

Abrusci, P., Vergara-Irigaray, M., Johnson, S., Beeby, M. D., Hendrixson, D. R., Roversi, P., Friede, M. E., Deane, J. E., Jensen, G. J., Tang, C. M., & Lea, S. M. (2013). Architecture of the major component of the type III secretion system export apparatus. *Nature Structural and Molecular Biology*, *20*(1), 99–104. https://doi.org/10.1038/nsmb.2452

Agrain, C., Sorg, I., Paroz, C., & Cornelis, G. R. (2005). Secretion of YscP from Yersinia enterocolitica is essential to control the length of the injectisome needle but not to change the type III secretion substrate specificity. *Molecular Microbiology*, *57*(5), 1415–1427. https://doi.org/10.1111/j.1365-2958.2005.04758

Akeda, Y., & Galán, J. E. (2005). Chaperone release and unfolding of substrates in type III secretion. *Nature*, *437*(7060), 911–915. https://doi.org/10.1038/nature03992

Al-Otaibi, N. S., Taylor, A. J., Farrell, D. P., Tzokov, S. B., DiMaio, F., Kelly, D. J., & C Bergeron, J. R. (2020). *The cryo-EM structure of the bacterial flagellum cap complex suggests a molecular mechanism for filament elongation*. https://doi.org/10.1038/s41467-020-16981-4

Arnold, R., Brandmaier, S., Kleine, F., Tischler, P., Heinz, E., Behrens, S., Niinikoski, A., Mewes, H. W., Horn, M., & Rattei, T. (2009). Sequence-Based Prediction of Type III Secreted Proteins. *PLoS Pathogens*, *5*(4). https://doi.org/10.1371/journal.ppat.1000376

Bajaj, V., Hwang, C., & Lee, C. A. (1995). hilA is a novel ompR/toxR family member that activates the expression of Salmonella typhimurium invasion genes. *Molecular Microbiology*, *18*(4), 715–727. https://doi.org/10.1111/j.1365-2958.1995.mmi_18040715

Beverin, S., & Sheppard, D. E. (1971). D-Fucose as a Gratuitous Inducer of the L-Arabinose Operon in Strains of Escherichia coli B/r Mutant in Gene araC' Downloaded from. In *Journal of Bacteriology* (Vol. 107, Issue I). http://jb.asm.org/

Birtalan, S. C., Phillips, R. M., & Ghosh, P. (2002). Three-dimensional secretion signals in chaperone-effector complexes of bacterial pathogens. *Molecular Cell*, *9*(5), 971–980. https://doi.org/10.1016/S1097-2765(02)00529-4

Birtalan, S., & Ghosh, P. (2001). Structure of the Yersinia type III secretory system chaperone SycE. *Nature Structural Biology*, *8*(11), 974–978. https://doi.org/10.1038/nsb1101-974

Botteaux, A., Sani, M., Kayath, C. A., Boekema, E. J., & Allaoui, A. (2008). Spa32 interaction with the inner-membrane Spa40 component of the type III secretion system of Shigella flexneri is required for the control of the needle length by a molecular tape measure mechanism. *Molecular Microbiology*, *70*(6), 1515–1528. https://doi.org/10.1111/j.1365-2958.2008.06499

Burkinshaw, B. J., Deng, W., Lameignère, E., Wasney, G. A., Zhu, H., Worrall, L. J., Brett Finlay, B., & Strynadka, N. C. (2015). *Structural Analysis of a Specialized Type III Secretion System Peptidoglycan-cleaving Enzyme **. https://doi.org/10.1074/jbc.M115.639013

Butan, C., Lara-Tejero, M., Li, W., Liu, J., & Galán, J. E. (2019). *High-resolution view of the type III secretion export apparatus in situ reveals membrane remodeling and a secretion pathway*. https://doi.org/10.1073/pnas.1916331116/-/DCSupplemental

Buttner, D. (2012). Protein Export According to Schedule: Architecture, Assembly, and Regulation of Type III Secretion Systems from Plant- and Animal-Pathogenic Bacteria. *Microbiology and Molecular Biology Reviews*, *76*(2), 262–310. https://doi.org/10.1128/mmbr.05017-11

Cao, Y. Q., Li, Q., Xia, P. F., Wei, L. J., Guo, N., Li, J. W., & Wang, S. G. (2017). AraBAD based toolkit for gene expression and metabolic robustness improvement in synechococcus elongatus. *Scientific Reports*, *7*(1), 1–10. https://doi.org/10.1038/s41598-017-17035-4

Cheng, L. W., Kay, O., & Schneewind, O. (2001). Regulated secretion of YopN by the type III machinery of Yersinia enterocolitica. *Journal of Bacteriology*, *183*(18), 5293–5301. https://doi.org/10.1128/JB.183.18.5293-5301.2001

Cherradi, Y., Hachani, A., & Allaoui, A. (2014). Spa13 of Shigella flexneri has a dual role: Chaperone escort and export gate-activator switch of the type III secretion system. *Microbiology (United Kingdom)*, *160*(PART 1), 130–141. https://doi.org/10.1099/mic.0.071712-0

Christie, P. J. (2019). The Rich Tapestry of Bacterial Protein Translocation Systems. *Protein Journal*, *38*(4), 389–408. https://doi.org/10.1007/s10930-019-09862-3

Collazo, C. M., & Galán, J. E. (1996). Requirement for exported proteins in secretion through the invasion- associated type III system of Salmonella typhimurium. *Infection and Immunity*, *64*(9), 3524–3531. https://doi.org/10.1128/iai.64.9.3524-3531.1996

Cornelis, G. R. (2006). The type III secretion injectisome. *Nature Reviews Microbiology*, *4*(11), 811–825. https://doi.org/10.1038/nrmicro1526

Creasey, E. A., Delahay, R. M., Bishop, A. A., Shaw, R. K., Kenny, B., Knutton, S., & Frankel, G. (2003). CesT is a bivalent enteropathogenic Escherichia coli chaperone required for translocation of both Tir and Map. *Molecular Microbiology*, *47*(1), 209–221. https://doi.org/10.1046/j.1365-2958.2003.03290

Darwin, K. H., & Miller, V. L. (2000). The putative invasion protein chaperone SicA acts together with InvF to activate the expression of Salmonella typhimurium virulence genes. *Molecular Microbiology*, *35*(4), 949–960. https://doi.org/10.1046/j.1365-2958.2000.01772

Dasanayake, D., Richaud, M., Cyr, N., Caballero-franco, C., Finn, R. M., Ausió, J., Luo, W., Donnenberg, M. S., & Jardim, A. (2012). *EspD IS REQUIRED FOR MEMBRANE INSERTION AND*. *81*(3), 734–750. https://doi.org/10.1111/j.1365-2958.2011.07727

de Nisco, N. J., Rivera-Cancel, G., & Orth, K. (2018). The biochemistry of sensing: Enteric pathogens regulate type iii secretion in response to environmental and host cues. *MBio*, *9*(1), 1–15. https://doi.org/10.1128/mBio.02122-17

Deane, J. E., Graham, S. C., Mitchell, E. P., Flot, D., Johnson, S., & Lea, S. M. (2008). Crystal structure of Spa40, the specificity switch for the Shigella flexneri type III secretion system. *Molecular Microbiology*, *69*(1), 267–276. https://doi.org/10.1111/j.1365-2958.2008.06293

Deane, J. E., Roversi, P., Cordes, F. S., Johnson, S., Kenjale, R., Daniell, S., Booy, F., Picking, W. D., Picking, W. L., Blocker, A. J., & Lea, S. M. (2006). Molecular model of a type III secretion system needle: Implications for host-cell sensing. *Proceedings of the National Academy of Sciences of the United States of America*, *103*(33), 12529–12533. https://doi.org/10.1073/pnas.0602689103

Demers, J. P., Sgourakis, N. G., Gupta, R., Loquet, A., Giller, K., Riedel, D., Laube, B., Kolbe, M., Baker, D., Becker, S., & Lange, A. (2013). The Common Structural Architecture of Shigella flexneri and Salmonella typhimurium Type Three Secretion Needles. *PLoS Pathogens*, *9*(3), 1–11. https://doi.org/10.1371/journal.ppat.1003245

Deng, W., Marshall, N. C., Rowland, J. L., McCoy, J. M., Worrall, L. J., Santos, A. S., Strynadka, N. C. J., & Finlay, B. B. (2017). Assembly, structure, function and regulation of type III secretion systems. *Nature Reviews Microbiology*, *15*(6), 323–337. https://doi.org/10.1038/nrmicro.2017.20

Deng, W., Puente, J. L., Gruenheid, S., Li, Y., Vallance, B. A., Vázquez, A., Barba, J., Ibarra, J. A., O'Donnell, P., Metalnikov, P., Ashman, K., Lee, S., Goode, D., Pawson, T., & Finlay, B. B. (2004). Dissecting virulence: Systematic and functional analyses of a pathogenicity island. *Proceedings of the National Academy of Sciences of the United States of America*, *101*(10), 3597–3602. https://doi.org/10.1073/pnas.0400326101

Diepold, A., Amstutz, M., Abel, S., Sorg, I., Jenal, U., & Cornelis, G. R. (2010). Deciphering the assembly of the Yersinia type III secretion injectisome. *EMBO Journal*, *29*(11), 1928–1940. https://doi.org/10.1038/emboj.2010.84

Diepold, A., Sezgin, E., Huseyin, M., Mortimer, T., Eggeling, C., & Armitage, J. P. (2017). A dynamic and adaptive network of cytosolic interactions governs protein export by the T3SS injectisome. *Nature Communications*, *8*(May), 1–12. https://doi.org/10.1038/ncomms15940

Diepold, A., & Wagner, S. (2014). Assembly of the bacterial type III secretion machinery. *FEMS Microbiology Reviews*, *38*(4), 802–822. https://doi.org/10.1111/1574-6976.12061

Dietsche, T., Tesfazgi Mebrhatu, M., Brunner, M. J., Abrusci, P., Yan, J., Franz-Wachtel, M., Schärfe, C., Zilkenat, S., Grin, I., Galán, J. E., Kohlbacher, O., Lea, S., Macek, B., Marlovits, T. C., Robinson, C. V., & Wagner, S. (2016). Structural and Functional Characterization of the Bacterial Type III Secretion Export Apparatus. *PLoS Pathogens*, *12*(12), 1–25. https://doi.org/10.1371/journal.ppat.1006071

El Hajjami, N., Moussa, S., Houssa, J., Monteyne, D., Perez-Morga, D., & Botteaux, A. (2018). The inner-rod component of Shigella flexneri type 3 secretion system, MxiI, is involved in the transmission of the secretion activation signal by its interaction with MxiC. *MicrobiologyOpen*, *7*(1), 1–11. https://doi.org/10.1002/mbo3.520

Erhardt, M., Hirano, T., Su, Y., Paul, K., Wee, D. H., Mizuno, S., Aizawa, S. I., & Hughes, K. T. (2010). The role of the FliK molecular ruler in hook-length control in Salmonella enterica. *Molecular Microbiology*, *75*(5), 1272–1284. https://doi.org/10.1111/j.1365-2958.2010.07050.x

Erhardt, M., Namba, K., & Hughes, K. T. (2010). *Bacterial Nanomachines: The Flagellum and Type III Injectisome*. https://doi.org/10.1101/cshperspect.a000299

Erhardt, M., Singer, H. M., Wee, D. H., Keener, J. P., & Hughes, K. T. (2011). An infrequent molecular ruler controls flagellar hook length in Salmonella enterica. *EMBO Journal*, *30*(14), 2948–2961. https://doi.org/10.1038/emboj.2011.185

Fàbrega, A., & Vila, J. (2013). Salmonella enterica serovar Typhimurium skills to succeed in the host: Virulence and regulation. *Clinical Microbiology Reviews*, *26*(2), 308–341. https://doi.org/10.1128/CMR.00066-12

Farrell, I. S., Toroney, R., Hazen, J. L., Mehl, R. A., & Chin, J. W. (2005). Photo-cross-linking interacting proteins with a genetically encoded benzophenone. In *Nature Methods* | (Vol. 2, Issue 5). http://www.nature.com/naturemethods

Galan, J. E., & Iii, R. C. (1989). Cloning and molecular characterization of genes whose products allow Salmonella typhimurium to penetrate tissue culture cells (cell invasion/bacterial pathogenesis/bacterial adhesion/TnphoA). In *Proc. Nati. Acad. Sci. USA* (Vol. 86).

Gaytán, M. O., Martínez-Santos, V. I., Soto, E., & González-Pedrajo, B. (2016). Type three secretion system in attaching and effacing pathogens. *Frontiers in Cellular and Infection Microbiology*, *6*(OCT), 1–25. https://doi.org/10.3389/fcimb.2016.00129

Gaytán, M. O., Monjarás Feria, J., Soto, E., Espinosa, N., Benítez, J. M., Georgellis, D., & González-Pedrajo, B. (2018). *Novel insights into the mechanism of SepL-mediated control of effector secretion in enteropathogenic Escherichia coli*. *7*, 17. https://doi.org/10.1002/mbo3.571

Gibson, D. G., Young, L., Chuang, R. Y., Venter, J. C., Hutchison, C. A., & Smith, H. O. (2009). Enzymatic assembly of DNA molecules up to several hundred kilobases. *Nature Methods*, *6*(5), 343–345. https://doi.org/10.1038/nmeth.1318

Gophna, U., Ron, E. Z., & Graur, D. (2003). Bacterial type III secretion systems are ancient and evolved by multiple horizontal-transfer events. *Gene*, *312*(1–2), 151–163. https://doi.org/10.1016/S0378-1119(03)00612-7

Guo, E. Z., Desrosiers, D. C., Zalesak, J., Tolchard, J., Berbon, M., Habenstein, B., Marlovits, T., Loquet, A., & Galán, J. E. (2019). A polymorphic helix of a Salmonella needle protein relays signals defining distinct steps in type III secretion. *PLoS Biology*, *17*(7). https://doi.org/10.1371/journal.pbio.3000351

Guzman, L.-M., Belin, D., Carson, M. J., & Beckwith, J. (1995). Tight Regulation, Modulation, and High-Level Expression by Vectors Containing the Arabinose P BAD Promoter. In *Journal of Bacteriology* (Vol. 177, Issue 14)

Hansen-Wester, I., & Hensel, M. (2001). Salmonella pathogenicity islands encoding type III secretion systems. In *Microbes and Infection* (Vol. 3, Issue 7, pp. 549–559). Elsevier Masson SAS. https://doi.org/10.1016/S1286-4579(01)01411-3

Haraga, A., Ohlson, M. B., & Miller, S. I. (2008). Salmonellae interplay with host cells. *Nature Reviews Microbiology*, *6*(1), 53–66. https://doi.org/10.1038/nrmicro1788

Hirano, T., Shibata, S., Ohnishi, K., Tani, T., & Aizawa, S. I. (2005). N-terminal signal region of FliK is dispensable for length control of the flagellar hook. *Molecular Microbiology*, *56*(2), 346–360. https://doi.org/10.1111/j.1365-2958.2005.04615

Hoiseth, S. K., & Stocker, B. A. D. (1981). *and Effective As Live Vaccines*. *291*(May), 238–239.

Hu, B., Morado, D. R., Margolin, W., Rohde, J. R., Arizmendi, O., Picking, W. L., Picking, W. D., & Liu, J. (2017). *Visualization of the type III secretion sorting platform of Shigella flexneri*. https://doi.org/10.1073/pnas.1411610112

Hu, B., Morado, D. R., Margolin, W., Rohde, J. R., Arizmendi, O., Picking, W. L., Picking, W. D., & Liu, J. (2015). Visualization of the type III secretion sorting platform of Shigella flexneri. *Proceedings of the National Academy of Sciences of the United States of America*, *112*(4), 1047–1052. https://doi.org/10.1073/pnas.1411610112

Hu, J., Worrall, L. J., Hong, C., Vuckovic, M., Atkinson, C. E., Caveney, N., Yu, Z., & Strynadka, N. C. J. (2018). Cryo-EM analysis of the T3S injectisome reveals the structure of the needle and open secretin. *Nature Communications*, *9*(1), 1–11. https://doi.org/10.1038/s41467-018-06298-8

Hu, Jinhong, Worrall, L. J., Vuckovic, M., Hong, C., Deng, W., Atkinson, C. E., Brett Finlay, B., Yu, Z., & Strynadka, N. C. J. (2019). T3S injectisome needle complex structures in four distinct states reveal the basis of membrane coupling and assembly. *Nature Microbiology*, *4*(11), 2010–2019. https://doi.org/10.1038/s41564-019-0545-z

Ide, T., Laarmann, S., Greune, L., Schillers, H., Oberleithner, H., & Schmidt, M. A. (2001). Characterization of translocation pores inserted into plasma membranes by type III-secreted Esp proteins of enteropathogenic Escherichia coli. *Cellular Microbiology*, *3*(10), 669–679. https://doi.org/10.1046/j.1462-5822.2001.00146

Izoré, T., Job, V., & Dessen, A. (2011). Biogenesis, regulation, and targeting of the type III secretion system. *Structure*, *19*(5), 603–612. https://doi.org/10.1016/j.str.2011.03.015

Job, V., Matteï, P. J., Lemaire, D., Attree, I., & Dessen, A. (2010). Structural basis of chaperone recognition of type III secretion system minor translocator proteins. *Journal of Biological Chemistry*, *285*(30), 23224–23232. https://doi.org/10.1074/jbc.M110.111278

Journet, L., Agrain, C., Broz, P., & Cornelis, G. R. (2003). The Needle Length of Bacterial Injectisomes Is Determined by a Molecular Ruler. *Science*, *302*(5651), 1757–1760. https://doi.org/10.1126/science.1091422

Kaniga, K., Tucker, S., Trollinger, D., & Galan, J. E. (1995). Homologs of the Shigella IpaB and IpaC invasins are required for Salmonella typhimurium entry into cultured epithelial cells. *Journal of Bacteriology*, *177*(14), 3965–3971. https://doi.org/10.1128/jb.177.14.3965-3971.1995

Kaniga, Koné, Bossio, J. C., & Galán, J. E. (1994). The Salmonella typhimurium invasion genes invF and invG encode homologues of the AraC and PulD family of proteins. *Molecular Microbiology*, *13*(4), 555–568. https://doi.org/10.1111/j.1365-2958.1994.tb00450

Kato, J., Dey, S., Soto, J. E., Butan, C., Wilkinson, M. C., De Guzman, R. N., & Galan, J. E. (2018). A protein secreted by the salmonella type iii secretion system controls needle filament assembly. *ELife*, *7*, 1–23. https://doi.org/10.7554/eLife.35886

Kauer, J. C., Erickson-Viitanen, S., Wolfe, H. R., & DeGrado, W. F. (1986). p-Benzoyl-L-phenylalanine, a new photoreactive amino acid. Photolabeling of calmodulin with a synthetic calmodulin-binding peptide. *Journal of Biological Chemistry*, *261*(23), 10695–10700. https://doi.org/10.1016/S0021-9258(18)67441-1

Khlebnikov, A., Datsenko, K. A., Skaug, T., Wanner, B. L., & Keasling, J. D. (2001). Homogeneous expression of the PBAD promoter in Escherichia coli by constitutive expression of the low-affinity high-capacity araE transporter. *Microbiology*, *147*(12), 3241–3247. https://doi.org/10.1099/00221287-147-12-3241

Khlebnikov, A., Risa, Skaug, T., Carrier, T. A., & Keasling, J. D. (2000). Regulatable arabinose-inducible gene expression system with consistent control in all cells of a culture. *Journal of Bacteriology*, *182*(24), 7029–7034. https://doi.org/10.1128/JB.182.24.7029-7034.2000

Kubori, T., Matsushima, Y., Nakamura, D., Uralil, J., Lara-, M., Kubori, T., Matsushima, Y., Nakamura, D., Galn, J. E., & Aizawa, S. (2016). *Supramolecular Structure of the Salmonella typhimurium Type III Protein Secretion System Tejero , Anand Sukhan , Jorge E . Gálan and Shin-Ichi Aizawa Published by : American Association for the Advancement of Science Stable URL : http://www.jstor.org/stab*. *280*(5363), 602–605.

Kubori, T., Sukhan, A., Aizawa, S. I., & Galán, J. E. (2000). Molecular characterization and assembly of the needle complex of the Salmonella typhimurium type III protein secretion system. *Proceedings of the National Academy of Sciences of the United States of America*, *97*(18), 10225–10230. https://doi.org/10.1073/pnas.170128997

Kuhlen, L., Abrusci, P., Johnson, S., Gault, J., Deme, J., Caesar, J., Dietsche, T., Mebrhatu, M. T., Ganief, T., Macek, B., Wagner, S., Robinson, C. V., & Lea, S. M. (2018). Structure of the core of the type iii secretion system export apparatus. *Nature Structural and Molecular Biology*, *25*(7). https://doi.org/10.1038/s41594-018-0086-9

Kuhlen, L., Johnson, S., Zeitler, A., Bäurle, S., Deme, J. C., Caesar, J. J. E., Debo, R., Fisher, J., Wagner, S., & Lea, S. M. (2020). *The substrate specificity switch FlhB assembles onto the export gate to regulate type three secretion*. https://doi.org/10.1038/s41467-020-15071-9

Kurtz, J. R., Goggins, J. A., & Mclachlan, J. B. (2017). *Salmonella infection: interplay between the bacteria and host immune system*. https://doi.org/10.1016/j.imlet.2017.07.006

Lara-Tejero, M., Kato, J., Wagner, S., Liu, X., & Galán, J. E. (n.d.). *A Sorting Platform Determines the Order of Protein Secretion in Bacterial Type III Systems*. https://doi.org/10.1126/science.1201476

Lavander, M., Sundberg, L., Edqvist, P. J., Lloyd, S. A., Wolf-Watz, H., & Forsberg, Å. (2002). Proteolytic cleavage of the FlhB homologue YscU of Yersinia pseudotuberculosis is essential for bacterial survival but not for type III secretion. *Journal of Bacteriology*, *184*(16), 4500–4509. https://doi.org/10.1128/JB.184.16.4500-4509.2002

Lefebre, M. D., & Gálan, J. E. (2014). The inner rod protein controls substrate switching and needle length in a Salmonella type III secretion system. *Proceedings of the National Academy of Sciences of the United States of America*, *111*(2), 817–822. https://doi.org/10.1073/pnas.1319698111

Loquet, A., Sgourakis, N. G., Gupta, R., Giller, K., Riedel, D., Goosmann, C., Griesinger, C., Kolbe, M., Baker, D., Becker, S., & Lange, A. (2012). Atomic model of the type III secretion system needle. *Nature*, *486*(7402), 276–279. https://doi.org/10.1038/nature11079

Lorenz, C., & Büttner, D. (2011). Secretion of early and late substrates of the type III secretion system from Xanthomonas is controlled by HpaC and the C-terminal domain of HrcU. *Molecular Microbiology*, *79*(2), 447–467. https://doi.org/10.1111/j.1365-2958.2010.07461.x

Lunelli, M., Hurwitz, R., Lambers, J., & Kolbe, M. (2011). Crystal structure of prgi-sipd: Insight into a secretion competent state of the type three secretion system needle tip and its interaction with host ligands. *PLoS Pathogens*, *7*(8). https://doi.org/10.1371/journal.ppat.1002163

Lunelli, M., Lokareddy, R. K., Zychlinsky, A., & Kolbe, M. (2009). IpaB-IpgC interaction defines binding motif for type III secretion translocator. *Proceedings of the National Academy of Sciences of the United States of America*, *106*(24), 9661–9666. https://doi.org/10.1073/pnas.0812900106

Lunelli, M., Kamprad, A., Bürger, J., Mielke, T., T Spahn, C. M., & Kolbe, M. (2020). *Cryo-EM structure of the Shigella type III needle complex*. https://doi.org/10.1371/journal.ppat.1008263

Marenne, M. N., Journet, L., Mota, L. J., & Cornelis, G. R. (2003). Genetic analysis of the formation of the Ysc-Yop translocation pore in macrophages by Yersinia enterocolitica: Role of LcrV, YscF and YopN. *Microbial Pathogenesis*, *35*(6), 243–258. https://doi.org/10.1016/S0882-4010(03)00154-2

Marlovits, T. C., Kubori, T., Lara-Tejero, M., Thomas, D., Unger, V. M., & Galán, J. E. (2006). Assembly of the inner rod determines needle length in the type III secretion injectisome. *Nature*, *441*(7093), 637–640. https://doi.org/10.1038/nature04822

Marlovits, T. C., Kubori, T., Sukhan, A., Thomas, D. R., Galán, J. E., & Unger, V. M. (2004). *Structural Insights into the Assembly of the Type III Secretion Needle Complex*. Science; 306(5698): 1040–1042.

Michiels, T., & Cornelis, G. R. (1991). Secretion of hybrid proteins by the Yersinia Yop export system. *Journal of Bacteriology*, *173*(5), 1677–1685. https://doi.org/10.1128/jb.173.5.1677-1685.1991

Minamino, T., Saijo-Hamano, Y., Furukawa, Y., González-Pedrajo, B., Macnab, R. M., & Namba, K. (2004). Domain organization and function of Salmonella FliK, a flagellar hook-length control protein. *Journal of Molecular Biology*, *341*(2), 491–502. https://doi.org/10.1016/j.jmb.2004.06.012

Monjarás Feria, J. V., Lefebre, M. D., Stierhof, Y. D., Galán, J. E., & Wagner, S. (2015). Role of autocleavage in the function of a type iii secretion specificity switch protein in salmonella enterica serovar typhimurium. *MBio*, *6*(5), 1–8. https://doi.org/10.1128/mBio.01459-15

Monlezun, L., Liebl, D., Fenel, D., Grandjean, T., Berry, A., Schoehn, G., Dessein, R., Faudry, E., & Attree, I. (2015). PscI is a type III secretion needle anchoring protein with in vitro polymerization capacities. *Molecular Microbiology*, *96*(2), 419–436. https://doi.org/10.1111/mmi.12947

Moriya, N., Minamino, T., Hughes, K. T., Macnab, R. M., & Namba, K. (2006). The Type III Flagellar Export Specificity Switch is Dependent on FliK Ruler and a Molecular Clock. *Journal of Molecular Biology*, *359*(2), 466–477. https://doi.org/10.1016/j.jmb.2006.03.025

Mota, L. J., Journet, L., Sorg, I., Agrain, C., & Cornelis, G. R. (2005). Bacterial injectisomes: Needle length does matter. *Science*, *307*(5713), 1278. https://doi.org/10.1126/science.1107679

Mueller, C. A., Broz, P., Müller, S. A., Ringler, P., Sorg, I., Kuhn, M., Engel, A., Cornelis, G. R., & Iii, W. (2016). *The V-Antigen of Yersinia Forms a Distinct Structure at the Tip of Injectisome Needles Published by : American Association for the Advancement of Science Stable URL : http://www.jstor.org/stable/3842714 REFERENCES Linked references are available on JSTOR* . *310*(5748), 674–676.

Nambu, T., Minamino, T., Macnab, R. M., & Kutsukake, K. (1999). Peptidoglycan-Hydrolyzing Activity of the FlgJ Protein, Essential for Flagellar Rod Formation in Salmonella typhimurium. In *Journal of bacteriology* (Vol. 181, Issue 5).

Ohnishi, K., Ohto, Y., Aizawa, S. I., Macnab, R. M., & Iino, T. (1994). FlgD is a scaffolding protein needed for flagellar hook assembly in Salmonella typhimurium. *Journal of Bacteriology*, *176*(8), 2272–2281. https://doi.org/10.1128/jb.176.8.2272-2281.1994

Binder, D., Probst, C., Grünberger, A., Hilgers, F., Loeschcke, A., & Jaeger, K.-E. (2016). Comparative Single-Cell Analysis of Different E. coli Expression Systems during Microfluidic Cultivation. *PLoS ONE*, *11*(8), 160711. https://doi.org/10.1371/journal.pone.0160711

Pallen, M. J., Francis, M. S., & Fütterer, K. (2003). Tetratricopeptide-like repeats in type-III-secretion chaperones and regulators. *FEMS Microbiology Letters*, *223*(1), 53–60. https://doi.org/10.1016/S0378-1097(03)00344-6

Parsot, C., Hamiaux, C., & Page, A. L. (2003). The various and varying roles of specific chaperones in type III secretion systems. *Current Opinion in Microbiology*, *6*(1), 7–14. https://doi.org/10.1016/S1369-5274(02)00002-4

Portaliou, A. G., Tsolis, K. C., Loos, M. S., Balabanidou, V., Rayo, J., Tsirigotaki, A., Crepin, V. F., Frankel, G., Kalodimos, C. G., Karamanou, S., & Economou, A. (2017). Hierarchical protein targeting and secretion is controlled by an affinity switch in the type III secretion system of enteropathogenic Escherichia coli . *The EMBO Journal*, *36*(23), 3517–3531. https://doi.org/10.15252/embj.201797515

Rathinavelan, T., Lara-Tejero, M., Lefebre, M., Chatterjee, S., Mcshan, A. C., Guo, D.-C., Tang, C., Galan, J. E., & De Guzman, R. N. (2014). NMR Model of PrgI-SipD Interaction and its Implications in the Needle-Tip Assembly of the Salmonella Type III Secretion System. *J Mol Biol*, *426*(16), 2958–2969. https://doi.org/10.1016/j.jmb.2014.06.009

Roehrich, A. D., Guillossou, E., Blocker, A. J., & Martinez-Argudo, I. (2013). Shigella IpaD has a dual role: Signal transduction from the type III secretion system needle tip and intracellular secretion regulation. *Molecular Microbiology*, *87*(3), 690–706. https://doi.org/10.1111/mmi.12124

Romo-Castillo, M., Andrade, A., Espinosa, N., Feria, J. M., Soto, E., Díaz-Guerrero, M., & González-Pedrajo, B. (2014). EscO, a functional and structural analog of the flagellar fliJ protein, is a positive regulator of EscN ATPase activity of the enteropathogenic Escherichia coli injectisome. *Journal of Bacteriology*, *196*(12), 2227–2241. https://doi.org/10.1128/JB.01551-14

Russo, B. C., Duncan, J. K., Wiscovitch, A. L., Hachey, A. C., & Goldberg, M. B. (2019). Activation of Shigella flexneri type 3 secretion requires a host-induced conformational change to the translocon pore. *PLoS Pathogens*, *15*(11), 1–20. https://doi.org/10.1371/journal.ppat.1007928

Ryu, Y., & Schultz, P. G. (2006). *Efficient incorporation of unnatural amino acids into proteins in Escherichia coli*. https://doi.org/10.1038/NMETH864

Schleif, R. (2000a). Regulation of the L-arabinose operon of Escherichia coli. *Trends in Genetics*, *16*(12), 559–565. https://doi.org/10.1016/S0168-9525(00)02153-3

Schraidt, O., Lefebre, M. D., Brunner, M. J., Schmied, W. H., Schmidt, A., Radics, J., Mechtler, K., Galán, J. E., & Marlovits, T. C. (2010). Topology and organization of the Salmonella typhimurium type III secretion needle complex components. *PLoS Pathogens*, *6*(4), 1–12. https://doi.org/10.1371/journal.ppat.1000824

Siegele, D. A., & Hu, J. C. (1997). Gene expression from plasmids containing the araBAD promoter at subsaturating inducer concentrations represents mixed populations. *Proceedings of the National Academy of Sciences of the United States of America*, *94*(15), 8168–8172. https://doi.org/10.1073/pnas.94.15.8168

Silva, Y. R. de O., Contreras-Martel, C., Macheboeuf, P., & Dessen, A. (2020). Bacterial secretins: Mechanisms of assembly and membrane targeting. *Protein Science*. https://doi.org/10.1002/pro.3835

Sorg, I., Wagner, S., Amstutz, M., Müller, S. A., Broz, P., Lussi, Y., Engel, A., & Cornelis, G. R. (2007). YscU recognizes translocators as export substrates of the Yersinia injectisome. *EMBO Journal*, *26*(12), 3015–3024. https://doi.org/10.1038/sj.emboj.7601731

Sory, M. P., Boland, A., Lambermont, I., & Cornelis, G. R. (1995). Identification of the YopE and YopH domains required for secretion and internalization into the cytosol of macrophages, using the cyaA gene fusion approach. *Proceedings of the National Academy of Sciences of the United States of America*, *92*(26), 11998–12002. https://doi.org/10.1073/pnas.92.26.11998

Spreter, T., Yip, C. K., Sanowar, S., André, I., Kimbrough, T. G., Vuckovic, M., Pfuetzner, R. A., Deng, W., Yu, A. C., Finlay, B. B., Baker, D., Miller, S. I., & Strynadka, N. C. J. (2009). A conserved structural motif mediates formation of the periplasmic rings in the type III secretion system. *Nature Structural and Molecular Biology*, *16*(5), 468–476. https://doi.org/10.1038/nsmb.1603

Stanley, A. M., Carvalho, P., & Rapoport, T. (2011). *Recognition of an ERAD-L substrate analyzed by site-specific in vivo photocrosslinking*. https://doi.org/10.1016/j.febslet.2011.04.009

Stecher, B., Macpherson, A. J., Hapfelmeier, S., Kremer, M., Stallmach, T., & Hardt, W.-D. (2005). Comparison of Salmonella enterica Serovar Typhimurium Colitis in Germfree Mice and Mice Pretreated with Streptomycin. *Infection and Immunity*, *73*(6), 3228–3241. https://doi.org/10.1128/IAI.73.6.3228-3241.2005

Storz, G., Kato, J., Dey, S., Soto, J. E., Butan, C., Wilkinson, M. C., De Guzman, R. N., & Galan, J. E. (2018). *A protein secreted by the Salmonella type III secretion system controls needle filament assembly*. https://doi.org/10.7554/eLife.35886.001

Sukhan, A., Kubori, T., Wilson, J., Gala, J. E., Iii, T., & Prgh, T. (2001). Genetic Analysis of Assembly of the. *Society*, *183*(4), 1159–1167. https://doi.org/10.1128/JB.183.4.1159

Tamano, K., Katayama, E., Toyotome, T., & Sasakawa, C. (2002). Shigella Spa32 is an essential secretory protein for functional type III secretion machinery and uniformity of its needle length. *Journal of Bacteriology*, *184*(5), 1244–1252. https://doi.org/10.1128/JB.184.5.1244-1252.2002

Torres-Vargas, C. E., Kronenberger, T., Roos, N., Dietsche, T., Poso, A., & Wagner, S. (2019). The inner rod of virulence-associated type III secretion systems constitutes a needle adapter of one helical turn that is deeply integrated into the system's export apparatus. *Molecular Microbiology*, *112*(3), 918–931. https://doi.org/10.1111/mmi.14327

Torruellas, J., Jackson, M. W., Pennock, J. W., & Plano, G. V. (2005). The Yersinia pestis type III secretion needle plays a role in the regulation of Yop secretion. *Molecular Microbiology*, *57*(6), 1719–1733. https://doi.org/10.1111/j.1365-2958.2005.04790.x

Tsirigotaki, A., De Geyter, J., Šoštaric, N., Economou, A., & Karamanou, S. (2016). Protein export through the bacterial Sec pathway. *Nature Reviews | Microbiology*, *15*. https://doi.org/10.1038/nrmicro.2016.161

Wagner, S., & Diepold, A. (2020). *A Unified Nomenclature for Injectisome-Type Type III Secretion Systems*. Curr Top Microbiol Immunol. 2020;427:1-10. doi: 10.1007/82_2020_210. PMID: 32415388

Wagner, S., Grin, I., Malmsheimer, S., Singh, N., Torres-Vargas, C. E., & Westerhausen, S. (2018). Bacterial type III secretion systems: A complex device for the delivery of bacterial effector proteins into eukaryotic host cells. *FEMS Microbiology Letters*, *365*(19), 1–13. https://doi.org/10.1093/femsle/fny201

Wagner, S., Königsmaier, L., Lara-Tejero, M., Lefebre, M., Marlovits, T. C., & Galán, J. E. (2010). Organization and coordinated assembly of the type III secretion export apparatus. *Proceedings of the National Academy of Sciences of the United States of America*, *107*(41), 17745–17750. https://doi.org/10.1073/pnas.1008053107

Warawa, J., Finlay, B. B., & Kenny, B. (1999). Type III secretion-dependent hemolytic activity of enteropathogenic Escherichia coli. *Infection and Immunity*, *67*(10), 5538–5540. https://doi.org/10.1128/iai.67.10.5538-5540.1999

Wee, D. H., & Hughes, K. T. (2015). *Molecular ruler determines needle length for the Salmonella Spi-1 injectisome*. https://doi.org/10.1073/pnas.1423492112

Westerhausen, S., Nowak, M., Torres-Vargas, C. E., Bilitewski, U., Bohn, E., Grin, I., & Wagner, S. (2019). A NanoLuc luciferase-based assay enabling the real-time analysis of protein secretion and injection by bacterial type III secretion systems. *BioRxiv*, *October 2019*, 745471. https://doi.org/10.1101/745471

Worrall, L. J., Hong, C., Vuckovic, M., Deng, W., Bergeron, J. R. C., Majewski, D. D., Huang, R. K., Spreter, T., Finlay, B. B., Yu, Z., & Strynadka, N. C. J. (2016). Near-atomic-resolution cryo-EM analysis of the Salmonella T3S injectisome basal body. *Nature*, *540*(7634), 597–601. https://doi.org/10.1038/nature20576

Yonekura, K., Maki, S., Morgan, D. G., DeRosier, D. J., Vonderviszt, F., Imada, K., & Namba, K. (2000). The bacterial flagellar cap as the rotary promoter of flagellin self-assembly. *Science*, *290*(5499), 2148–2152. https://doi.org/10.1126/science.290.5499.2148

Yonekura, Koji, Maki-Yonekura, S., & Namba, K. (2003). Complete atomic model of the bacterial flagellar filament by electron cryomicroscopy. *Nature*, *424*(6949), 643–650. https://doi.org/10.1038/nature01830

Yu, X. J., Grabe, G. J., Liu, M., Mota, L. J., & Holden, D. W. (2018). Ssav interacts with SsaL to control the translocon-to-effector switch in the salmonella SPI-2 type three secretion system. *MBio*, *9*(5). https://doi.org/10.1128/mBio.01149-18

Yu, X. J., McGourty, K., Liu, M., Unsworth, K. E., & Holden, D. W. (2010). pH sensing by intracellular salmonella induces effector translocation. *Science*, *328*(5981), 1040–1043. https://doi.org/10.1126/science.1189000

Zarivach, R., Deng, W., Vuckovic, M., Felise, H. B., Nguyen, H. V., Miller, S. I., Finlay, B. B., & Strynadka, N. C. J. (2008). Structural analysis of the essential self-cleaving type III secretion proteins EscU and SpaS. *Nature*, *453*(7191), 124–127. https://doi.org/10.1038/nature06832

Zhang, Y., Lara-Tejero, M., Bewersdorf, J., & Galán, J. E. (2017). Visualization and characterization of individual type III protein secretion machines in live bacteria. *Proceedings of the National Academy of Sciences of the United States of America*, *114*(23), 6098–6103. https://doi.org/10.1073/pnas.1705823114

Zilkenat, S., Franz-Wachtel, M., Stierhof, Y.-D., Galá, J. E., Macek, B., & Wagner, S. (2016). *Determination of the Stoichiometry of the Complete Bacterial Type III Secretion Needle Complex Using a Combined Quantitative Proteomic Approach*. https://doi.org/10.1074/mcp.M115.056598

Acknowledgements

I want to thank Prof. Samuel Wagner for the chance to work on this challenging and ambitious scientific project, I truly appreciate the confidence you showed in me. I value the insight and guidance you provided throughout my stay in your team. Finally, I express my deepest admiration towards you for being an exceptional person and a brilliant scientist.

Many thanks to PD Dr. rer. nat. Monika Schütz, Prof. Dr. Doron Rapaport and Prof. Dr. Gabriele Dodt for their willingness to serve as examiners at my PhD dissertation defense.

I express my deepest gratitude to the University of Tübingen for supporting my doctoral studies with a fellowship of the excellence initiative.

My sincere appreciation to Dr. Julia Monjarás-Feria and Dr. Libera Lo Presti for their valuable and constructing feedback on this thesis.

Many thanks to all members of AG Wagner (2014-2019) for their support and contributions to my research projects. MTA Andrea Eipper is worthy of a special mention for her outstanding technical support.

I want to thank our collaboration partners Prof. Antti Poso and Thales Kronenberger, PhD, for their contribution to this work. In the same line, I thank Dr. York D. Stierhof and his working team for performing the TEM analysis of injectisomes.

Gisela Bauer-Haffter and Dr. Iwan Grin, you have my everlasting gratitude for your hospitality and guidance.

This work was supported by the Alexander von Humboldt Foundation in the framework of the Sofja Kovalevskaja Award to Prof. Samuel Wagner.